10\242
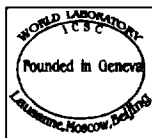
NASA-CR-205550

ECOLEN
SCIENTIFIC RESEARCH CENTER
2, Aviamotornaya st., Moscow, 111250, Russia

VERIFICATION AND IMPROVEMENT OF FLAMELET APPROACH FOR NON−PREMIXED FLAMES

Principal Investigator: *S. Zaitsev*

Participants: *Yu.Buriko,
O.Guskov,
V.Kopchenov,
D.Lubimov,
S.Tshepin,
D.Volkov*

Scientific consultant: *Prof. A.Secundov*

Moscow
August 1997

CONTENT

(to be continued)

INTRODUCTION

Studies in the mathematical modeling of the high-speed turbulent combustion has received renewal attention in the recent years. The review of fundamentals, approaches and extensive bibliography was presented by *Bray, Libbi and Williams (1994)*.

In order to obtain accurate predictions for turbulent combustible flows, the effects of turbulent fluctuations on the chemical source terms should be taken into account. The averaging of chemical source terms requires to utilize probability density function (PDF) model. There are two main approaches which are dominant in high-speed combustion modeling now. In the first approach, PDF form is assumed based on intuitia of modelliers (see, for example, *Spiegler et.al.,1976; Girimaji, 1991; Baurle et.al.,1992*). The second way is much more elaborate and it is based on the solution of evolution equation for PDF. This approach was proposed by *S.Pope (1981)* for incompressible flames. Recently, it was modified for modeling of compressible flames in studies of *Farschi (1989); Hsu (1991); Hsu, Raji, Norris (1994); Eifer, Kollman (1993)*. But its realization in CFD is extremely expensive in computations due to large multidimensionality of PDF evolution equation (*Baurle, Hsu, Hassan,1994*).

Promising way for development of computationally non-expensive procedure for PDF construction is flamelet approach (FL) formulated for subsonic turbulent flames in studies of *Bilger (1980), Kuznetsov (1977,1982), Peters (1984)* and *Williams (1975)*. The simplification of the turbulence/chemistry interaction modeling is achieved here based on the assumption that chemical processes are mostly confined to the local vicinity of the stoichiometric surfaces. This assumption allows to reduce instantaneous conservation equations for reactive scalars to the system of ordinary differential equations (flamelet equations). Its solution gives relations for reactive species mass fraction and temperature depending on mixture fraction z and its scalar dissipation $N = D(\nabla z)^2$ where D is molecular diffusivity. The FL solutions are used to present joint PDF of reactive scalars $\mathscr{P}(C_1,...,C_J,T)$ as a function of mixture fraction and scalar dissipation joint PDF $\mathscr{P}(z,N)$ only. So consideration of the reactive scalars statistics is reduced to the modeling of large- and small-scale statistics for the passive scalar. Additional benefits of the FL approach are connected with the fact that flamelet equations can be integrated before starting hydrodynamics calculations for many cases of turbulent flames. So, CFD modeling can be performed using tabulated solutions for reactive scalars versus mixture fraction z and scalar dissipation N (so-called flamelet library approach). By such a manner, very complex detailed kinetics schemes can be incorporated into the CFD codes without significant computational time increasing.

Previously, FL approach demonstrated satisfactory results in predictions of reactive species and temperature for subsonic laboratory nonpremixed flames (*Liew,Bray,Moss, 1984; Buriko,Kuznetsov, 1988; Buriko et.al., 1994*). Currently, FL model capabilities are studied for simulation of the combustion and pollutants

emissions in gas-turbine combustors (*Buriko et.al. 1996; Bai,Fuchs 1995; Amin et.al. 1995; etc.*).

The flamelet modeling of the supersonic flames is much more complex compare to the case of low-Mach number flames The main problems which complicated FL modeling of compressible flames are connected with:

(i) *Large input of flow kinetic energy term* in energy conservation equation and pressure variation inside the flow field which provide dependence of the reactive scalars on the additional parameters i.e. on flow velocity V and pressure p:
$C_\alpha = C_\alpha(z, N, V, p)$.
So, dependencies for the reactive scalars became 4-parametric instead of 2-parametric ones for low-Mach number flows. This feature complicates procedure for flamelet library development and averaging. The dependence of C_α on V and p worsen the accuracy of hydrodynamics and kinetics splitting also.

(ii) *Large ignition delay.* Often supersonic jet flames are not stabilized at nozzle lip and ignition takes place in some cross section downstream the nozzle exit. The ignition delay distance can be significant for supersonic flames. The basic assumptions of the FL approach are violated in the vicinity of self-ignition point since reagents can be partially-premixed in self-ignition region and chemical processes can occur in some volumes or near-premixed flame fronts.

Nevertheless, possible benefits, which can provide flamelet approach for the simplification of the turbulence/chemistry interaction modeling, requires modeliers to look for possible ways for model modifications and its implementation into the simulation of combustion processes in supersonic flames. The estimations of possible combustion regimes in hydrogen/air systems for application to scramjet combustors were reported by *Balakrishnan and Williams (1993)*. Their results indicated that, close to flamelet, combustion regimes are likely exist in supersonic combustors at typical operational conditions of hypersonic airplanes.

First studies toward flamelet model generalization for supersonic flames have been performed recently by *Zheng and Bray (1994)*, *Bezgin et.al. (1995)*, *Morgenthaler et.al. (1997)*. In particular, extension of the *Kuznetsov (1982)* flamelet approach for the expanded supersonic jet flames was done in 1995-1996 under implementation of the NASA Cooperative Agreement NCCW-75 by our group *(Bezgin et.al. 1996)*. It was found that FL approach allowed to describe satisfactory main features of supersonic H_2/air jet flames. Model demonstrated also high capabilities for reduction of the computational expenses in CFD modeling of the supersonic flames taking into account detailed oxidation chemistry. However, disadvantages and limitations of the existing version of FL approach were found in that study also. They were: i) inaccuracy of reactive scalars predictions obtained in flamelet modeling for well-known *Burrows—Kurkov (1973)* test case; ii) significant inaccuracy in predictions of the ignition delay distance; iii) improper model operation in the vicinity of self-ignition point.

So, studies toward further improvement of the FL approach capabilities were continued this year under NASA LeRC Cooperative Agreement NCC3-496. They were performed in two main directions:

1. Analysis and improvement of previously found inaccuracy in model predictions and consideration of the new test cases for more careful verification of the model capabilities.

2. Searching possible way for modification of the FL approach for its more correct operation in the case of flames with large ignition delay distance.

The current Report summarizes results of the performed studies. It is organized as follows:

Sec.I contains cumulative summary of the flamelet approach which is necessary for explanations in the next Sections of the Report.

Sec.II contains brief description of the test cases which were used both for the analysis of the previously obtained discrepancy and in the current CFD tests of the flamelet approach.

Brief analysis of the previous results and current model modifications are given in Sec.III.

The results and analysis of the current CFD tests are presented in Sec.IV. In current study, we considered 4 tests cases which covered 3 main types of the flow field (round jet, planar wall jet and planar mixing layer) and two classes of flames (with and without large ignition delay distance). All the considered test cases were calculated based on the averaged system of 2-D Navier-Stokes equations and using the same turbulence and detailed chemistry models. The description of the obtained results is presented in:

Sec.IV.1 - for *Burrows and Kurkov (1973)* wall-jet test;

Sec.IV.2 - for Beach round jet test reported in *Evans et.al (1978)*;

Sec.IV.3 - for *Cheng et.al. (1994)* round jet test;

Sec.IV.4 - for *Chang et.al. (1993)* planar mixing layer experiment.

The supplemented information about CFD tests is submitted to the Appendixes (description of the mathematical model, thermodynamics and kinetics reference data, etc.). Only brief description of applied computational procedures is presented in current Report since we used the same codes as those described in our previous Final Report to NASA *(Bezgin et.al., 1996)*.

Sec.V contains results of our investigations toward modification of the flamelet approach for flames with large ignition delay distance. Our reasons and modified flamelet equations (MFL) are presented in Sec.V.1. Computational procedure, which was used for their solution, is outlined in Sec.V.2. Results of modeling tests of the MFL equations are presented in Sec.V.3 together with suggestions concerning possible way for model improvement.

The Report is finished by Summary and suggestions for further investigations.

I. FLAMELET APPROACH

The current concept of the flamelet approach (FL) remained the same as that presented in *Bezgin et.al. (1996)*. The schematic of the approach is given in Fig.1. It is based on the assumption that chemical reactions are mostly occur in narrow regions (flamelets) located in the vicinity of the surfaces with stoichiometric composition.

The stoichiometric surface is highly curved and randomly fluctuated in turbulent flows. So, the mixture fraction z is used to characterize its location. The mixture fraction z is introduced as the total mass fraction of all kinds of atoms initially been contained in fuel and then converted to other chemical species arising in the flame. It obeys conservation equation without source term:

$$\frac{\partial \rho z}{\partial t} + \frac{\partial \rho u_k z}{\partial x_k} = \nabla \rho D \nabla z \qquad (I.1)$$

Value of $z = 1$ corresponds to pure fuel and $z = 0$ - to pure air; mixture fraction has value $z = z_s = 1/(1 + St)$ at the stoichiometric surface (St is the stoichiometric factor).

The assumption about small thickness of the reaction zones allows to simplify modeling of the turbulence/chemistry interaction problem (Fig.1). First of all, it is possible to reduce instantaneous conservation equations for reactive scalars to the system of ordinary differential equations (flamelet equations). Its solution gives relations for reactive species mass fractions and temperature depending on mixture fraction z and its scalar dissipation $N = D(\nabla z)^2$ where D is molecular diffusivity i.e. $C_\alpha = C_\alpha(z,N)$, $T = T(z,N)$. These relations are used to present joint PDF for reactive scalars $\mathcal{P}(C_1,...,C_J,T)$ depending on mixture fraction and its scalar dissipation joint PDF $\mathcal{P}(z,N)$ only. Let us present flamelet equations and passive scalar statistics model in a little more details.

Flamelet Equations. Based on assumption about small thickness of the reaction zones, the unsteady and convective terms in the instantaneous conservation equations for reactive scalars are dropped out and mixture fraction is used as independent variable instead of space coordinate. Full account was done by *Kuznetsov (1982)* and it was repeated in our previous Final Report *(Bezgin et.al., 1996)*. The same kind of reasoning is applied to the energy conservation equation also. Resulting system of flamelet equations has the form:

$$N^s \frac{d^2 C_\alpha}{dz^2} + R_\alpha = 0 \qquad (I.2)$$

$$\frac{d^2 H}{dz^2} = 0 \qquad (I.3)$$

where C_α is mass fraction of α-specie ($\alpha = 1,...,J$); J is total number of reactive species; R_α is the chemical production term; H is total enthalpy defined as

$$H = h + \frac{(\vec{V} \cdot \vec{V})}{2}; \qquad h = \sum_{\alpha=1}^{J} h_\alpha C_\alpha \qquad \text{is static enthalpy; species specific enthalpies}$$

$h_\alpha = \int_{T_0}^{T} Cp_\alpha dT + \Delta h_\alpha(T_0)$ are used taking into account species heats of formation Δh_α

at reference temperature T_0; $\vec{V}$ is velocity vector. The parameter $N^S = D\left(\dfrac{dz}{dn}\right)^2$ is

the value of instantaneous scalar dissipation $N = D(\nabla z)^2$ at the stoichiometric surface which characterizes the reagents fluxes to the reaction zones; n is coordinate normal to the stoichiometric surface $z = z_s$ (Fig.1).

The boundary conditions (BC) for the flamelet equations (I.2)-(I.3) are posed at $z = 1$ (pure fuel) and $z = 0$ (pure oxidizer):

$$z = 0 \quad H = H^A; C_\alpha = C_\alpha^A \tag{I.4}$$

$$z = 1 \quad H = H^F; C_\alpha = C_\alpha^F \qquad\qquad \alpha = 1,...,J$$

where superscripts F and A denote composition and total enthalpies of fuel and oxidizer respectively.

The eq.(I.3) is integrated over z from 0 to 1 and the total enthalpies of fuel (at $z = 1$) and air (at $z = 0$) are used to define the constants in the obtained linear relation. As the result, flamelet model equations (I.2),(I.3) are re-written in a form:

$$N^S \frac{d^2 C_\alpha}{dz^2} + R_\alpha = 0 \qquad\qquad \alpha = 1,...,J \tag{I.5}$$

$$h = (H^F - H^A)z + H^A - \frac{V^2}{2}$$

The formulated flamelet model boundary problem (I.5) with the boundary conditions (I.4) give the solution for C_α and static temperature T in the following parametric form:

$$C_\alpha = C_\alpha(z, \; N^S, \; p_s, \; \frac{V^2}{2}, \; BC); \qquad\qquad \alpha = 1,...,J \tag{I.6}$$

$$T = T(z, \; N^S, \; p_s, \; \frac{V^2}{2}, \; BC)$$

where p_s is pressure in the reaction zone and BC denotes boundary conditions (I.4). The solution (I.6) is considered in the flamelet approach as an instantaneous relations between the reactive species mass fractions and temperature on the one hand and mixture fraction, scalar dissipation at the stoichiometric surface, local flow velocity and pressure on the other. Additional simplifications were adopted in *Bezgin et.al (1996)* to decrease number of variables in parametric relations (I.6). These simplifications were:

i) the role of the pressure fluctuations on the combustion chemistry was ignored;

9

ii) correlation between flow velocity and mixture fraction distributions was applied in eq.(I.5) in a simplified form, which is approximately valid for unconfined jets *(Abramovich et.al., 1984):*

$$\frac{V - V^A}{V^F - V^A} \approx z^\beta$$

where V^A, V^F are the mean flow velocities in the air and fuel core flows respectively, β is some exponent which was chosen as $\beta \approx 1/Sc_t$ (Sc_t is the turbulent Schmidt number).

Recently, practically the same kind of reasoning was applied by *Morgenthaler et.al. (1997)* in their FL modeling of supersonic jet flames.

Such simplifications allowed to split flamelet equations from the hydrodynamical ones and to apply flamelet library concept. This reduces flamelet modeling of reacting flows to the two-step procedure schematically shown in Fig.2. At the first step, flamelet eqs.(I.5) are solved for different values of N^s and pressure p_s. The obtained solutions are collected into the flamelet library in a parametric form on z, N^s and pressure p_s. At the second step, the obtained flamelet library is used together with CFD code for the flow hydrodynamics modeling. This two-step procedure is described in Appendix A more detailed.

It is important to note flamelet model behavior in the vicinity of ignition/extinction conditions. Let us illustrate it using typical dependence of the calculated maximum flame temperature T_m vs scalar dissipation N^s which is schematically shown in Fig.3. It is seen that increasing of the scalar dissipation N^s (i.e. growth of reagents mixing rate) lead to increasing of the chemical nonequilibriumness in the reaction zone and hence it decreases maximum flame temperature T_m. It is seen that burning solution exists only if $N^s < N_{cr}^{(1)}$. The flame quench occurs when N^s becomes higher than $N_{cr}^{(1)}$. This means that the flame extincts when the mixing rate (which is controlled by scalar dissipation) becomes too high compare to reactants consumption in chemical reactions due to the limitations of the finite rate chemistry. It is seen also (Fig.3) that there is the second critical value of the scalar dissipation $N_{cr}^{(2)}$ which corresponds to the transition from pure mixing to combustion regimes. As a rule, $N_{cr}^{(1)} >> N_{cr}^{(2)}$. Both $N_{cr}^{(1)}$ and $N_{cr}^{(2)}$ values can be obtained from the flamelet calculations for each particular operational conditions (pressure, air and fuel temperatures) and given detailed chemistry model for fuel oxidation.

The existence of the critical values of scalar dissipation allows to restrict flamelet parametric calculations during flamelet library production by the range $N^s \in [0, N_{cr}^{(1)})$. For the higher values of N^s the pure mixing solution can be used to calculate the mixture composition and thermodynamics properties.

Passive Scalar Statistics Model. The flamelet solutions (I.6) allows to present joint PDF for reactive scalars and temperature in a form:

$$P(z, N^S, C_1, ..., C_J, T) = P(z, N^S)\delta(T - T^{Fl})\prod_{\alpha=1}^{J}\delta(C_\alpha - C_\alpha^{Fl})$$

where $T^{Fl} = T(z, N^s)$ and $C_\alpha^{Fl} = C_\alpha(z, N^s)$ are the solutions of flamelet equations. It is seen that only passive scalar joint PDF $P(z,N)$ is needed to obtain mean values of reactive scalars. It can be obtained from the numerical solution of the evolved PDF equation for passive scalar or using the algebraic models for passive scalar PDF. We used the second approach.

The Favre joint PDF of mixture fraction z and scalar dissipation $\mathscr{P}(z, N^S)$ was considered in a following form:

$$\mathscr{P}(z, N^S) \equiv \frac{\rho}{\bar{\rho}}P(z, N^S) = (1 - \gamma)\delta(z)\delta(N^S) + \gamma P_t(z)\delta(N^S - \tilde{N}_t^S)$$

where γ is the intermittency factor; P_t is the mixture fraction probability density function in a turbulent mixing layer; δ is the Dirac function.

The intermittency factor γ and probability density function in a turbulent mixing layer P_t were approximated based on self-similar solutions of PDF equation presented in *Kuznetsov and Sabelnikov (1990)* and used by us previously *(Bezgin et al. 1996)*. The intermittency factor γ was calculated using approximate relation:

$$\gamma = \begin{cases} 1.31/(1 + \sigma^2/\tilde{z}^2) & \text{if} \quad \sigma/\tilde{z} > 0.555 \\ 1 & \text{if} \quad \sigma/\tilde{z} < 0.555 \end{cases} \tag{I.7}$$

where $\tilde{z} = \overline{\rho z}/\bar{\rho}$ is Favre averaged mixture fraction and $\sigma^2 = \overline{\rho z''z''}/\bar{\rho}$ is mixture fraction variance. The conditional PDF in the turbulent mixing layer $P_t(z)$ was taken in Airy/Gaussian form reported in Appendix A.

The conditionally averaged value of scalar dissipation at the stoichiometric surface was approximated as:

$$\overline{N}_t^S = \frac{\tilde{N}\big|_{\tilde{z}=zs}}{\gamma\big|_{\tilde{z}=zs}} \tag{I.8}$$

where $\tilde{N}\big|_{\tilde{z}=zs}$, $\gamma\big|_{\tilde{z}=zs}$ are the mean values of the scalar dissipation $\tilde{N}$ and intermittency factor γ calculated under the condition that mean value of mixture fraction $\tilde{z} = z_s$.

The conventional approximation for the mean scalar dissipation $\tilde{N}$ was used:

$$\tilde{N} = c_{diss}\frac{K \cdot \sigma^2}{\nu_t} \tag{I.9}$$

where K is turbulence kinetic energy, ν_t is eddy viscosity, c_{diss} is empirical factor.

In such a treatment, only turbulence kinetic energy K, eddy viscosity ν_t, mean mixture fraction $\tilde{z} = \overline{\rho z}/\bar{\rho}$ and its variance $\sigma^2 = \overline{\rho z''z''}/\bar{\rho}$ are needed to calculate the PDF in any given point of the flowfield. These turbulent mixing

characteristics were calculated using conventional semi-empirical transport equations of the turbulence modeling (see, Appendix A) which were solved together with averaged hydrodynamics equations as it is sketched in Fig.2.

Self—ignition criterion. Often supersonic flames are not stabilized at nozzle lip and self-ignition takes place in some cross section downstream the nozzle exit as it is schematically shown in Fig.2. The ignition delay distance can be significant for supersonic flames and should be modeled.

The reactants can be partially-premixed in the vicinity of the self-ignition point. So, chemical processes can occur, particularly, in some volumes or near-premixed flame fronts. Unfortunately, accurate calculations in the vicinity of ignition point can not be performed using FL since this model was constructed for thin diffusion front (some model modification which can provide more accurate modeling in the near-ignition regions is presented in Sec.V of the Report). However, upstream (in the mixing region) and downstream (in the diffusion flame region) self-ignition region, flamelet approach can be used. That is why, we applied somehow simplified approach for prediction of self-ignition point.

The combustion in the vicinity of the self-ignition point was expected to be in diffusion flame mode. Possible existence of the multiple combustion regimes or volume exothermic reactions was ignored. The self-ignition point location was predicted approximately, as a point on the mean stoichiometric surface, where conditionally averaged value of scalar dissipation $\overline{N}_t^s$ became lower than its critical value N_{cr}. This simplified treatment is schematically shown in Fig.2. Additional explanations regarding applied, in the current study, approach for the prediction of the self-ignition point location are presented in Sec.III.

II. SUMMARY OF THE TEST CASES

Complexity of the measurements in compressible flames significantly decreases number of the test cases which can be used for CFD validation of the turbulent combustion model. The analysis of the known unclassified literature and consultations with our supervisor Dr. Povinelli (LeRC) allowed to select 4 test cases where sufficiently detailed information about test conditions, flowfield and reactive scalars characteristics was reported. They cover 3 main types of the flow field (round jet, planar wall jet and planar mixing layer) and two classes of flames (with and without large ignition delay distance). The brief summary of the selected test cases is presented in Table 1. More detailed information and sketches are presented in Sec.IV which reports final results of current CFD.

Table 1. TEST CASES SUMMARY

SOURCE	CASE	FLAME	M_{H2}	M_a	T_{H2} [K]	T_{air} [K]	P_{H2}/P_{air} [MPa/MPa]	Ignition delay	TOOLS
Burrows& Kurkov (1973) NASA TM X-2828	planar wall-jet	H2-air[') mixing	1.	2.44	254	1150	0.1/0.1		P', P_w, GS, TC
		H_2-air[') flame	1.	2.44	254	1270	0.1/0.1	large	
Beach et.al. (1978) NASA TP 1169	round-jet	H_2-air[') flame	2.	1.9	251	1495	0.1/0.1	small or none	P', GS,
Cheng et.al. (1994) Comb&Fl. v.99	round-jet	H_2-air[') flame	1.	2.	545	1250	0.1/0.1	mid	Spont. Raman LIF
Chang et.al. (1993) AIAA- 93-2381	planar mixing layer	air-air mixing	0.39	0.72	303	824	0.1/0.1		LDV TC
		H_2/N_2- air flame["]	0.3	0.71	348	817	0.106/0.106	pilot flame	

[') vitiated air (obtained by burning of H_2 in enriched by O_2 air)

["] pilot H_2 flame in air flow for combustion process stabilization

Tools are diagnostics techniques: P'- pitot pressure probes, P_w- wall static pressure measurements; GS-gas sampling, TC - thermocouple.

III. PREVIOUS TESTS and CURRENT MODEL MODIFICATIONS

The Beach experiment reported in *Evans et.al. (1978)* and *Burrows,Kurkov (1973)* test were considered in previous studies *(Bezgin et.al. ,1996)*. The mostly important, for further explanations, results of the previous tests are summarized in Fig.4. Here FL predictions for water concentration are plotted together with data for both considered previously test cases. It is seen that accuracy of FL predictions was quite different. The FL predictions were quite satisfactory for Beach test case. However, unsatisfactory results were obtained for the Burrows-Kurkov experiment. The significant discrepancy (about 40%) between experimental data and results of computations was found not only in H_2O concentration peak value but in static temperature distributions and ignition delay distance (predicted 0.08 m downstream fuel injector instead of ≈ 0.18m reported by Burrows and Kurkov). Trying to improve accuracy of predictions, we performed a large number of draft parametric tests, where we varied turbulence models (Secundov's one parametric "v_t-90" model presented in Appendix A, standard k-ε model of *Jones&Launder (1973)* and *Chein (1982)* k-ε model were used). We varied also shape of the inflow profiles and level of the turbulence intensity at the entrance of the test section. Unfortunately, all these modifications did not provide any reasonable improvement of the predictions (or even made them worse). Nevertheless, analysis started in *(Bezgin et.al.,1996)* allowed to clarify two possible roots of the discrepancy. They are: (i) too high level of the mixture fraction fluctuations intensity $INT = \sigma / \tilde{z}$ predicted by the turbulence model equation for mixture fraction variance and/or (ii) too high chemical nonequilibriumness predicted by the used detailed kinetics model. The relative role of these two effects on the previous (and unsatisfactory) model predictions for Burrows&Kurkov experiment is illustrated by Fig.5 taken from *Bezgin et.al. (1996)*. Here, the measured by Burrows and Kurkov, H_2O mole fractions (denoted by crosses) are plotted versus mixture fraction z. The dashed line denotes the equilibrium chemistry solution for water mole fraction $\chi_{H2O}^{(eq)}$ plotted vs mixture fraction z also. It was calculated based on the assumption that both chemical nonequilibriumness and scalar field fluctuations are absent in the flow so it is the upper limit for possible water concentration distributions. It is seen that experimentally measured H_2O mole fraction distribution is very close to the equilibrium limit $\chi_{H2O}^{(eq)}$ and so role of both chemical nonequilibriumness and fluctuations intensity were not too high in this conditions. The flamelet model overpredicted role of these effects as it is shown in Fig.5. The instantaneous flamelet model solution obtained in calculations for water mole fraction $\chi_{H2O} = \chi_{H2O}(z,N^s,p_s)$ is plotted vs mixture fraction z by fine solid line. The averaged distribution of water mole fraction:

$$\tilde{\chi}_{H2O} = \int \chi_{H2O} \, \mathcal{P}(z,N^S) \, dz dN^s$$

is plotted by fat solid line. It is seen approximately 50%:50% input of both chemistry nonequilibriumness and averaging procedure into the resulting averaged water

mole fraction distribution $\tilde{\chi}_{H2O}$ predicted by the FL approach. It is seen that averaged concentration peak value is 40% lower than the peak value for $\chi_{H2O}^{(eq)}$ distribution. Such a predictions were very far from the experimental data of Burrows and Kurkov.

Previously we connected this model uncertainties with improper operation of only mixture fraction variance equation in our turbulence model. However, additional tests of the detailed chemistry approximations performed in the current study required us to change this point of view and to introduce modifications not only into the mixture fraction variance equation but into the detailed chemistry model also. Trying to improve flamelet model predictions for self-ignition point location, we changed self-ignition criterion also. Our reasoning and account of introduced modifications are presented below.

Mixture Fraction Variance Equation. To decrease intensity of the mixture fraction fluctuations we somewhat changed values of empirical coefficients in balance equation for mixture fraction variance $\sigma^2 = \overline{\rho z'' z''} / \overline{\rho}$. Its general form remained the same as that used by us previously and widely distributed between modeliers (see, for example, *Jones&Whitelaw 1982*):

$$\frac{\partial \overline{\rho} \sigma^2}{\partial t} + \nabla \overline{\rho} \tilde{V} \sigma^2 = \underbrace{\frac{\partial}{\partial x_\alpha}\left[\overline{\rho}\left(c_\sigma v_t + \frac{v}{Sc}\right)\frac{\partial \sigma^2}{\partial x_\alpha}\right]}_{\text{diffusion}} + \underbrace{\frac{2\overline{\rho} v_t}{Sc_t}(\nabla \tilde{z})^2}_{\text{production}} - \underbrace{2\overline{\rho}\tilde{N}}_{\text{dissipation}} \qquad \text{(III.1)}$$

where c_σ is empirical constant which is usually chosen as $c_\sigma \approx 1/Sc_t$; $\tilde{N}$ is mean value of the scalar dissipation.

The changes were made in the value of empirical factor in approximation for the mean scalar dissipation. We used in our previous predictions the following relation:

$$\tilde{N} = c_{diss}\frac{K \cdot \sigma^2}{v_t} \qquad \text{(III.2)}$$

where K is turbulence kinetic energy, v_t is eddy viscosity, c_{diss} is empirical factor. Previously, we used value of $c_{diss} = 0.07$.

Somewhat different form for approximation of the mean scalar dissipation is commonly used by modeliers:

$$\tilde{N} = c\frac{\varepsilon \cdot \sigma^2}{K}$$

where ε is the turbulence energy dissipation rate and value of empirical factor c is usually chosen as $c \approx 0.95$-1 *(Jones&Whitelaw, 1982; Bilger, 1989; etc.)*. So, one can obtain that $c_{diss} \approx 0.1c$ based on conventional, in turbulence modeling, relation $\varepsilon \approx 0.1\frac{K^2}{v_t}$. That is why, we somehow increased role of the dissipative term (and

decreased intensity of fluctuations) by increasing coefficient c_{diss} in (III.2) from previously used value 0.07 to 0.1.

Detailed Chemistry Approximation. Previous tests of the flamelet model were done using slightly simplified hydrogen oxidation block taken from the detailed kinetics scheme proposed by *Miller and Bowman (1989)*. The resulting detailed kinetics model included 21 reactions between 11 species (H_2, O_2, H_2O, H, O, OH, H_2O_2, HO_2, N_2, N, NO). The used, previously, simplification was that the difference in third-body efficiencies for three-molecular reactions (like $H+H+M=H_2+M$, $OH+H+M=H_2O+M$, etc.) were ignored. It was expected that efficiencies of all molecules, which act as third body M in three-molecular reactions, are the same as that of molecular nitrogen N_2. Previously, we expected that such simplification did not significantly influence results of chemistry calculations. Unfortunately, additional tests showed that such simplification of the detailed chemistry model is too rough.

We performed separate flamelet model calculations for typical values of the scalar dissipation in the reaction zone which corresponded to mid and far field of supersonic jet flames ($N^s = 5$-$50 sec^{-1}$). Three detailed kinetics mechanisms were used in sensitivity tests. They were:

(i) previously used simplified H_2 oxidation block from Miller&Bowman kinetics scheme;

(ii) the same H_2 oxidation block from Miller&Bowman scheme with different third body efficiencies which were taken into account in accordance with the data reported by Miller and Bowman.

(iii) *Jachimowski (1988)* scheme, which was developed in NASA for modeling of H_2/air oxidation chemistry in supersonic flames. This model utilizes different third body efficiencies also.

The kinetic schemes and third-body efficiencies are presented in Appendix C.

Typical results of flamelet calculations for conditions of Burrows-Kurkov experiment are presented in Fig.6. It was found that introduction of the different third body efficiencies should increase equilibriumness of the flame in the regions of "well-developed" combustion. It is seen that Miller&Bowman scheme with selective third-bodies efficiencies predicted somehow higher flame nonequilibriumness compare to the Jachimowski scheme but, in general, Miller-Bowman and Jachimowski detailed kinetics schemes gave close to each other results.

It was found also that such detalization of the kinetics scheme significantly influenced predictions of critical values of the scalar dissipation N_{cr}. The summary of the $N_{cr}^{(1)}$ and $N_{cr}^{(2)}$ values obtained in sensitivity tests is presented in Table 2.

Table 2. DETAILED KINETICS TESTS

(Burrows&Kurkov test case conditions)

Kinetics model	$N_{cr}^{(1)}$, sec^{-1}	$N_{cr}^{(2)}$, sec^{-1}
Miller&Bowman scheme (selective efficiencies are ignored)	641.0	89.6
Miller&Bowman scheme (selective efficiencies are used)	942.9	14.2
Jachimowski scheme (selective efficiencies are used)	1091.4	15.2

The same influence of the third bodies selective efficiencies was obtained for other test cases also.

The obtained result required us to introduce selective third body efficiencies into the detailed chemistry model. Additionally, we choose Jachimowski H_2/air oxidation scheme for final CFD tests since it was specially developed for supersonic flames modeling (it was tested by *Casimir Jachimowski (1988)* using data for high enthalpy flows at the conditions close to the regimes which were investigated in the current study).

Self—Ignition Criterion. The previously found *(Bezgin et.al., 1996)* significant underprediction of the ignition delay distance required us to modify self-ignition criterion.

As it was reported in Sec.I, the self-ignition point location is predicted in flamelet approach approximately, as a point on the stoichiometric surface, where scalar dissipation $\overline{N_t^S}$ became lower than its critical value N_{cr} ($\overline{N_t^S} < N_{cr}$). However, the flamelet solutions provide two values of critical scalar dissipation ($N_{cr}^{(1)}$ and $N_{cr}^{(2)}$) as it was discussed in Sec.I and schematically shown in Fig.3. The value of $N_{cr}^{(1)}$ corresponds to the flame quenching and $N_{cr}^{(2)}$ corresponds to the mixing/burning transition. As a rule $N_{cr}^{(1)} >> N_{cr}^{(2)}$ as it is illustrated by data presented in Table.2. So, using $N_{cr}^{(1)}$ or $N_{cr}^{(2)}$ as an indicator in self-ignition criterion will lead to different results regarding ignition point location.

Previously, we used value of $N_{cr}^{(1)}$ as an indicator for ignition point location. However, additional analysis led us to the assumption that it is much more correctly to use value of $N_{cr}^{(2)}$ for prediction of self-ignition point location in supersonic delayed flames. Our reasoning regarding this choice is presented below.

The using of $N_{cr}^{(1)}$ as an indicator of critical conditions is widely distributed in flamelet modeling *(Liew et.al, 1984; Morgenthaler et.al.,1997; etc.)*. The existence of the second critical value of scalar dissipation is usually ignored. Such a choice is justified for low-speed flames at near-room or slightly elevated conditions. As a rule, at such conditions, combustion wave initialization requires external ignitor (spark device or pilot flame). Flameholders are usually applied for combustion wave stabilization. That is why, flame is initiated and stabilized by external tools and so combustion model should control possible flame quenching due to too high mixing rate only. The using of $N_{cr}^{(1)}$ is justified in such situation. Moreover, if flame ignites in some point of the low-speed mixing layer far downstream fuel injector, it can move upstream up to the fuel injector or to the point where conditions for its extinction will occur (so-called "flashback" effect). As the result, the steady-state combustion zone would exist in the whole region downstream the point where scalar dissipation became lower than $N_{cr}^{(1)}$.

One can expect that this reasoning is violated for self-ignition in supersonic flows since flame movement upstream self-ignition point is quite questionable due to very high value of the flow velocity. So, we expected that it is more justified to use $N_{cr}^{(2)}$ for approximate prediction of self-ignition point location in high-speed flows since it is the parameter $N_{cr}^{(2)}$ responsible for mixing/burning transition of the flamelet solutions.

Final CFD tests (Sec.IV) showed, that using of $N_{cr}^{(2)}$ in self-ignition criterion provided much better predictions. However, first attempts to apply $N_{cr}^{(2)}$ as an indicator in self-ignition criteria were unsatisfactory. The reported in Table 2 values of $N_{cr}^{(2)}$ lead to significant overprediction of the ignition delay distance for the Burrows-Kurkov test case. The same results were obtained for *Cheng et.al. (1994)* test case conditions also. This discrepancy required us to introduce one more modification into our flamelet modeling of supersonic flames which is described below.

Vitiated Air Composition. The important feature of three, among considered test cases, is the air flow pre-heating by the burning of the H_2 in air enriched by O_2. As a rule, this leads to the presence of non-zero radicals concentrations (H,O,OH) in the high-temperature vitiated air flowing into the test section. Previously , we did not take into account this feature. We considered vitiated air flow consisted of stable species only. Our reasoning was based on the results of FL calculations which showed that both burning solutions of FL equations for reactive species and scalar dissipation at quench limit $N_{cr}^{(1)}$ were practically insensitive to such modification of air composition. However, this feature influenced parameter $N_{cr}^{(2)}$ and hence prediction for self-ignition point location as it is illustrated by Table 3.

Table 3. VITIATED AIR COMPOSITION INFLUENCE

(Jachimowski scheme, Burrows&Kurkov test case conditions)

Vitiated air composition	$N_{cr}^{(1)}$, sec^{-1}	$N_{cr}^{(2)}$, sec^{-1}
Stable species only (0.258 O_2 + 0.486N_2 + 0.256H_2O by mass)	1091.4	15.2
Equilibruim composition[*)] (0.258 O2 + 0.486N2 + 0.256H_2O + + 10^{-5}OH + 2.8·10^{-4} NO by mass)	1089.7	33.8

[*)]Species with mass fraction <10^{-5} are not shown

Unfortunately, data about radicals concentrations were presented in only one *(Cheng et.al., 1994)* among the considered tests. So, to model this effect in the other test cases, we considered vitiated air flow as mixture with equilibrium composition. It did not change (with accuracy about 0.05%) concentrations of the main species compared to the values reported by authors for the considered experiments but it led to the presence of small amount of radicals and nitric oxides (with mass fraction about 10^{-4}-10^{-5}) in the vitiated air flow. We expect that it is more realistic approach than modeling of the vitiated air flow as a mixture of stable species only.

In general, input of each among the introduced modifications on the results of predictions was not very high but their collective influence allowed to obtain reasonable improvement of the flamelet predictions in the current tests (Sec.IV) compare to those reported previously in Bezgin et.al.(1996).

IV. CURRENT RESULTS OF CFD TESTS

CFD tests of the flamelet approach were done for four test cases summarized in Sec.II. The same as previously used, flamelet library concept sketched in Fig.2 was applied in current CFD. The modeling of each test case included two sequential steps. At the first step, flamelet equations (I.5) were solved parametrically and obtained solutions were collected into the flamelet library. At the second step, flamelet library was used together with the CFD solver for the flowfield calculations. All current CFD tests were done using full system of averaged 2D Navier-Stokes equations. The Secundov's one-equation model "v_t-90" was used for turbulence modeling. Full description of the mathematical model and coupling procedure is presented in Appendix A.

In flamelet calculations, hydrogen combustion chemistry was approximated by the detailed H_2/air kinetics scheme proposed by *C.Jachimowski (1988)*. The Jachimowski detailed kinetics model (please, see Appendix C) includes 33 reactions between 13 species (H_2, O_2, H_2O, H, O, OH, HO_2, H_2O_2, N_2, N, NO, NO_2, HNO). The species specific enthalpies were used in a form of 7-th order polynomial approximations over temperature taken from Alemasov *et.al. (1971)* and presented in Appendix C also. The flamelet solver FLSLV and all details of the flamelet libraries generation procedure were fully the same as those reported in *Bezgin et.al. (1995,1996)*. As previously, flamelet libraries were verified by the interpolation accuracy and Richardson extrapolation to zero-length grid step (both were better than 1%). The summary CPU requirements for flamelet libraries production and its accuracy tests did not exceed 5-10% of total CPU required for CFD modeling.

The CFD modeling was done using the same modified version of FNAS2D code which was used by our group in previous tests of the flamelet approach. It was described in our previous Report *(Bezgin et.al. 1996)*.

The same, as applied in *Bezgin et.al., (1996)* smoothing of the heat, released in the vicinity of the self-ignition point was used in current calculations to avoid nonphysical flow disturbances of the flowfield in these regions and to provide better convergence of computations.

The main part of CFD tests was done using HP 9000/735 workstation except modeling of the *Chang et.al (1993)* test case which was modeled using conventional PC Pentium 200MHz.

IV.1 BURROWS-KURKOV WALL-JET EXPERIMENT

IV.1.1. TEST CASE

Scheme of the setup and test conditions of *Burrows and Kurkov (1973)* experiment are given in Fig.7. The test section was rectangular duct having the constant width (0.051m). The air supply duct had 0.089m height. Hydrogen was injected parallel to the vitiated air flow. It was injected with a sonic speed through the two-dimensional slot located at the backward step in the initial cross section. Slot height was $h = 0.004m$. Lip thickness at the top of the step was $0.76 \cdot 10^{-3}$ m. Test section total height expanded linearly from 0.0938m in the initial cross section to 0.105m at the exit cross section. Composition measurements were done at the exit plane of the test section located at $x = 0.356m$ downstream the injector location.

As it was discussed in Sec.III., this test case was studied previously and we met serious difficulties in flamelet modeling. So, the goal of the current calculations was both to study how the introduced modifications changed results of predictions and to get final conclusions about model accuracy.

IV.1.2. COMPUTATIONS

All details of the computational procedure were not differ from that used in our previous modeling of Burrows&Kurkov test case presented in *Bezgin et.al. (1996)*.

The flow field was expected 2-D. The role of the boundary layer at the upper duct wall was neglected The simplest molecular transport model was applied i.e. the mixture molecular viscosity and diffusivity were estimated based on H_2 molecular diffusivity and fixed laminar Prandtl and Schmidt numbers $Pr = Sc = 0.72$. The values of the turbulent Schmidt number and constant c_σ in turbulent diffusivity term of mixture fraction variance equation (III.1) were $Sc_t = 1$ and $c_\sigma = 0.67$.

The computational domain together with summary of the boundary conditions is given in Fig.8. The left boundary was located in the hydrogen injection cross-section where all parameters distributions were supposed to be known in all opened parts of cross-section excluding the slot lip. No-slip velocity conditions were posed on the lip wall and on the lower wall of the duct. It was expected also that the lip surface and lower wall were adiabatic with zero temperature gradient. The turbulent kinetic energy and turbulent viscosity were equal to zero at the lower wall and lip. The mean mixture fraction and mixture fraction variance normal derivatives were equal zero at the lower wall and lip. The upper wall was considered as inviscid with zero transversal velocity component. All normal derivatives, which were needed to estimate viscous stresses and corresponding diffusion fluxes on the wall, were equal to zero. The so-called drift boundary conditions with normal derivatives of all parameters determination from computational domain were posed in the exit plane of computational domain.

The parameters distributions at the inlet boundary were obtained by the same manner as it was done previously in *(Bezgin et.al.,1996)*. The longitudinal velocity and eddy viscosity distributions in the incoming air flow were derived in accordance with the procedure described in Appendix B and using estimated from the experimental data boundary layer thickness ($\delta \approx 0.016$m). The same procedure was used for calculations of u, v_t and K distributions in the exit plane of the hydrogen injection slot. The 2% velocity fluctuations were expected in free air stream. The non-dimensional initial distributions of the longitudinal component of

the flow velocity $\overline{U} = \dfrac{\tilde{u}}{u_a}$; eddy viscosity $\overline{V}_t = \dfrac{V_t}{u_a h}$; turbulent kinetic energy $\overline{K} = \dfrac{K}{u_a^2}$

and total enthalpy $\overline{H} = \dfrac{H}{u_a^2}$ are given in Fig.9 where u_a is the flow velocity in the air core flow and h is hydrogen injector slot height. The uniform step initial profile was expected for mixture fraction z. The transverse component of the velocity v and mixture fraction variance σ^2 were expected to be zero at the entry boundary.

The reliability of the adopted initial distributions was studied previously *(see Bezgin et.al. 1996)* for non-reacting counterpart of Burrows-Kurkov experiment. The satisfactory agreement was found.

Calculations were done using the same nonuniform grid with 100 cells in longitudinal direction and 90 cells in transversal direction (Fig.8). Grid was clustered to the lower wall and to backward-facing step in accordance with geometrical progressions. Detailed description of the grid generation procedure was given in our previous Final Report also. Both previous and current tests of the discretization influence on the results of calculations showed that it was confined in small (about 5%) variation of the peak values of turbulence characteristics. The flow hydrodynamics parameters were practically insensitive to the grid variation.

The convergence was estimated by the L_2 norm for the residual of continuity equation. The L_2 norm behavior vs iteration number did not changed compare to the previous results reported in *Bezgin et.al.(1996)*. It decreased by 4 orders during 600 iterations which required about 2 hours CPU of workstation HP 9000/735.

IV.1.3 RESULTS and DISCUSSION

Ignition delay distance. The obtained Mach number field is given in Fig.10. It is seen that the flamelet model predicted self-ignition point location ≈ 0.23m downstream hydrogen injector. This prediction correlates with accuracy about 20% with data reported by Burrows and Kurkov ($x \approx 0.18$m). Additional tests showed high sensitivity of the self-ignition point location to the value of radical concentrations in the vitiated air flow. The OH concentration increasing from equilibrium value 10^{-5} to 10^{-4} allowed to displace self-ignition point practically into the same position where it was observed by Burrows and Kurkov. However, information about radicals concentration in vitiated air flow was absent in specification presented by Burrows and Kurkov. Their possible level would depend on both pre-heater and air nozzle

constructive features. So, we decide to use in our further predictions equilibrium values of radicals concentrations in vitiated air as the lower but justified limit.

Previously, flamelet model prediction was x = 0.08m i.e. the ignition delay distance was twice underpredicted. The modifications of the detailed chemistry model and ignition criterion improved correlation for the location of self-ignition point. It was predicted with the accuracy about 20% (at least).

Reactive scalars and temperature. The comparison of the obtained reactive species mole fraction distributions (solid lines) with the experimental data is given in Fig.11 for test section x = 0.356m where the composition measurements were done by Burrows and Kurkov. The results of our previous predictions reported in *Bezgin et.al. (1996)* are plotted by dashed lines. It is seen that introduced modifications improved model predictions of the reactive scalars. The same improvement was obtained for the static temperature distribution also (Fig.12). The peak values of both H_2O and static temperature were correlated with the accuracy about 10% instead of 35-40% discrepancy obtained previously *(Bezgin et.al., 1996)*.

The additional analysis showed that predictions improvement was obtained by the collective influence of all modifications introduced into the current version of the approach. The relative input of the chemical nonequilibriumness and mixture fraction fluctuations provided by the current version is illustrated in Fig.13. The relative influence of these factors obtained in the previous unsatisfactory tests is presented in Fig.13 for comparison also. It is seen that both decreasing of the fluctuations intensity (approximately by 50% in near stoichiometric zones as it is reported in Fig.14) and increasing of the chemistry equilibriumness provided approximatelly 50% by 50% improvement of the results for reactive scalars.

It is necessary to note that decreasing of the mixture fractions fluctuations intensity was obtained not only due to changes in empirical coefficients of the turbulence model equation for mixture fraction variance but due to improvement in positioning of self-ignition point also. Self-ignition in conditions of Burrows-Kurkov experiment was accompanied by essential transversal expansion of the mixing layer in the vicinity of ignition point due to heat release as it is shown in Fig.15a. Mixing layer became much thicker downstream the ignition point and, as a result, mixture fraction transversal gradients became lower. Some additional turbulence was generated in the vicinity of the ignition point (Fig.15c). These effects lead to the decreasing of the mixture fraction fluctuations intensity (Fig.15b) through the decreasing of the role of production term (which depend on the mean mixture fraction gradient) and increasing of the dissipation term in the equation for mixture fraction variance.

We consider the obtained results as quite encouraging however even the reported version of the model somehow underpredicted (about 10%) the mainly important indicators of heat release, such as H_2O and temperature peak values. So, we tried to obtain better correlation. Unfortunately all these attempts were unsuccessful. We expect now that further improvement of predictions for the used version of the flamelet model was prohibited due to very large ignition delay

distance leading to possible input of the partially-premixed combustion mechanisms (volume reactions or multiple flame configurations) additionally to the main diffusion flame mode. These our assumption is based on the comparison of calculated and measured wall pressure distributions.

Wall pressure distribution. Additionally to the gas-sampling and temperature measurements, Burrows and Kurkov measured pressure distributions along the lower wall of the duct. Unfortunately, as a rule, modeliers do not present results provided by their models for this distribution. We know the only publication of *Kolesnikov (1981)* who presented such predictions provided by his assumed PDF modeling with *Spiegler et.al. (1976)* averaging procedure.

We compared wall pressure distribution provided by current flamelet approach with the data of Burrows and Kurkov. It is presented in Fig.16. Experimental data variation in x<0.1m region was attributed by Burrows and Kurkov to some uncertainties in positioning of the test section elements and existence of the shock wave from the air nozzle so it could not be modeled in our calculations. However, it is seen that monotonic pressure increasing downstream self-ignition point was obtained along the wall in experiments of Burrow and Kurkov. The flamelet model gave rapid pressure rise in the vicinity of the self-ignition point (x≈0.2m) with the pressure decreasing in the far field. It indicates that model overpredicted heat release in the vicinity of the self-ignition point and underpredicted it in the far field. Such difference can be explained by improper model operation in the vicinity of the self-ignition point. Flamelet predicts very rapid transition from mixing to diffusion flame regime and so, it predicts that partially premixed reagents should rapidly react in the nearest vicinity of the self-ignition point. At the same time it is known that their consumption can realize in premixed flames which formed in fuel rich and fuel lean zones additionally to the main diffusion front (so-called multiple flame configurations studied ,in particular, by *Kioni, Rogg, Bray and Linan, 1993*) and/or due to volume exothermic reactions. The diffusion flame mode input into the total heat release rate would become dominant in such a case only sufficiently far downstream self-ignition point.

We tried to estimate region where such element of partially-premixed combustion could be important for conditions of Burrows-Kurkov experiment. For this purpose, we varied in our calculations length of domain where we redistributed heat initially released by flamelet model in the vicinity of self-ignition point. The calculated wall pressure distribution became close to the experimental one only when we re-distributed this heat along the whole combustion region up to the exit cross-section (see dashed line in Fig.16). This indicates that the possible input of the partially premixed combustion mechanisms can be important up to the exit of the test section.

Based on results of current CFD, it was concluded that introduced modifications allowed to improve flamelet approach predictions significantly. Reactive species and temperature distributions were correlated with the accuracy

about 10-15%. We obtained also much better prediction of self-ignition point location. However, additional indirect estimations showed that role of the partially premixed combustion mechanisms could be important for this test case and further modification of the flamelet approach is needed for more accurate operation in such cases. We expect that this feature worsen correlation between reactive scalars and mixture fraction and required us to use slightly different values of empirical constants (Sc_t and $1/c_\sigma$) in diffusivity terms of turbulence model equations for mean and variance mixture fraction equations.

Additional estimations for conditions of Burrows -Kurkov test case were done using modified FL equations and they are presented in Sec.V of the Report. These estimations correlated with the formulated conclusions.

IV.2 BEACH ROUND-JET EXPERIMENT

IV.2.1.TEST CASE

The sketch of the Beach test case reported in *Evans et.al.(1978)* is given in Fig.17 together with the inflow conditions. The hydrogen was injected through supersonic axisymmetric nozzle with the Mach number $M_{H2} = 2$. The hot air was obtained by burning of hydrogen in air enriched by oxygen. High-enthalpy vitiated air flow was expanded through supersonic nozzle with the Mach number $M_a = 1.9$. The hydrogen injector tube had external diameter $d_j = 0.009525m$ with a lip thickness 0.0015m. The air nozzle free stream diameter D was 0.0653m.

This test case was investigated in our previous study where CFD modeling was done using PNS approximation of the hydrodynamics equations. The Beach experiment did not meet any serious difficulties in our previous tests except some underprediction of the H_2O mass fraction for the nearest to the injector test section ($x/d_j = 8.26$). However, modifications introduced into the approach required us to re-calculate it in the current tests also.

IV.2.2. COMPUTATIONS

The assumption about H_2 jet in co-flowing infinite air stream was adopted in CFD modeling. The role of the vitiated air flow mixing with ambient air was neglected. The flowfield was expected axisymmetrical. The mixture molecular viscosity and diffusivity were estimated based on H_2 molecular diffusivity and fixed laminar Prandtl and Schmidt numbers $Pr = Sc = 0.72$. The calculations were done for the value of the turbulent Schmidt number $Sc_t = 0.7$ and the value of constant $c_\sigma = 1/Sc_t$ in eq.(III.1) for mixture fraction variance.

The schematic of computational domain is given in Fig.18. The left boundary was located in the hydrogen injection cross-section where all parameters distributions were supposed to be known in all opened parts of cross-section excluding the injector lip. No-slip velocity conditions were posed on the lip wall. It was expected also that the lip wall was adiabatic and non-catalytic. The turbulent kinetic energy and turbulent viscosity were equal to zero at the lip. The mean mixture fraction and mixture fraction variance normal derivatives were equal zero at the lip also. The upper boundary of computational domain was at $y/d_j = 2$ position. The no-reflection conditions were posed at the upper boundary. The symmetry conditions were posed at the axis of symmetry. The drift boundary conditions with normal derivatives of all parameters determination from computational domain were posed in the exit plane of computational domain.

The calculations were done in two sequential domains sketched in Fig.18 to increase computations accuracy in the vicinity of the injector. The first computational domain was located in $0 \leq x/d_j \leq 1.5$ region and the second one was in $1.5 \leq x/d_j \leq 27.9$ region. The drift boundary conditions were applied at the exit plane of the first computational domain. All parameters on the inflow boundary of the

second computational domain were taken from the calculations in the first domain. The computational grid in the first domain was clustered to the lip in both transversal and streamwise directions. The grid nodes were clustered to the mixing layer in both computational domains.

The parameters distributions at the inlet boundary of the Domain I were obtained by the same manner as it was done in the case of Burrows-Kurkov test case. The longitudinal velocity and eddy viscosity distributions in the incoming air flow were derived from the estimations of the boundary layer thickness ($\delta = 0.002$m) in accordance with the procedure described in Appendix B. The same procedure was used for calculations of u, v_t and K distributions in the exit plane of the hydrogen injection slot. The 2% velocity fluctuations were expected in free stream outside the boundary layers. The uniform step initial profile was expected for mixture fraction z. The transverse component of the velocity v and mixture fraction variance σ^2 were expected to be zero at the entry boundary.

The computations with typical 100x90 grids in each computational domain required about 1 hour of HP9000/735 work station. The L_2 norm behavior for the residual of continuity equation vs iteration number is presented in Fig.19.

The same as in the case of Burrows-Kurkov tests case, series of calculations with separate increasing of nodes number in longitudinal or in transversal directions was done to control accuracy of computations. In the first series, the main computational domain (Domain II in Fig.18) was divided into 4 subregions and calculations were done with patched grids consisted of 100x90 nodes in each sub-region. So, the total number of the grid nodes in longitudinal direction was increased from 100 to 400 to estimate influence of the discretization in longitudinal direction. Additional series of calculations was done using 200x170 (for Domain I and 100x170 (for Domain II) adaptive grids. The grid adaptation was realized in accordance with spring analogy reported by *Baruzzi (1993)*. In each cross-section all grid nodes were supposed to be connected by springs with the stiffness proportional to the gradient of Mach number. The obtained adaptive grids are presented in Fig.20 (for Domain I) and in Fig.21 (for Domain II).

These tests showed small influence of discretization in both longitudinal and transversal directions on the results of calculations. It mostly confined in 2-3% variation of the turbulence energy and mixture fraction variance peak values. All final results reported below were obtained using presented adaptive grids.

IV.2.3. RESULTS and DISCUSSION

Flowfield near injector. Our previous CFD modeling of the Beach test case was done using PNS approximation of the hydrodynamics equations. So the flowfield features in the vicinity of the injector lip were ignored and PNS marching calculations were started from $x/d_j = 0.33$ cross section with some presumed inflow profiles of parameters. In the current study we performed CFD modeling using full system of averaged Navier-Stokes equations. So, we were able to calculate flowfield

27

in the vicinity of the injector and to control reliability of the inflow conditions adopted in our previous tests.

The obtained flowfield patterns (Mach number field and static pressure contours) in the domain near injector are presented in Fig.22. It is seen compression and expansion waves which arise due to turning and interaction of supersonic flows near injector lip. The parameters distributions in $x/d_j = 0.33$ cross section, obtained in current NS computations, were close to "presumed" distributions which were used as inflow conditions for our previous PNS modeling. So detalization of the computational model for near-injector region did not significantly influence results of the model predictions.

Ignition delay distance. The obtained water mass fraction field is given in Fig.23. It is seen that the flamelet model predicted self-ignition point location very close to the injector ($x/d_j \approx 4$) which is reasonably correlates with the our previous predictions. The inflow air temperature was high ($T \approx 1500K$) in conditions of Beach test case. So, value of $N_{cr}^{(2)}$ was high ($N_{cr}^{(2)} \approx 462 sec^{-1}$) and changes introduced into the self-ignition criterion influenced results of computations very weakly for this test case. It is seen also (Fig.23) that maximum water mass fraction sufficiently rapidly trend to the near-equilibrium values downstream self-ignition point.

The obtained Mach number field is given in Fig.24. The flowfield is slightly disturbed in the vicinity of the ignition point and weak compression wave is generated in this region.

In general, reported pictures are in good agreement with our previous results.

Reactive scalars. The comparison of the obtained reactive species mass fractions distributions (solid lines) with the experimental data is given in Fig.25a-d for four test sections where experimental data were available. The results of our previous predictions are presented also by dashed lines. It is seen that results of current predictions well correlates with both experimental data and our previous results. The mostly essential difference is reasonable improvement of the water peak value predictions in the first test section due to decreasing of the chemical nonequilibriumness of the detailed chemistry model compare to that used in the previous tests.

So, it was concluded that introduced modifications allowed to obtain better prediction of the water peak value (better that 10%) for the first test section where previous tests gave higher discrepancy (about 25%). The accuracy for the other test stations remained reasonably good.

IV.3 CHENG et.al. ROUND-JET EXPERIMENT

IV.3.1. TEST CASE

The spontaneous Raman scattering and laser induced pre-dissociative fluorescence (LIPF) methods were employed by *Cheng et.al. (1994)* to measure simultaneously the temperature and concentrations of species in supersonic coaxial burner. The scheme of setup is sketched in Fig.26 together with inflow conditions. The hydrogen was injected with the Mach number $M_{H2} = 1$. The injector internal diameter was $d = 2.36 \cdot 10^{-3}$m. The vitiated air was obtained by burning of hydrogen in air. The high-enthalpy vitiated air was expanded through convergent-divergent nozzle with the Mach number $M_a = 2$ at the exit. There was small shift ($\approx d$) in longitudinal positioning for exit cross-sections of the hydrogen injector and the air nozzle. The hydrogen injector had thick lip. The lip thickness ($h \approx 0.7 \cdot 10^{-3}$m) was compatible with hydrogen jet radius.

The flowfield was characterized by the interaction between coaxial jets with ambient air. So, two mixing layers were formed in the flowfield. The first one (where combustion mostly occurred) was between hydrogen jet and vitiated air. The second one was between vitiated air flow and ambient air. It was reported that the flame was lift-off from the nozzle lip to $x/d \approx 25$ but self-ignition was asymmetric.

The used vitiated air generator was small enough and, probably, it was difficult to obtain perfect premixing of contaminants after pre-burner. So, the inflow species and temperature distributions in the vitiated air flow were nonuniform. The vitiated air composition was characterized by high level of OH radicals (about 10^{-3} by volume fraction). However, independently of these disadvantages, the unique data about mean and fluctuating scalars in supersonic flame were obtained in this experiment.

IV.3.2. COMPUTATIONS

In the current tests, we tried to take into account presence of the ambient air in the computational domain. Vitiated and ambient air had different atomic composition. So, we applied simplified generalization of our approach to model presence of two mixing layers between three flows having different atomic composition. Two mixture fractions z_1 and z_2 were introduced to describe state of mixing in hydrogen/vitiated air and vitiated/ambient air mixing layers respectively. It was expected also that combustion processes occur due to interaction of the hydrogen with vitiated air only. Possible role of the ambient air in chemical reactions was neglected. This assumption was approximately valid in the main part of the flame up to $x/d \approx 45$ cross section as it can be concluded from the consideration of the data reported by *Cheng et.al. (1994)*.

Let us present adopted modification in more details.

First, summary mixture fraction z was introduced in the same manner as it was done previously. It was defined as total mass fraction of hydrogen atoms H in

all species. It was varied from z=1 in the H_2 jet to z=0 in the ambient air, since ambient air did not contain hydrogen-laden species (ambient air humidity was neglected). The total mixture fraction had value $z = z^* = 2\dfrac{\mu_H}{\mu_{H2O}}C^*_{H2O} + \dfrac{\mu_H}{\mu_{OH}}C^*_{OH}$ in the vitiated air flow since vitiated air contained water and hydroxyl radicals with mass fractions C^*_{H2O} and C^*_{OH} respectively.

The first mixture fraction z_1 was used to model state of mixing and combustion in the internal (H_2/vitiated air) mixing layer in the same manner as it was done by *Cheng et.al. (1994)* in their processing of the experimental data. The z_1 was introduced as the normalized excess of the hydrogen atoms mass fraction z over its value in the vitiated air flow:

$$z_1 = \frac{z - z^*}{1 - z^*} H(z - z^*)$$

where H is the Heaviside step function, which was introduced to reject negative values. The first mixture fraction z_1 equals 1 in the pure fuel and it equals 0 in both vitiated and ambient air.

The second mixture fraction z_2 was introduced to model state of mixing between vitiated and ambient air in the external mixing layer. It was defined as:

$$z_2 = \frac{z}{z^*} + (1 - \frac{z}{z^*})H(z - z^*)$$

The second mixture fraction z_2 equals 1 for both hydrogen jet and vitiated air and it equals 0 for ambient air.

It was expected that instantaneous values of z_1 and z_2 satisfy diffusivity equation in form (I.1). So, conventional Favre-averaged form of the turbulence modeling equations was used to calculate their mean $(\tilde{z}_1, \tilde{z}_2)$ and variance (σ^2_1, σ^2_2) values:

$$\nabla(\overline{\rho}\vec{V}\tilde{z}_1) = \nabla\overline{\rho}(\nu_t / Sc_t + \nu / Sc)\nabla\tilde{z}_1;$$

$$\nabla(\overline{\rho}\vec{V}\sigma^2_1) = \nabla\overline{\rho}(\nu_t / Sc_t + \nu / Sc)\nabla\sigma^2_1 + 2\overline{\rho}\frac{\nu_t}{Sc_t}(\nabla\tilde{z}_1)^2 - 2\overline{\rho}\tilde{N}_1;$$

etc.

These four additional equations were solved together with the main system of the hydrodynamics equations and turbulence model. The obtained mean and variance values were used for calculations of mixture fractions PDF's in internal and external mixing layers. The reactive scalars distributions were calculated from the flamelet equations which were solved vs z_1. The mixing solution vs z_2 was used for calculation of reactive species in the external mixing layer. The averaging procedure was applied in CFD for both internal and external mixing layers using mixture fractions PDF's. All other details of computations were not differed from those reported for other considered test cases.

The flow field was expected axisymmetric. The small longitudinal shift in positioning of the hydrogen injector and air nozzle exit cross sections was ignored. It was expected that they were positioned in the same cross section. The calculations were done for the same as those for the Beach test case set of the laminar and turbulent Prandtl and Schmidt numbers ($Pr = Sc = 0.72$; $Pr_t = Sc_t = 0.7$; $c_\sigma = 1/Sc_t$).

Computational domain. The scheme of computational domain is presented in Fig.27. The exit cross-section of the vitiated air nozzle was chosen as left boundary of computational domain. The exit computational boundary was posed in cross-section $x/d = 43.3$. The lower computational boundary was at the axis of symmetry of the burner. The upper computational boundary was located in ambient air. The transverse dimension of computational domain was equal to $y/d = 12$ in the initial cross-section and it increased linearly downstream to take into account the growth of the external mixing layer between vitiated and ambient air.

Boundary conditions. The left boundary included hydrogen jet, lip surface, vitiated air stream and ambient air. The parameters distributions in the vitiated air flow and in hydrogen jet were supposed to be know. The lip surface was expected adiabatic with no-slip velocity conditions and zero values of turbulent viscosity and turbulent kinetic energy.

The flow parameters at the ambient air part of the left boundary were calculated using the left Riemann invariant, defined from the computational domain, and known total parameters for the undisturbed ambient air. The vertical velocity component was supposed to be equal to zero at this part of the left boundary. The same procedure was applied for flow parameters calculation at the upper boundary of computational domain

The drift boundary conditions were used for the supersonic part of the right computational boundary. The condition of given pressure was used for subsonic part of this boundary. It was expected that pressure in this part of the exit boundary was 1% less than that in undisturbed ambient air.

Inflow parameters distributions. The parameters distributions (normalized by mass-averaged velocity of the hydrogen jet U_{H2} and internal injector diameter d) which were used as inflow conditions at the left boundary of computational domain are presented in Fig.28. They were obtained by the following manner.

The internal flow in the convergent - divergent nozzle of the vitiated air pre-burner was calculated using our NS CFD code up to the nozzle exit cross-section. The nozzle geometry was taken from the sketch presented in *Cheng et.al.(1994)*. The total parameters after pre-heater were taken in accordance with specification presented in their paper also. The calculated vitiated air flow parameters in the core flow were very close to that reported by Cheng et.al. (1994) in their specification of the test case, except the vitiated air was just slightly closer to the fully expanded

conditions. The obtained, at the exit of the nozzle, parameters distributions were used as inflow profiles in the vitiated air flow.

The fully developed turbulent pipe flow was assumed in the hydrogen injector. It was expected that turbulent boundary layers thickness was equal to radius of the tube. The longitudinal velocity, turbulent viscosity and turbulent energy distributions were calculated using procedure outlined in Appendix B. The pressure and density were supposed to be constant across hydrogen jet. The vertical velocity component was equal to zero in the injection tube.

Computational grids and convergence. The overlapping grids were used to increase calculations accuracy near the injector lip surface. The first domain ($0 \leq x/d \leq 3$) included 120x140 grid nodes and the second domain ($2 \leq x/d \leq 43.3$) included 100x140 grid nodes. The computational grids are presented in Figs.29,30. The boundary conditions at the right boundary of the first computational domain ($x/d = 3$) were formulated as it was discussed above for the right computational boundary of the whole computational domain.

The CFD computations of this test case required about 3500 iterations and 15 hours of our HP workstation. The behavior of the residual L2 norm vs iterations number is presented in Fig.31. Sufficiently slow convergence was due to the presence of very low-speed ambient air in the external part of the computational domain. After the first 1000 iterations, the main residual was located in these regions and further decreased very slowly.

IV.3.3. RESULTS and DISCUSSION

Flow field patterns. The obtained in computations static pressure contours and Mach number field are presented in Fig.29 for the region near injector. It is seen series of expansion and compression waves generated in the flows of hydrogen jet and vitiated air around injector lip (its height was compatible with the hydrogen injector diameter).

The Mach number field for the far domain is given in Fig.32. It is clear seen development of two mixing layers. The inner layer (between H_2 and vitiated air) is reactive and the outer layer corresponds to the mixing between vitiated air and ambient air. It was found that the inner flow alternates periodically from being supersonic to subsonic before becoming supersonic again. The similar complex flowfield structure was reported previously by CFD modeliers who studied this test case using different turbulent combustion models *(Eklund,Drummond,Hassan,1990; Hsu,Raju,Norris, 1994).* Qualitative remarks regarding existence of the wave structure were presented by authors of the experiment also.

Ignition delay distance. The flamelet predicted self-ignition point location in $x/d \approx 12$ cross-section. The authors of the experiment reported value $x/d \approx 25$ as the estimation for ignition delay distance based on the long exposure visual photograph of the flame. From our point of view, such difference in predictions and

observations is explained by asymmetric ignition which was observed in the experiment. We expect also that the inhomogenity of composition and temperature of the vitiated air flow was the mostly probable cause responsible for this asymmetry. The inflow vitiated air inhomogenity is well-seen in Figs.33f,34 for the nearest test station x/d = 0.85. For example, the measured in the inflow OH mole fraction (Fig.33f) decreased, approximately, 3-4 times from positive (over y-axis) to the negative side of the vitiated air jet. We were not able to take into account all details of such inflow composition nonuniformity in our current axisymmetrical CFD. So, OH concentration ($\approx 10^{-3}$ by mole fraction) was chosen in the inflow conditions as its typical value observed in the experiment at the positive side of the vitiated air jet. Thus, our predictions better reproduced behavior of the positive side of the jet. The temperature and H_2O flame peaks in experimental data are well-seen on the positive side of the jet even in x/d = 21.5 cross section while they are absent on the negative side of the jet in this cross section (please see Figs.33d and 34).

We performed computations where we decreased, approximately by an order, inflow OH concentration to its typical value for the negative side of the vitiated air jet. This resulted in ignition point displacement more close to its position reported by *Cheng et.al. (1994)*. Such sensitivity of ignition delay distance prediction to the inflow radicals concentrations was mentioned for this test case by another modeliers also.

Mean reactive scalars and temperature. The results of predictions for mean values of mixture fraction and species concentrations are given in Figs.33a-f. Our predictions for the positive side of the jet are re-plotted for its negative side also for more clearness.

The radial distributions of the mixture fraction are presented in Fig.33a. It is seen that calculations correlate fairly well with experimental data for the first three test sections (x/d = 0.85, 10.8 and 21.5). However, it is seen that turbulence model somewhat underpredicted mixing rate near the axis of symmetry for the far field of the jet. The same tendency was found in H_2 profiles as it is seen from Fig.33b. We expect that such difference can be explained by the aforementioned asymmetry of the self-ignition in the experiment which could provide increasing of the 3-D effects in the internal mixing layer downstream self-ignition region.

Predictions of the N_2 mole fractions were well-correlated with the experimental data (Fig.33c) for all test sections.

The obtained H_2O distributions are presented in Fig.33d. We expected the obtained correlation as fairly good since reported CFD was done for the inflow conditions which approximately reproduced positive side of the jet. It is seen that, according to the experimental data, the positive side of the jet is within combustion regime, at least, from x/d<21. Only mixing was observed in experiment at the negative side of the jet in both 21.5 and 32.3 cross sections. As it was discussed previously, it was possible to reproduce such behavior of the negative side of the jet by decreasing of the OH inflow concentration. In any case, flamelet model predictions reasonably correlated with the experimental data except only slightly

underpredicted peak value for x/d = 32.3 cross section. However, measured for this test section H_2O peak value is somewhat questionable taking into account reported by Cheng et.al. data on instantaneous realizations. It is seen (Fig.38b) that H_2O instantaneous data collapsed to the peak value which is about 0.6-0.65. These values are approximately 15% higher than that for chemically equilibrium limit. Such effect did not observed in another test stations and probably can be attributed to some instrumentation effects..

The reasonable correlation between experimental data and predictions was obtained for O_2 mole fraction in the inner mixing layer as it is reported in Fig.33e. The discrepancy between data and predictions in the outer mixing layer is explained by significant non-uniformity of the inflow O_2 distribution provided by the vitiated air generator (please see data for x/d = 0.85 cross section in Fig.33e). This nonuniformity was ignored in current CFD.

The calculated distributions of the OH mole fraction are presented in (Fig.33f). It is seen that both peak values and width of the profile were reproduced with the accuracy about 20-30% for the right hand side of the flame in the region (x/d>20). We expected this correlation as reasonable taking into account that reported accuracy of OH measurements was about 13%. The correlation was not so good upstream the ignition point (x/d≤10.8). It can be explained by both aforementioned inflow nonuniformity and existence of slow chemical processes in the induction region which were neglected in our simplified criterion for self-ignition.

The performed tests show reasonable correlation between measured and predicted by the flamelet model static temperature distributions in the combustion zones and internal mixing layer as it is reported in Fig.34. Here, averaged solution of flamelet equations for static temperature is plotted together with experimental data. The obtained correlation indicates that adopted in the flamelet calculations simplified treatment for conditionally averaged flow velocity V = V(z) (please see Sec.I) operated reasonably well and it did not introduce significant inaccuracy in the static temperature distributions even in the case where Mach number was varied in wide range from 0 (ambient air) to 2 (vitiated air flow). Nevertheless, it should be mentioned some underprediction of the static temperature distributions for the external mixing layer in the final test sections (x/d = 32.3 and 43.1). We hope that it is not the property of our model since the same discrepancy was found in the Evolved and Assumed PDF modeling reported by *Hsu,Raju,Norris, (1994); Baurle, Hsu, Hassan, (1994)* and other modeliers. Followed *Hsu,Raju,Norris, (1994)*, it can be expected that such discrepancy could be attributed to some instrumentation inaccuracy for measurements in low temperature regions reported by *Cheng et.al.(1994)*.

Reactive scalars RMS. The obtained distributions of the mixture fraction rms are presented in Fig.35 together with the experimental data. It is seen that obtained distributions well correlated with experimental data except only x/d = 10.8 cross section where computations somehow overpredicted mixture fraction rms.

The flamelet predictions for reactive scalars rms are reported for $x/d = 10.8$ and 43.1 cross sections in Figs.36 and 37.

It is seen from consideration of Fig.36 that rms distributions for reactive scalars correlate in main features with experimental data in $x/d = 10.8$. Some difference between predictions and data can be explained taking into account both adopted in modeling simplifications and specific features of the test case. For example, it is seen difference in predictions of rms fluctuations in regions near $y/d = 2.5$ and $y/d = -2.5$. These regions corresponds to the vitiated air flow. The nature of the experimentally observed fluctuations is the inhomogenity of the vitiated air composition provided by pre-heater. We did not take into account this feature of the inflow conditions in our modeling. Followed *Hsu,Raju,Norris, (1994)*, we expect that experimentally observed values 0.01 for O_2 and 0.04 for N_2 in the outer regions of the external mixing layer could be attributed to the background fluctuations since the data for the other test stations indicate the same level for these fluctuations. We expect that underprediction of the OH radical rms value was due to very simplified treatment of the ignition phenomenon in the flamelet approach. If one take into account aforementioned features, the flamelet model predictions for reactive scalars rms reasonably correlates in this cross section with results of PDF modeling reported by *Hsu,Raju,Norris, (1994)* except some underprediction of the peak rms temperature near the axis of symmetry.

It is much more difficult to present conclusions regarding quality of the rms predictions for $x/d = 43.1$ cross section. The peak values are predicted reasonably well, but displacement of their locations could be attributed to the flow asymmetry in the experiment.

In general, flamelet modeling provided predictions of the reactive scalars rms compatible with that reported for other approaches.

Instantaneous patterns for reactive scalars. The authors of the experiment reported data regarding instantaneous realizations for the reactive scalars measured by their Raman system. The original data of Cheng et.al. are presented in Figs.38a,b by green points. So, we tried to use their data for simplified estimations of realisticity of the instantaneous reactive scalars distributions provided by the flamelet approach.

It was expected that scattering of instantaneous values of reactive scalars (at fixed value of mixture fraction) was due to the scalar dissipation fluctuations *(Bilger,1989)*. The increasing of the scalar dissipation leads to the growth of the chemical nonequilibriumness in the reacting zones due to increasing of the reagents fluxes. Otherwise, its decreasing equilibrates the state of combustion chemistry. So, fluctuations of the scalar dissipation would lead to arising of different instantaneous patterns of the reactive scalars in the reaction zones and hence, the scatter plots can be used for indirect estimation of the realisticity of instantaneous solutions provided by the combustion model.

Unfortunately, statistical properties of the scalar dissipation are not so well-investigated now as those for mixture fraction. However, both experimental data

(Namazian et.al., 1988) and theoretical estimations *(Monin, Yaglom, 1965)* show that its PDF can be approximately modeled using so-called log-norm low:

$$\Omega(N) = \frac{1}{(2\pi)^{1/2} N\sigma} \exp[-\frac{1}{2\sigma^2}(\ln(N/\overline{N}) + \sigma^2/2)^2] \qquad (IV.1)$$

where $\sigma^2 \approx 0.5\ln(L_t/\eta)$, L_t is integral length scale and η is Kolmogorov scale. Using this PDF model, it is possible to estimate upper and lower values of scalar dissipation which corresponds to the given probability of expectations. We choose the range 99% probability and calculated N_{max} and N_{min} values using log-norm PDF distribution for scalar dissipation. The mean value of $\overline{N}$ in relation (IV.1) was chosen to be equal to the value of conditionally averaged scalar dissipation at the stoichiometric surface $\overline{N}_t^S$ provided by our CFD. The data on integral and Kolmogorov turbulence scales (L_t and η) were taken from experimental estimations reported by *Cheng et.al. (1994)*. Further, the upper and lower possible flamelet distributions, predicted by the model in the range of N^S variation $N_{min} < N^S < N_{max}$, were taken from the flamelet library. The comparison of such upper and lower limits for possible instantaneous solutions with the scatter data and conditionally averaged flamelet solution is presented in Fig.38a,b for point $y/d = 1.1$ in $x/d = 32.3$ cross section ($\overline{N}_t^S = 17\,\mathrm{sec}^{-1}$). It is seen that upper and lower boundaries for temperature and main species are within scatter distributions and they are located close to the upper and lower boundaries of scatter plots. The conditionally averaged solutions are located close to the regions where scatter points clustered except H_2O distribution. However, as it was discussed earlier, the observation of scatter points with the H_2O mole fraction about 0.6-0.65 is questionable. These values are approximately 15% higher than equilibrium chemistry peak value for H_2O. Additionally, this feature was not observed both upstream and downstream considered test section. So, probably, it would be attributed to some instrumentation uncertainty.

The flamelet somewhat underpredicted possible peak distribution of the OH radical as it is shown in Fig.38b[)]. This means that model slightly underpredicted maximum nonequilibriumness in this point of the flame. Followed *Cheng et.al.(1994)*, we can expect that this underpredictions could be due to neglecting of the velocity fluctuations in the flamelet calculations. The velocity fluctuations can cause additional temperature fluctuations and, probably, influence combustion chemistry in supersonic flames.

The same kind of estimations was made for another test sections where scatter plots were available. They gave basically the same results. So we expect that these indirect estimations indicate that flamelet model correctly reproduced main features of the combustion processes for the supersonic flames at moderate Mach numbers. We expect that simplified treatment of the kinetic energy term adopted in the current flamelet calculations did not lead to any significant errors in

---

[)] The maximum OH distribution corresponded to $N^S \approx 17\,\mathrm{sec}^{-1}$ so conditionally averaged and maximum OH distributions were very close one to the other.

predictions. However, the modeling of supersonic flames at higher Mach numbers can require more accurate treatment for this term.

Based on obtained results, it was concluded that flamelet approach gave satisfactory results for this test case. Specific features of this experiment (asymmetric ignition, imperfect premixing in vitiated air flow and presence of the ambient air) required us to introduce additional assumptions for its flamelet modeling. Nevertheless, both temperature and reactive scalar distributions in the reaction zones were predicted reasonably good. The correlation for reactive scalars rms was somewhat worse but accuracy of the flamelet predictions was compatible with that reported for Assumed and Evolved PDF modeling. Additional indirect estimations demonstrated that instantaneous flamelet solutions were within scatter distributions provided by the Raman measurements. Some underprediction of the upper limit for OH radical instantaneous distributions can indicate possible necessity to use more accurate treatment of the kinetic energy term in flamelet equations. However, we expect that such modifications can became important for modeling of the supersonic flames at much higher Mach numbers than that considered here.

It should be noted also, that we are not fully satisfied by the pure computational results of the performed simulation. Unfortunately, CFD of this test case were very expansive and we were practically at the limit of our HP workstation capabilities. We attributed this feature to the presence of the low-speed air and somewhat simplified formulations of the boundary conditions at the ambient air part of the computational domain. It is possible to hope, that the influence of these assumed conditions appears essential in the external part of the shear layer between vitiated air and ambient air and it did not influenced region of hydrogen - vitiated air interaction. Nevertheless, we expect to reconsider the aforementioned numerical aspects of this test configuration in further investigations to obtain less-expensive and correct modeling.

IV.4 CHANG et.al. PLANAR MIXING LAYER

IV.4.1. TEST CASE

Scheme of setup and test conditions of *Chang et al. (1993)* experiment are given in Fig.39. The test section was rectangular duct having the constant width (0.2m). Air and fuel streams converged at the splitter plate tip with a 6 degree convergence angle. Both air and fuel ducts were 0.05m height at the splitter tip. Non-reacting and reacting flow regimes were studied. Lower and upper duct walls were parallel in the non-reacting case. They were 1.3 degree diverged in the reacting case. Velocity profiles and turbulence characteristics were measured in several cross sections using LDV. Temperature measurements were done in cross sections 0.006, 0.15 and 0.3 m for the reacting case. The hydrogen-fueled torch was used for the flame stabilization in the reacting case. It was located in the air supplying duct upstream the splitter plate. Ignition in this case was observed in a region close to the splitter plate tip, as it can be seen from OH emission images, presented by *Chang et al. (1995)*.

VI.4.2. COMPUTATIONS

The flow field was expected 2-D. The role of the boundary layers at the upper and lower duct walls was neglected. The molecular viscosity and diffusivity were estimated based on air molecular diffusivity and fixed laminar Prandtl and Schmidt numbers $Pr = Sc = 0.72$. The computations were done for values of $Sc_t = 1/c_\sigma = 0.5$.

Probability of $z = 1$ value was non-negligible along the whole flowfield for the considered mixing layer case. So, small modification of the PDF model was applied to take into account flow intermittency effects at fuel-rich edge of the mixing layer ($z = 1$). Followed *Kuznetsov and Sabelnikov (1990)*, the mixture fraction PDF was expected to be symmetrical with respect to $\tilde{z} = 0.5$. Probability to observe both $z = 0$ and $z = 1$ values in the same point of the mixing layer was neglected. Based on such assumptions, mixture fraction PDF was modified to the form suggested in *Kuznetsov and Sabelnikov,(1990)*. In regions where $\tilde{z} < 0.5$, conventional relations of Sec.I were applied for calculations of mixture fraction PDF and intermittency factor:

$$\mathcal{P}(z) = (1 - \gamma)\delta(z) + \gamma P_t(z); \quad \gamma = \min\left\{1.31\tilde{z}^2 / (\tilde{z}^2 + \sigma^2); \ 1\right\}.$$

In regions where $\tilde{z} \geq 0.5$, the mixture fraction PDF and intermittency factor were calculated as:

$$\mathcal{P}(z) = (1 - \gamma_1)\delta(1 - z) + \gamma_1 P_t(1 - z); \quad \gamma_1 = \min\left\{1.31(1 - \tilde{z})^2 / ((1 - \tilde{z})^2 + \sigma^2); \ 1\right\}.$$

The flamelet model calculations showed that $N_{cr}^{(2)}$ was very small ($N_{cr}^{(2)} < 10^{-3}$ sec^{-1}) for conditions of this test case. It indicated that self-ignition was impossible inside the test section and it was necessary to apply external device for initialization of combustion wave. This qualitative prediction correlates with the

necessity to use hydrogen-fueled torch in the experiment for flame stabilization inside test section. So, it was expected that flame was stabilized due to the presence of the torch. That is why, flamelet library solutions up to the extinction critical value of scalar dissipation $N_{cr}^{(1)}$ were used. All other features connected with the presence of torch (some temperature rise in the part of air stream; presence of small amount of combustion products) were not taken into account.

The scheme of computational domain is given in Fig.40. The left boundary $(x = 0)$ was located near the splitter tip cross-section. Right boundary was set at $x = 0.4m$, which is 0.07m downstream the last presented test section. Conditions at the inlet and exit boundaries were posed in the same way as it is often done for subsonic flows. Velocity and static temperature profiles, profiles of turbulent characteristics and mixture fraction were supposed to be known at the inlet boundary while the pressure was extrapolated to the inlet boundary from the computational domain. Fixed pressure condition (0.1MPa) was applied at the exit boundary. Normal derivatives of all other parameters at the exit plane were determined from computational domain. The upper and lower walls were considered as inviscid with zero normal velocity component. All normal derivatives, which were needed to estimate viscous stresses and corresponding diffusion fluxes on the wall, were equal to zero.

The parameters distributions at the inlet boundary were taken from LDV data at the first test section reported by *Chang et.al. (1993)*. Streamwise velocity in core flows was set equal to that measured in the experiment, i.e. 394 m/s at the air side and 134 m/s at the fuel side for non-reacting case; 390 m/s and 137 m/s respectively for reacting case. Static temperature in core flows was estimated using measured values of total temperature and Mach number. Approximate analytical fit to the experimental data was used to model the inlet profile of the cross-stream velocity component. The thickness of the boundary layers on the lower and upper surfaces of the splitter plate was adjusted to the measured streamwise velocity profile. The eddy viscosity and streamwise velocity profiles inside the mixing layer were obtained using the procedure described in Appendix B and they were slightly smoothed near splitter lip. The value of turbulent kinetic energy in the core flows was estimated using experimental data on velocity components rms as $K \approx u'^2/2 + v'^2$. In the non-reacting case, inlet turbulent kinetic energy profile in the mixing layer was obtained using procedure of Appendix B. In the reacting case, turbulent kinetic energy was approximated using experimental data on velocity components rms as $K \approx u'^2/2 + v'^2$. The uniform step initial profile was expected for mixture fraction z. The mixture fraction variance σ^2 was expected to be zero at the entry boundary.

To estimate the value of turbulent viscosity in the core flows, an approximate relation, which is often used in turbulence modeling, was used: $v_t \approx 0.1u'L_t$ where L_t is the turbulence integral length scale. Unfortunately, no data were available on turbulence scale in this flow, so the value of L_t was approximately estimated as 0.1 of the supplying duct height, i.e. $L_t \approx 5$ mm. As it was found in computations (see

below), the flowfield was sensitive to the inlet value of L_t, especially in the reacting case.

The non-dimensional initial distributions of the streamwise and cross-stream components of the flow velocity $\overline{U} = \dfrac{\tilde{u}}{u_a}$ and $\overline{V} = \dfrac{\tilde{v}}{u_a}$; eddy viscosity $\overline{v}_t = \dfrac{v_t}{u_a h}$ and turbulent kinetic energy $\overline{K} = \dfrac{K}{u_a^2}$ are given in Fig.41 where u_a is the air flow velocity in the core flow and h is the test section height at the splitter tip cross-section (h = 0.1m).

Calculations were done using the nonuniform grid with 100 cells in longitudinal direction and 80 cells in transversal direction (see Fig.42). Grid was clustered to the duct centerline and to the inlet plane.

The convergence was estimated by the L_2 norm for the residual of continuity equation. The L_2 norm decreased 4 order during 800 iterations which required about 5 hours of Pentium-200 PC.

VI.4.3. RESULTS and DISCUSSION

Non—reacting case. The obtained profiles of mean streamwise velocity are presented in Fig.43 for eight cross-sections where experimental data were available. It can be seen that streamwise velocity profiles were in good agreement with the experimental data. The mean cross-stream velocity distributions were not predicted so accurately (see Fig.44). The calculated cross-stream velocity distribution rapidly decayed downstream the splitter, while experimental data showed existence of its sufficiently high negative values far downstream the splitter plate.

Profiles of calculated turbulence kinetic energy are compared to that, obtained from experimental data in Fig.45. The relation $K \approx u'^2/2 + v'^2$ was used here to estimate turbulence kinetic energy from experimental data on rms velocity components. The agreement is reasonably good for the first four test stations (x<150mm). Some disagreement in turbulent kinetic energy distributions was found far downstream splitter plate (x = 300 and 330mm test sections). However, as a whole, predictions of the turbulence kinetic energy distributions were acceptable taking into account simplified relations for its estimation from experimental data.

The significant disagreement between calculated and measured Reynolds stress profiles was obtained. The Reynolds stress provided by our CFD was obtained using relation $\langle u'v' \rangle = -v_t \left(\dfrac{\partial \overline{u}}{\partial y} + \dfrac{\partial \overline{v}}{\partial x} \right)$. The computations overpredicted experimental data several times (usually 5-7) as it is reported by Fig.46 where the calculated and measured Reynolds stress normalized by the slip speed square vs. self-similar coordinate $\eta = y/x$ are shown for x = 300mm test station. The same result was found for other test sections also. This result was unexpected since we sufficiently accurately predicted distributions of the mean streamwise velocity component. So

we compared results of our CFD with data regarding $\langle u'v'\rangle$ behavior in planar mixing layers obtained in different experiments and summarized in *Abramovich et.al.(1984)*. It is seen (Fig.46) that our results correlate with these data reasonably well.

The obtained discrepancy can not be explained by the influence of the discretization as it is reported by Figs.47a,b where results obtained for three different grids are shown (100x80, 150x120 and 200x160). Followed *Lai and Raju (1993)*, who performed CFD modeling of this experiment, we can conclude that even results presented for "rough" 100x80 grid mesh provided good resolution for the parameters distributions in the mixing layer.

We expect that the obtained result indicates that even non-reacting counterpart of the *Chang et.al.(1993)* experiment contained some abnormal features of the turbulence spectra which could not be reproduced using conventional turbulence modeling relations.

Reacting case. The difference between predictions and experimental data was found for the reacting counterpart of the Chang et.al. experiment also. The calculated streamwise velocity distributions are compared with the experimental data in Fig.48. It is seen that our results correlate with the experimental data in region x<150mm. Significant difference between results of computations and data was found for the far field (x = 300 and 330mm cross-sections). The experiment indicates a much significant penetration of the mixing layer into the upper fuel-laden stream. It is seen the underprediction of the mixing layer growth obtained in computations. Again, as in the non-reacting case, it was impossible to reproduce correctly cross-steam velocity distributions as it is reported in Fig.49. The maximum in the turbulent kinetic energy distributions was predicted more correctly but significant underprediction of the mixing layer width and its positioning was found in the far field also (Fig.50).

As for the non-reaction case, it was found that grid influence could not explain obtained discrepancy as it is reported by Fig.51a,b. It is seen that the use of finer grid influenced the results of computations very slightly.

One could expect that operation of the torch ignitor in the air supplied duct could lead to the development of the large scale fluctuations in the reacting case. So, we tried to estimate possible influence of such large-scale fluctuations on the results of predictions. For this purpose, the turbulent viscosity in the incoming air flow was increased ten times which corresponded to the increasing of the integral length scale approximately up to the value compatible with the air supply duct height ($L_t \approx 50$mm). Such modification provided much better correlation of both width and location of the mixing layer in the far field as it is reported in Fig.52. The cross-stream velocity distributions became slightly closer to the experimental data also (Fig.53). However, both abnormally high value of the integral length scale which was necessary to obtain such improvement and absence of data about its behavior in the experiment, does not allow to consider obtained result as any kind

41

of final predictions. It should be considered as rough estimation which indirectly indicates possible role of some unconventional scales distributions in the turbulence spectra or presence of some large-scale fluctuations in the experiment.

The predicted by the model mean temperature distributions are presented in Fig.54 for $x = 300$mm cross section. It is seen that the maximum in the temperature distribution is reproduced by the model but pure accuracy in flowfield predictions lead to pure accuracy in predictions of both width of the temperature distribution and positioning of the mixing layer. The estimation provided by the "large-L_t" computations is presented also. It is seen that such modification somewhat improve predictions but, as it was discussed previously, it can not be considered as the final result since the presence of the turbulent fluctuations having the integral length scale compatible with the duct height is quite questionable.

As a whole, results of the current calculations correlates with those reported by *Lai and Raju (1993)*, who studied capabilities of their RPLUS and composite PDF models for this test case. As the aforementioned modeliers, we obtained the same discrepancy in predictions. We agree with them that presence of the hydrogen torch provided some element of uncertainty in inflow conditions for the considered test case. Such feature could be responsible, in particular, for discrepancy between results of predictions and experimental data. However, it should be mentioned that we found difference for Reynolds stress distributions even in non-reacting case. This finding makes this test case different from typical ones. We hope that obtained discrepancy can not be attributed directly to the flamelet model since:

(i) discrepancy was observed even for nonreacting counterpart of the experiment;

(ii) the same discrepancy was obtained by *Lai and Raju (1993)*, who studied this test case using other turbulent combustion models.

We expect that performed estimations showed some abnormal behavior of the turbulence spectra or presence of some large-scale fluctuations in the experimental setup. The observations of the authors of the experiment indicated presence of the "large-scale shear layer flapping motion" in the test section. Probably, better correlation could require to model more accurately features of inflow and outflow ducts of this experimental setup. Unfortunately, in spite of the good contact with one of the experiment authors (Dr.C.Chang, LeRC), causes of such behavior of the mixing layer are not quite clear for us yet. This require us to retain further consideration of this test case for the next investigations.

V. MODELING TESTS OF MODIFIED FLAMELET APPROACH FOR FLAMES WITH LARGE IGNITION DELAY DISTANCE

V.1. MODIFIED FLAMELET EQUATIONS (MFL)

In the previous tests, including those presented in Sec.IV of the current Report, we used the following form of the flamelet equations:

$$N^s \frac{d^2 C_\alpha}{dz^2} + R_\alpha = 0 \qquad\qquad \alpha = 1,...,J \qquad\qquad (V.1)$$

where C_α is mass fraction of α-specie; z is mixture fraction; N^s is scalar dissipation at the flame front; R_α is chemical production term. All quantities in (V.1) are considered as conditionally averaged over mixture fraction z. Such form of flamelet equations is obtained from the instantaneous conservation equations for reactive scalars by neglecting the convective terms and using the mixture fraction as an independent variable instead of space coordinate. The account, presented by *Peters (1984), Bilger (1982)* and *Kuznetsov (1982),* showed that, formally, such equations are valid in the regions where thickness of the reaction zones is small enough. As a rule, such situation is observed in flames far downstream ignition point. These equations are approximately valid in the mixing region located upstream ignition point due to similarity of the scalars transport equations when the difference in molecular diffusivities is ignored. However, the rejected terms can play important role in the ignition region where transition from mixing to diffusion flame combustion regime is occurred and reaction zone can be sufficiently thick.

The improper behavior of the flamelet model in the vicinity of self-ignition point significantly restricts its capabilities for lift-off diffusion flames. It is a serious disadvantage for the modeling of the high-enthalpy compressible flames since, in many cases of such flames, test geometry does not contain flameholders for reliable flame stabilization near injector and flame self-ignite far downstream injection point.

Trying to improve flamelet behavior in self-ignition region, we introduce into our flamelet equations convective term. For the first approximation, the longitudinal convection was expected to be dominant, since analysis presented by *Li, Bilger (1993)* and *Klimenko (1995)* showed that variation of conditionally averaged values across mixing layer is not too significant as a rule. As the result, modified flamelet equations had the form close to the simplified form of the Conditional Moment Closure (CMC) equations proposed by *Bilger (1993)* and *Klimenko(1990):*

$$V_z \frac{\partial C_\alpha}{\partial x} = N \frac{\partial^2 C_\alpha}{\partial z^2} + R_\alpha \qquad\qquad (V.2)$$

where V_z is flow velocity conditionally averaged over z; x is space coordinate.

It is necessary to note that, even in the steady-state case, full CMC equations are much more complex and 4-D (3 space coordinates + mixture fraction z are used as independent variables). Their accurate realization in CFD is too computationally expensive procedure. So, the goal of our current modeling tests was not to test

capabilities of CMC modeling. Our studies were confined by searching of minor modifications of the flamelet model which can provide its more reliable operation in near-ignition regions without much complication of the approach as a whole. That is why, the form of eqs.(V.2) was chosen as possible candidate.

The simplest closure hypothesis were applied in the current tests. It was expected that the conditionally averaged flow velocity V_z equals to the mean value of the streamwise velocity component at the stoichiometric surface:

$$V_z = \tilde{u}\big|_{\tilde{z}=z_s}$$

The scalar dissipation N and mixture fraction z were expected statistically independent in fully turbulent regions. Conditionally averaged value of scalar dissipation at the stoichiometric surface was used for approximation of N in eqs.(V.2) in the same manner as it was done in FL approach (please, see eq.I.8):

$$\overline{N}_t^s = \frac{\tilde{N}\big|_{\tilde{z}=z_s}}{\gamma\big|_{\tilde{z}=z_s}}$$

where $\tilde{N}\big|_{\tilde{z}=z_s}$, $\gamma\big|_{\tilde{z}=z_s}$ are the mean values of the scalar dissipation $\tilde{N}$ and intermittency factor γ calculated under the condition that mean value of mixture fraction $\tilde{z} = z_s$.

In such treatment only mean flow velocity distributions and turbulence mixing characteristics were necessary for the modeling tests of the modified flamelet equations (MFL). For modeling tests of MFL approach, we extracted these distributions from results of our flamelet CFD reported in Sec.IV. So, inverse influence of the combustion model on the mean and fluctuating flow fields was neglected in current modeling tests.

V.2. SOLUTION PROCEDURE

To solve MFL eqs. (V.2), we slightly modified our flamelet solver FLSLV described in *Bezgin et.al. (1996)*. The approximation of the derivatives remained the same, i.e. second order central difference for the diffusive term and first order upwind difference for convective term. The treatment of chemical source term was not changed also, i.e Jacobian $\left(\dfrac{\partial R_\alpha}{\partial C_\beta}\right)$ was used to provide implicit treatment of the source term. The resulting algebraic system was solved using matrix sweeping at every level in marching direction x. The accuracy of the solution was provided by the small limiting value of concentrations increment at each marching step. Usually the increment of all concentrations was set to be less than 1%. This condition was used for the choice of the step in marching direction. The accuracy of the solution was checked by the variation of the mentioned limit of the increment.

V.3. COMPARISON OF THE FL AND MFL SOLUTIONS BEHAVIOR.

Conditions of the previously considered *Cheng et.al.(1994)* and *Burrows–Kurkov (1973)* test cases were used for comparative modeling tests. The $\tilde{u}\big|_{z,zs}$ and $\overline{N}_!^s$ distributions were taken from the results of our FL CFD reported in Sec.IV of the Report.

The comparison of the FL and MFL instantaneous solutions is presented in Figs.55a-d where reactive scalars (H_2O, O_2 and O) and static temperature are plotted vs mixture fraction z and scalar dissipation N. Here, decreasing of the scalar dissipation corresponds to the increasing of the distance downstream inlet boundary. It is seen significant difference in properties of FL and MFL instantaneous solutions near self-ignition point. FL generated "instantaneous" (and non-physical) consumption of the partially premixed reactants which initially penetrated into fuel-rich and fuel-lean parts of the mixing layer upstream ignition point. The FL equations predicted instantaneous formation of thin diffusion flame reaction zone near stoichiometric surface which is accompanied by mixing in fuel-rich and fuel-lean parts of the mixing layer. The MFL demonstrated more gentle consumption of the partially premixed reactants with relatively slow formation of the diffusion flame reaction zone in the vicinity of the stoichiometric surface. The development of the diffusion flame front was accompanied in MFL calculations by decaying chemical reactions between partially premixed reactants in fuel-rich and fuel-lean parts of the mixing layer. It is seen that behavior of the MFL and FL solutions became closer one to the other in the "well-developed" combustion regions far downstream ignition point. However, even in these regions there is some difference in predictions. The MFL predicted that some amount of the oxygen initially penetrated deeply into the fuel-rich part of the mixing layer does not react since temperature in these regions is small enough. Such unburned oxygen "bump" in fuel rich zones is well seen far downstream self-ignition point as it is reported by Fig.55a.

In general, MFL solutions demonstrated more realistic properties in self-ignition regions. They predicted gentle consumption of the partially premixed reactants and finite rate development of the diffusion flame front. Qualitatively, MFL predictions correlated with known observations of the diffusion flame formation in lifted flames with significant ignition delay distance *(Kioni, et.al. 1993)*. However, MFL equations demonstrated more non-equilibrium properties of instantaneous solutions compare to the FL predictions downstream self-ignition region. The predictions of FL and MFL equations became the same only in the near-equilibrium region very far downstream ignition point.

Further estimations were done for the averaged solutions of the MFL equations. Using mean and variance mixture fraction distributions provided by FL CFD, we estimated possible ignition delay distance and mean reactive scalars distributions for MFL equations in conditions of Burrows-Kurkov test case. It was found that MFL significantly overestimated ignition delay distance compare to both

45

experimental data and FL predictions. Only increasing of OH concentration (by an order from its equilibrium value which was used in FL predictions) in vitiated air allowed to obtain self-ignition region, in MFL estimations, approximately in the same location where it was predicted by the FL and observed in the experiment. So, quantitative correlation of the current MFL predictions with experimental data was sufficiently poor. But qualitative results of its predictions were reasonably realistic. The most interesting of them are given in Figs.56,57.

The mean oxygen mass fraction behavior in the conditions of Burrows-Kurkov test case is illustrated by Fig.56 where both predictions of FL and estimations for MFL approach are presented. It is seen that averaged MFL solution predicted gentle transition from mixing to burning regimes with very slow reacting of the oxygen initially penetrated into the fuel-rich parts of the mixing layer upstream ignition region. It is important to note that such oxygen "bump" exists in fuel-rich regions up to the exit plane of the test section. This MFL prediction realistically reproduces mean O_2 behavior in conditions of Burrows-Kurkov experiment as it is shown in Fig.57. Here, both FL and MFL predictions for mean O_2 profile are given together with experimental data. It is seen the presence of unburned oxygen in the fuel-rich zone of the flame (y<0.01m). Thus, MFL indicated that elements of partially-premixed combustion could be important up to the exit plane of the test section. This prediction correlates with our conclusions regarding Burrows-Kurkov test case which were presented in Sec.IV.

Unfortunately, quantitative predictions of MFL were sufficiently poor as it is demonstrated by Fig.57 also. MFL significantly overestimated chemical nonequilibriumness and hence underestimated heat release in the flame. So, both peak value of the mean H_2O concentration and displacement of the mixing layer from the lower wall were in poor agreement with the data.

Nevertheless, we hope that current studies toward MFL development gave encouraging results. Of course, quantitative predictions of MFL were sufficiently poor but its qualitative behavior was quite realistic. The latter result correlates with the data of *Mell et. al. (1994)* who compared FL and CMC properties with the results of DNS for the case of diffusion flame development in homogeneous decaying turbulence for the system with one-step modeling reaction.

So, we hope that it is possible to develop non-expensive procedure based on minor modifications of the FL approach for much more realistic modeling of high-enthalpy delayed flames. We expect that the obtained discrepancy was due to the very simplified closure models for the scalar dissipation and conditionally averaged velocity which were used in current modeling tests. We hope to obtain better accuracy of predictions in next investigations using more justified treatments for these terms proposed in different studies *(Kuznetsov,Sabelnikov 1990; Li,Bilger, 1994; Bilger, Klimenko, 1993).*

SUMMARY and SUGGESTIONS FOR NEXT STUDIES

The current CFD tests for compressible flames were done using flamelet approach reported previously in *Bezgin et.al.(1996)*.

To improve previously obtained inaccuracy of model predictions, the following modifications were introduced:

(i) the modeling coefficients in mixture fraction variance equation were slightly changed within the range reported in the literature to decrease the mixture fraction fluctuations intensity provided by our turbulence model;

(ii) previously neglected, selective efficiencies for the molecules acting as a third bodies in three-molecular reactions were introduced into the detailed chemistry model;

(iii) the second critical value of the scalar dissipation $N_{cr}^{(2)}$ was used in self-ignition criterion instead of the critical value at quench limit $N_{cr}^{(1)}$ which was used in our previous predictions;

(iv) presence of free radicals was expected in the vitiated air provided by the pre-burners. Their mass fractions were taken according to the experimental data (if available) or were estimated from equilibrium composition computations.

All other details of current flamelet modeling were not differed from those reported in *Bezgin et.al.(1996)*.

We considered 4 test cases which covered 3 main types of the flow field (round jet, planar wall jet and planar mixing layer) and two classes of flames (with and without large ignition delay distance). All current CFD were done using full system of averaged 2D Navier-Stokes equations. The Secundov's one-equation model "v_t-90" was used for turbulence modeling. The hydrogen combustion chemistry was approximated by the detailed H_2/air kinetics scheme proposed by *C.Jachimowski (1988)* which included 33 reactions between 13 species.

It was found that introduced modifications allowed to improve results for the previously considered test cases (Beach round jet and Burrows-Kurkov wall jet experiments) and to obtain reasonable agreement with Raman data obtained by Cheng et.al. for round jet supersonic flame. As a rule, peak values of H_2O and static temperature were reproduced with the accuracy within 10-15% in these test cases. Reasonable correlation was found for reactive scalars rms for conditions of Cheng et.al. test case.

It was possible also to correlate location of the self-ignition point using modified self-ignition criterion with the accuracy about 20-30%. This result is much better than that obtained in our previous investigations (1.5-2 times). However it should be noted, that significant influence of the OH concentration value in the vitiated air flow on the prediction of self-ignition point location was found in current tests. This feature prohibited to obtain more accurate estimations for

capabilities of modified self-ignition criterion since only one of considered test cases (Cheng et.al. round jet experiment) contained information about OH radical value in vitiated air flow. However, even in this case, it was difficult to obtain more precise estimation due to inhomogenity of the vitiated air flow composition and temperature which led to asymmetric ignition in the experiment.

In general, introduced modifications allowed to obtain predictions of the reactive scalars and temperature distributions compatible (sometimes even better) with that reported for Evolved and Assumed PDF modeling. The model demonstrated good results for supersonic flames with small or moderate ignition delay distance, even in the case when very simplified modeling relations were used for its closure.

We met difficulties with modeling of *Chang et.al. (1993)* planar mixing layer experiment. But we hope that our explanations presented in Sec.IV.4 of the Report showed that the inaccuracy of predictions did not connected with flamelet model. Probably, more accurate treatment of the large-scales behavior in the turbulence model and/or inflow and outflow conditions of the experimental setup could improve accuracy of CFD predictions also. We hope to study possible directions for improvement in next investigations.

However, independently on relative success of the approach, tests showed that current flamelet version does not provide reliable predictions of all flame properties in situations when ignition delay distance is very large (Burrows-Kurkov test case). The situations, where diffusion flame is significantly lift-off from the fuel injector, can occur in supersonic flame sufficiently frequently. So, improvement of the flamelet behavior in self-ignition regions is the key problem for its further generalization for supersonic flames.

In the current study, we started development of modified flamelet approach (MFL) for more proper model operation in flames with large ignition delay distance. The convective term was introduced into the flamelet equations by analogy with the Conditional Moment Closure approach of Bilger-Klimenko. Modeling tests showed that, qualitatively, MFL predictions correlated with known observations of the diffusion flame formation in lifted flames with significant ignition delay distance. However, we obtained that MFL equations somewhat overpredicted nonequilibrium chemistry effects far downstream self-ignition point. So, quantitative correlation of the current MFL predictions with experimental data was poor. We expect that this was due to very simplified closure model for the conditionally averaged velocity which was used in current modeling tests. We belive that the obtained disadvantages can be improved in future by using more justified closure relations and it is possible to develop non-expensive procedure based on minor modifications of the FL approach for much more realistic modeling of high-enthalpy delayed flames.

48

Suggestions for next studies:

Based on results of performed study and preliminary discussions with our supervisor Dr.L.Povinelli (NASA LeRC) we propose the following main directions for future investigations:

1. Comparative tests of the flamelet and Evolved PDF modeling in the same "surrounding" conditions.
We expect to prepare Monte-Carlo simulator for Evolved PDF modeling and to perform comparative tests of the flamelet and Evolved PDF for the 3-4 cases of sub- and supersonic H_2/air diffusion flames. Other elements of the modeling (turbulence model, initial conditions, kinetics model) will be the same for both approaches in these tests. The results of such CFD will be used for more detailed analysis of similarity and difference of the approaches (joint PDF form, micromixing model, different high-order correlations, etc.). We expect that such comparative analysis would be helpful for further development of both approaches.

2. Further improvement of the flamelet modeling.
The current investigations showed that the incorporation of the convective term into the flamelet equations improves model behavior in the vicinity of the ignition point. However, its quantitative predictions are not satisfactory now. So, we propose to continue studies toward model improvement. For this purpose, we would like to test capabilities of different closure models for scalar dissipation and conditionally averaged velocity approximation. We would like also to develop approach for incorporation of such MFL model into CFD codes and to perform direct CFD tests.

3. Turbulence modeling
The accuracy of the turbulence model crucially influences results of turbulent combustion modeling. The main part of the current CFD tests was done using sufficiently old one-parametric "v_t-90" turbulence model. New versions of one- and two-equations turbulence models have been developed recently in ECOLEN&CIAM by Prof. A.Secundov. They include more accurate treatment of different effects which are important in modeling of the compressible flames (dilatation and compressibility effects, difference between turbulence in axisymmetrical and planar flows, role of the external large-scale turbulence, etc.). We propose to study their possible benefits in flamelet modeling of compressible jet flames.

We propose also to study possible benefits of the second order closure modeling in turbulence model equations for passive scalar since our current modeling was based on the simplest gradient diffusion model.

REFERENCES

Abramovich, G.N., Girshovich, T.A., Krasheninnikov, S.Yu., Secundov, A.N., Smirnova, I.P.,
> 1984. Theory of Turbulent Jets. Russian Ed., Moscow, Nauka.

Alemasov, V.E., Dregalin, A.F., Tishin, V.P., Hudyakov, V.A.,
> 1971. Thermodynamics and Thermophysics Properties of Combustion Products. Russian ed. by Glushko,V.P., v.1, Moscow.

Amin, E.M., Andrews G.E., Pourkashnian M., Williams, A., Yatter, R.A.,
> 1995. A Computational Study of Pressure Effects on Pollutants Generation in Gas Turbine Combustors. ASME Pap. 95-GT-304.

Bai X.-S., Fuchs L.,
> 1995. Sensitivity Study of Turbulent Reacting Flow Modeling in Gas Turbine Combustors. AIAA Journal, v.33, N10, pp.1857-1864.

Balakrishnan G., Williams F.A.,
> 1993. Turbulent Combustion Regimes for Hypersonic Propulsion Employing Hydrogen/Air Diffusion Flames. J.Propulsion and Power, v.10, N3, pp.434-436.

Baruzzi, G.,
> 1993. Structured Mesh Grid Adapting Based on a Spring Analogy. Conference of the CFD Society of Canada, Proceedings, Montreal, June 14-15.

Baurle, R.A., Alexopoulos, G.A.,Hassan, H.A.,Drummond, J.P.,
> 1992. An Assumed Joint-Beta PDF Approach for Supersonic Turbulent Combustion. AIAA Paper 92-3844.

Baurle, R.A., Hsu, A.T., Hassan,H.A.,
> 1994. Comparison of Assumed and Evolution PDF's in Supersonic Turbulent Combustion Calculations. AIAA Paper 94-3180.

Bezgin L., Buriko, Yu., Guskov O. et.al.
> 1995. Preliminary Study of the Flamelet Model Capabilities for Supersonic Non-Premixed Turbulent Combustion. First interim Report under Cooperative Agreement No.NCCW-75 with NASA, SRC "ECOLEN".
> 1996. Flamelet Model Application for Non-premixed Turbulent Combustion. Final ECOLEN Report under NASA Cooperative Agreement NCCW-75

Bilger,R.W.,

　　　　1980. Perturbation Analysis of Turbulent Non-Premixed Combustion.
　　　　　　Comb.Sci.&Tech., v.22, N3,p.251.

　　　　1980. Turbulent Flows with Non-premixed Reactants. In: Turbulent
　　　　　　Reacting Flows (eds.P. Libbi and F.Williams), Springer-Verlag,
　　　　　　Berlin, p.65.

　　　　1989. Turbulent Diffusion Flames. Ann. Rev. Fluid Mech., v.21,
　　　　　　pp.101-135.

　　　　1993. Conditional Moment Closure for Turbulent Reacting Flow. Phys.
　　　　　　Fluids A 5(2), pp.436-444.

Bilger, R.W., Klimenko, A.Yu.,

　　　　1993. Relationship Between Conserved Scalar PDFs and Scalar Dissipation in
　　　　　　Turbulent Flows. Report TN F-100, Charles Kolling Research
　　　　　　Laboratory, The University of Sydney.

Bray, K.N.C., Libbi, P.A. and Williams, F.A.,

　　　　1994. High-speed turbulent combustion. In: Turbulent Reacting
　　　　　　Flows (Eds. P.A.Libbi and F.A.Williams), Academic Press Inc.,
　　　　　　San Diego, pp.609-638.

Buriko Yu.Ya., Gorbatko A.A., Tchepin S.A., Zaitsev S.A., Volkov D.V.,

　　　　1995. NO predictions for aerocombustors and gas turbine engines
　　　　　　based on flamelet model for turbulent diffusion combustion.
　　　　　　1995 Yokohama International Gas Turbine Congress, Japan,
　　　　　　v.II, p.291.

Buriko, Yu.Ya., Kuznetsov, V.R.,

　　　　1988. Nitric Oxides Formation in Turbulent Duffusion Flames of
　　　　　　Hydrogen and Propane. Proc. of the 7-th World Hydrogen
　　　　　　Energy Conf., Moscow, USSR, v.3, p.2025.

Buriko,Yu.Ya.,Kuznetsov,V.R.,Uryvsky,A.F.,Volkov,D.V., Zaitsev,S.A.,

　　　　1994. A Test of a Flamelet Model for Turbulent Non-premixed
　　　　　　Combustion. Comb.&Flame, v.96, p.104,.

Burrows,M.C.,Kurkov,A.P.,

　　　　1973. Analytical and Experimental Study of Supersonic Combustion of
　　　　　　Hydrogen in a Vitiated Air Stream, NASA TM X-2828.

Chang, C.T., Marek, C.J., Wey, C., Jones, R.A., Smith, M.J.,

　　　　1993. Comparison of Reacting and Non-reacting Shear Layers at a High
　　　　　　Subsonic Mach Number. AIAA 93-2381.

Chang, C.T., Marek, C.J., Wey, C., Wey, C.C.,
    1995. Experimental Reacting Hydrogen Shear Layer Data at High Subsonic
    Mach Number. NASA Technical Publication 3342 (draft copy).

Chein, K.-Y.
    1982. Predictions of Channel and Boundary-Layer Flows with a
    Low-Reynolds-Number Turbulence Model. AIAA Journal,
    Vol. 20, Jan., pp.33-38.

Cheng T.S., Wehrmeyer, J.A., Pitz, R.W., Jarrett, O.Jr., Northam, G.B.,
    1994. Raman Measurements of Mixing and Finite-Rate Chemistry in a
    Supersonic Hydrogen-Air Diffusion Flame. Comb.&Flame, v.99,
    pp.157-173.

Eifer P., Kollman W.,
    1993. PDF Prediction of Supersonic Hydrogen Flames.
    AIAA-93-0448

Evans,J.S.,Schexnayder,C.J.,
    1980. Influence of Chemical Kinetics and Unmixedness on Burning in
    Supersonic Hydrogen Flames. AIAA Journal, v.18, N 7,.

Evans,J.S.,Schexnayder,C.J.,Beach,H.L.,
    1978. Application of Two-Dimentional Parabolic Computer Program
    to Prediction of Turbulent Reacting Flows, NASA TP-1169.

Farschi,M.
    1989. A PDF Closure Model for Compressible Turbulent Chemically
    Reacting Flows. AIAA-89-0390.

Gaffney,R.L.,White,J.A.,Girimaji,S.S.,Drummond,J.P.,
    1992. Modeling Turbulent Chemistry Interactions Using Assumed PDF
    Method. AIAA Paper 92-3638, 1992.

Girimaji,S.S.
    1991. Assumed β-pdf Model for Turbulent Mixing: Validation and
    Extension to Multiple Scalar Mixing. Combust. Sci. and Tech.
    v.78, pp.177-196.

Hsu,A.T.,
    1991. A Study of Hydrogen Diffusion Flames Using PDF Turbulence
    Model. AIAA Paper 91-1780.

Hsu,A.T.,Raji,M.S.,Norris,A.T.,
     1994. Application of a PDF Method to Compressible Turbulent
     Reacting Flows. AIAA Paper 94-0781.

Hsu,A.T.,Tsai,Y.-L.P.,Raji,M.S.,
     1993. A PDF Approach for Compressible Turbulent Reacting Flows.
     AIAA Paper 93-0087.

Jachimowski, C.J.,
     1988. An Analytical Study of the Hydrogen-Air Reaction Mechanism
     With Application to Scramjet Combustion. NASA LaRC,
     Technical Paper 2791.

Jones, W.P., Launder, B.E.,
     1973. The Calculation of Low-Reynolds-Phenomena with Two-
     Equation Model of Turbulence. Int. J. Heat and Mass Transfer,
     v.16, pp.1119-1130.

Jones, W.P., Whitelaw, J.H.
     1982. Calculation Methods for Reacting Turbulent Flows: a Review.
     Comb&Flame, v.48, N1, pp.1-26.

Kioni, P.N., Rogg, B., Bray, K.N.C., Linan, A.
     1993. Flame Spreading in Laminar Mixing Layers: The Triple Flame.
     Comb&Flame, v.95, pp.276-290.

Klimenko A.Yu.,
     1990. Multicomponent diffusion of various scalars in turbulent flows.
     Fluid Dynamics, 25, pp.327-334.
     1995. Note on the Conditional Moment Closure in Turbulent Shear
     Flows. Phys. Fluids &(2), p.446.

Kolesnikov,O.M.,
     1981. Concentrations Fluctuations Influence on Ignition of Wall
     Hydrogen Jet in Supersonic Flow. Fizika Gorenia i
     Vzriva (russian), v.21, N1, p.53, 1981.

Kuznetsov,V.R.,
     1977. Mixing up to a Molecular Level and the Development of a
     Chemical Reaction in a Turbulent Flow. Fluid Dynamics, v.12,
     No. 3, p.369.
     1982. Influence of Turbulence on the Formation of High
     Nonequilibrium Concentrations of Atoms and Free Radicals in
     Diffusion Flames. Fluid Dynamics, v.17, N 6, p.815.

Kuznetsov,V.R.,Sabelnikov,V.A.,
    1990. Turbulence and Combustion, (P.A.Libby ed.), Hemisphere Publ.,.

Lai, H.T., Raju M.S.,
    1993. CFD Validation of Subsonic Turbulent Planar Shear Layer.
    AIAA 93-1773.

Li, J.D, Bilger, R.W.,
    1993. Measurements and Predictions of the Conditional Variance in a
        Turbulent Reactive-Scalar Mixing Layer. Phys. Fluids A, 5(12),
        p.3255.
    1994. A Simple Theory of Conditional Mean Velocity in Turbulent Scalar-
        Mixing Layer. Phys. Fluids, v.6, N2, p.605.

Liew,S.K.,Bray,K.N.C.,Moss,J.B.,
    1984. A Stretched Laminar Flamelet Model of Turbulent Nonpremixed
        Combustion. Comb.&Flame, v.56, p.199.

Mell, W.E., Nilsen, V., Kosaly, G., Riley, J.J.,
    1994. Investigation of Closure Models for Nonpremixed Turbulent
        Reacting Flows. Phys. Fluids, 6(3), p.1331.

Miller,J.A.,Bowman,C.I.,
    1989. Mechanism and Modeling of Nitrogen Chemistry in
        Combustion. Progress in Energy Comb. Sci., v.15, p.287.

Monin A.S., Yaglom A.M.,
    1965. Statistical Fluid Dunamics, 1965(p.I), 1967(p.II), Moscow, Nauka.
        (russuan ed.)

Morgenthaler V., Figueira da Silva L.F., Deshaies B., Sabelnikov V.A.,
    1997. Numerical Analysis of Supersonic Turbulent Coflowing Jets:
        Influence of Turbulent Transport and Combustion Modeling.
        In: Advanced Computation&Analysis of Combustion. Eds.
        G.D.Roy, S.M.Frolov, P.Givi. ENAS Publishers, Moscow.

Namazian M.,Schefer R.W.,Kelly J., Scalar Dissipation Measurements in the
    1988. Developing Region of a Jet. Comb.&Flame, v.74,p.147-160.

Peters,N.,
    1984. Laminar Diffusion Flamelet Models in Non-Premixed
        Combustion. Progr.Energy Comb.Sci., 10, p. 319.

Pope,S.B.,

       1981. A Monte-Carlo Method for the PDF Equations of Turbulent
          Reactive Flows. Comb.Sci.&Tech. v.25, N5, p.159.

Sanyach M., Mathilu, J.

       1969. Zone de melange d'un jet plan-fluctuations induites dans le cone a
          potential-intermittence. Int. J. Heat&Mass Transfer, 1969, v.12, p.1679.

Schlichting,H.,

       1968. Boundary-Layer Theory, 6-th ed., McGraw-Hill Book
          Company,New York.

Spiegler, E., Wolfshtein, M., Manheimer-Timnat, Y.,

       1976. A Model of Unmixedness for Turbulent Reacting Flows.
          Acta Astronautica, v.3, p.265.

Wignanski, I.., Fiedler, H.,

       1969. Some Measurements in the selfpreserving jets. J.Fl.Mech., v.38, pt.3.

Williams,F.A.,

       1975. Turbulent Mixing in Non-Reactive and Reactive Flows. (S.N.B.
       Murthy ed.), p.189, Plenum, 1975.

Zheng,I.I., Bray,K.N.C.,

       1994. An Application of New Combustion and Turbulence Models to
          H_2-Air Nonpremixed Supersonic Combustion. Comb.&Flame,
          v.99, p.440.

Appendix A. DESCRIPTION OF THE MATHEMATICAL MODEL

The applied mathematical model consisted of the following main blocks:
  (i) hydrodynamics conservation equations;
  (ii) turbulence model;
  (iii) flamelet model;
  (iv) averaging procedure;
  (v) CFD/flamelet coupling procedure
  (vi) thermodynamics and detailed chemistry models of Appendix C.

A.1 Hydrodynamics Model

The Favre-averaged, steady-state conservation equations for 2-D or axisymmetric turbulent flows were written as:

$$\frac{\partial \vec{F}}{\partial x} + \frac{\partial \vec{G}}{\partial y} + j \frac{\vec{R}}{y} = 0 \tag{A.1}$$

where: x,y are axes of Cartesian (j=0) or cylindrical (j=1) coordinates. The fluxes and source term in (A.1) were given as:

$$\vec{F} = \begin{pmatrix} \overline{\rho}\tilde{u} \\ \overline{\rho}\tilde{u}^2 + \overline{p} - \overline{\tau}_{xx} \\ \overline{\rho}\tilde{u}\tilde{v} - \overline{\tau}_{xy} \\ \overline{\rho}\tilde{u}\tilde{H} - \tilde{u}\overline{\tau}_{xx} - \tilde{v}\overline{\tau}_{xy} + \overline{q}_x \end{pmatrix}, \quad \vec{G} = \begin{pmatrix} \overline{\rho}\tilde{v} \\ \overline{\rho}\tilde{u}\tilde{v} - \overline{\tau}_{yx} \\ \overline{\rho}\tilde{v}^2 + \overline{p} - \overline{\tau}_{yy} \\ \overline{\rho}\tilde{v}\tilde{H} - \tilde{u}\overline{\tau}_{yx} - \tilde{v}\overline{\tau}_{yy} + \overline{q}_y \end{pmatrix},$$

$$\tag{A.2}$$

$$\vec{R} = \begin{pmatrix} \overline{\rho}\tilde{v} \\ \overline{\rho}\tilde{u}\tilde{v} - \overline{\tau}_{yx} \\ \overline{\rho}\tilde{v}^2 - \overline{\tau}_{yy} + \overline{\tau}_{\theta\theta} \\ \overline{\rho}\tilde{v}\tilde{H} - \tilde{u}\overline{\tau}_{yx} - \tilde{v}\overline{\tau}_{yy} + \overline{q}_y \end{pmatrix}$$

where: $\overline{\rho}$ is mean density; $\tilde{u}, \tilde{v}$ are the Favre-averaged components of the velocity vector $\vec{U}$; $\overline{p}$ is pressure; $\tilde{H}$ is total enthalpy; $\overline{q}_x, \overline{q}_y$ are heat flux components. The viscous stresses and heat flux components in (A.2) were written as:

$$\overline{\tau}_{xx} = \overline{\rho}(v_t + v)(2\frac{\partial\tilde{u}}{\partial x} - \frac{2}{3}\nabla\cdot\vec{U}), \quad \overline{\tau}_{yy} = \overline{\rho}(v_t + v)(2\frac{\partial\tilde{v}}{\partial y} - \frac{2}{3}\nabla\cdot\vec{U}),$$

$$\overline{\tau}_{xy} = \overline{\tau}_{yx} = \overline{\rho}(\nu_t + \nu)\left(\frac{\partial \widetilde{u}}{\partial y} + \frac{\partial \widetilde{v}}{\partial x}\right), \quad \overline{\tau}_{\theta\theta} = \overline{\rho}(\nu_t + \nu)(2\frac{v}{y} - \frac{2}{3}\nabla \cdot \vec{U}),$$ (A.3)

$$\overline{q}_x = -\overline{\rho}(\nu_t / Pr_t + \nu / Pr)\frac{\partial \widetilde{h}}{\partial x}, \quad \overline{q}_y = -\overline{\rho}(\nu_t / Pr_t + \nu / Pr)\frac{\partial \widetilde{h}}{\partial y}$$

where ν_t is turbulent viscosity and ν is laminar kinematic viscosity; $\nabla \cdot \vec{U}$ is velocity divergence; $\widetilde{h}$ is static enthalpy; Pr and Pr_t are laminar and turbulent Prandtl numbers respectively.

A.2 Turbulence model

The turbulent viscosity ν_t in (A.3) was calculated using "ν_t-90" Secundov's turbulence model:

$$\frac{\partial \overline{\rho}\widetilde{u}\nu_t}{\partial x} + \frac{\partial \overline{\rho}\widetilde{v}\nu_t}{\partial y} + j\frac{\overline{\rho}\widetilde{v}\nu_t}{y} = \frac{\partial}{\partial x}\left[\overline{\rho}(c_1\nu_t + \nu)\frac{\partial \nu_t}{\partial x}\right] + \frac{\partial}{\partial y}\left[\overline{\rho}(c_1\nu_t + \nu)\frac{\partial \nu_t}{\partial y}\right] +$$

$$j\frac{\overline{\rho}(c_1\nu_t + \nu)\frac{\partial \nu_t}{\partial y}}{y} + c_2\overline{\rho}\nu_t|G| + c_3\nu_t\left(\overline{u}\frac{\partial \overline{\rho}}{\partial x} + \overline{v}\frac{\partial \overline{\rho}}{\partial y}\right) - c_4\overline{\rho}\nu_t^2\frac{G^2}{a^2} - \overline{\rho}\frac{c_5\nu_t^2 + c_6\nu_t\nu}{S^2}.$$ (A.4)

where: a is speed of sound; S is minimal distance to the wall;

$$c_2 = c_2'\left(\frac{y^4 G^2}{(30\nu_t)^2 + y^4 G^2}\right)^j \frac{\nu_t^2 + 11.2\nu_t\nu + 12.8\nu^2}{\nu_t^2 - 11.2\nu_t\nu + 64\nu^2}.$$

$$G^2 = 2[(\frac{\partial \widetilde{u}}{\partial x})^2 + (\frac{\partial \widetilde{v}}{\partial y})^2 + (\frac{\partial \widetilde{u}}{\partial y})(\frac{\partial \widetilde{v}}{\partial x})] + [(\frac{\partial \widetilde{u}}{\partial y})^2 + (\frac{\partial \widetilde{v}}{\partial x})^2 + 2j(\frac{\widetilde{v}}{y})^2],$$

c_1	c_2'	c_3	c_4	c_5	c_6
2	0.2	0.7	0.5	3	50

The Reynolds-averaged velocity components $\overline{u}, \overline{v}$ which met in the RHS of (A.4) were modeled using gradient diffusion relations:

$$\overline{u} = \widetilde{u} + \frac{\nu_t}{\overline{\rho} \cdot Sc_t}\frac{\partial \overline{\rho}}{\partial x}; \quad \overline{v} = \widetilde{v} + \frac{\nu_t}{\overline{\rho} \cdot Sc_t}\frac{\partial \overline{\rho}}{\partial y}, \text{ where } Sc_t \text{ is turbulent Schmidt number.}$$

The turbulence kinetic energy K, mean mixture fraction $\widetilde{z} = \overline{\rho z} / \overline{\rho}$ and its variance $\sigma^2 = \overline{\rho z''z''} / \overline{\rho}$ were calculated using semi-empirical transport equations of the turbulence modeling:

$$\frac{\partial \overline{\rho}\widetilde{u}K}{\partial x}+\frac{\partial \overline{\rho}\widetilde{v}K}{\partial y}+j\frac{\overline{\rho}\widetilde{v}K}{y}=\frac{\partial}{\partial x}\left[\overline{\rho}\left(1.4\nu_t+\nu\right)\frac{\partial K}{\partial x}\right]+\frac{\partial}{\partial y}\left[\overline{\rho}\left(1.4\nu_t+\nu\right)\frac{\partial K}{\partial y}\right]+$$

$$j\frac{\overline{\rho}\left(c_\sigma\nu_t+\nu\right)\dfrac{\partial K}{\partial y}}{y}+\overline{\rho}\nu_t G^2-0.1\frac{\overline{\rho}K^2}{\nu_t}.$$

$$\frac{\partial \overline{\rho}\widetilde{u}\widetilde{z}}{\partial x}+\frac{\partial \overline{\rho}\widetilde{v}\widetilde{z}}{\partial y}+j\frac{\overline{\rho}\widetilde{v}\widetilde{z}}{y}=\frac{\partial}{\partial x}\left[\overline{\rho}\left(\frac{\nu_t}{Sc_t}+\frac{\nu}{Sc}\right)\frac{\partial \widetilde{z}}{\partial x}\right]+\frac{\partial}{\partial y}\left[\overline{\rho}\left(\frac{\nu_t}{Sc_t}+\frac{\nu}{Sc}\right)\frac{\partial \widetilde{z}}{\partial y}\right]+\frac{j}{y}\overline{\rho}\left(\frac{\nu_t}{Sc_t}+\frac{\nu}{Sc}\right)\frac{\partial \widetilde{z}}{\partial y}$$

$$\frac{\partial \overline{\rho}\widetilde{u}\sigma^2}{\partial x}+\frac{\partial \overline{\rho}\widetilde{v}\sigma^2}{\partial y}+j\frac{\overline{\rho}\widetilde{v}\sigma^2}{y}=\frac{\partial}{\partial x}\left[\overline{\rho}\left(c_\sigma\nu_t+\nu\right)\frac{\partial \sigma^2}{\partial x}\right]+\frac{\partial}{\partial y}\left[\overline{\rho}\left(c_\sigma\nu_t+\nu\right)\frac{\partial \sigma^2}{\partial y}\right]+$$

$$j\frac{\overline{\rho}\left(c_\sigma\nu_t+\nu\right)\dfrac{\partial \sigma^2}{\partial y}}{y}+\frac{2\overline{\rho}\nu_t}{Sc_t}\left[\left(\frac{\partial \widetilde{z}}{\partial x}\right)^2+\left(\frac{\partial \widetilde{z}}{\partial y}\right)^2\right]-2\overline{\rho}\widetilde{N}$$

where mean scalar dissipation $\widetilde{N}$ was approximated as $\widetilde{N}=0.1\dfrac{K\cdot\sigma^2}{\nu_t}$.

A.3 Flamelet Model

The flamelet equations were taken in form (I.5) of Sec.I:

$$N^s\frac{d^2C_\alpha}{dz^2}+R_\alpha=0 \qquad\qquad \alpha=1,...,J \qquad\qquad (A.5)$$

$$h=(H^F-H^A)z+H^A-\frac{U^2}{2}$$

where C_α is mass fraction of α-specie; R_α is the chemical production term; J is total number of reactive species; H is total enthalpy; $h=\sum\limits_{\alpha=1}^{J} h_\alpha C_\alpha$ is static enthalpy; species specific enthalpies $h_\alpha=\int\limits_{T_0}^{T} Cp_\alpha dT+\Delta h_\alpha(T_0)$ are used taking into account species heats of formation Δh_α at reference temperature $T_0=298.15K$. The parameter N^s is the value of instantaneous scalar dissipation at the stoichiometric surface; superscripts F and A denote total enthalpies of fuel and oxidizer respectively.

The kinetic energy term in eqs.(A.5) was approximated using relation:

$$\frac{U - U^A}{U^F - U^A} \approx z^\beta$$

where U^A, U^F are the mean flow velocities in the air and fuel core flows respectively; β is exponent which was chosen as $\beta \approx 1/Sc_t$ (Sc_t is the turbulent Schmidt number).

The boundary conditions for eqs. (A.5) were posed in accordance with the test cases specifications at $z=1$ (pure fuel) and $z=0$ (pure oxidizer):

$$z=0 \quad H = H^A; C_\alpha = C_\alpha^A \qquad\qquad \alpha = 1,...,J \qquad\qquad (A.6)$$
$$z=1 \quad H = H^F; C_\alpha = C_\alpha^F$$

where superscripts F and A denote composition and total enthalpies for the flows of fuel and oxidizer respectively.

The flamelet eqs.(A.5) with boundary conditions (A.6) were solved parametrically over scalar dissipation $N^s \in [0, N_{cr}^{(1)})$ and pressure in reaction zone p_s. Here, $N_{cr}^{(1)}$ is critical value of scalar dissipation at quench limit. The obtained solutions were collected into the flamelet library in parametric form on z, N^s and pressure p_s:

$$C_\alpha = C_\alpha(z, N^s, p_s) \qquad\qquad \alpha = 1,...,J \qquad\qquad (A.7)$$

$$T = T(z, N^s, p_s)$$

The flamelet libraries for conditions of Beach test case (Sec.IV.2), Cheng et.al. test case (Sec.IV.3) and Chang et.al. test case (Sec.IV.4) were generated for fixed value of pressure in the reaction zone ($p_s = 0.1$MPa). The flamelet library for conditions of the Burrows-Kurkov test case was generated in the range of pressure variation 0.08-0.12MPa. Computational procedure for flamelet library generation was given in our previous Report (*Bezgin et.al, 1996*).

Averaging of the flamelet solutions and their coupling with CFD code was done in accordance with items A.4 and A.5.

A.4. Averaging Procedure

In the current tests, averaging procedure remained the same as that used by us previously (*Kuznetsov, Sabelnikov, 1990*). The Favre joint PDF of mixture fraction z and scalar dissipation $\mathcal{P}(z,N^s)$ was considered in a following form:

$$\mathcal{P}(z,N^S) = \frac{\rho}{\bar{\rho}} P(z, N^s) = (1 - \gamma)\delta(z)\delta(N^s) + \gamma P_t(z)\delta(N^s - \tilde{N}_t^s)$$

where γ is the intermittency factor; P_t is the mixture fraction probability density function in a turbulent mixing layer; δ is the Dirac function.

The intermittency factor γ was calculated using approximate relation:

$$\gamma = \begin{cases} 1.31/(1+\sigma^2/\tilde{z}^2) & \text{if} \quad \sigma/\tilde{z} > 0.555 \\ 1 & \text{if} \quad \sigma/\tilde{z} < 0.555 \end{cases} \tag{A.8}$$

where $\tilde{z} = \overline{\rho z}/\overline{\rho}$ is Favre averaged mixture fraction and $\sigma^2 = \overline{\rho z'' z''}/\overline{\rho}$ is mixture fraction variance. Self-similar solutions of PDF equation were used to approximate the mixture fraction PDF $P_t(z)$ in the turbulent mixing layer $(0 < z < 1)$:

$$P_t(z) = \begin{cases} \dfrac{1.404}{\tilde{z}_t} \text{Ai}(1.788\dfrac{z}{\tilde{z}_t} - 2.338) & \text{if} \quad \gamma < 1 \quad \text{(int ermittent \quad regions)} \\ \dfrac{1}{\sqrt{2\pi}\sigma} \exp\left(-\dfrac{(z-\tilde{z})^2}{2\sigma^2}\right) & \text{if} \quad \gamma = 1 \quad \text{(non - int ermittent regions)} \end{cases}$$

where $\tilde{z}_t = \tilde{z}/\gamma$ is the mixture fraction value conditionally averaged over the moments when the turbulent mixing layer is observed in a given point; Ai is Airy function.

The conditionally averaged value of scalar dissipation at the stoichiometric surface was approximated as:

$$\overline{N}_t^s = \dfrac{\tilde{N}\big|_{\tilde{z}=zs}}{\gamma\big|_{\tilde{z}=zs}} \tag{A.9}$$

where $\tilde{N}\big|_{\tilde{z}=zs}$, $\gamma\big|_{\tilde{z}=zs}$ are the mean values of the scalar dissipation $\tilde{N}$ and intermittency factor γ calculated under the condition that mean value of mixture fraction $\tilde{z} = z_s$.

A.5. Coupling with CFD solver.

The following procedure was used for the flamelet library incorporation into the compressible flow hydrodynamics solver. The "effective" heat capacities CP_α of the reactive species were introduced in the same manner as it was done by *Gaffney et.al. (1992)*:

$$CP_\alpha = \int_{T_0}^{T} C_{p\alpha} dT/(T - T_0) \tag{A.10}$$

where T_0 is the reference temperature.

Using the thermal equation of state for mixture $P = \rho RT/\mu$ and eqs.(A.10) one can obtain the following "effective" form for the total enthalpy H:

$$H = \dfrac{\Gamma}{(\Gamma-1)} \dfrac{P}{\rho} + Q + \dfrac{(\vec{U} \cdot \vec{U})}{2} \tag{A.11}$$

where:

$\Gamma = \dfrac{1}{(1 - \dfrac{R}{CP \cdot \mu})}$ is "effective" heat capacities ratio;

$Q = (\sum_\alpha C_\alpha \Delta h_\alpha - CP \cdot T_0)$ is "effective" heat of mixture formation;

μ is the mixture molar weight; Δh_α are species heats of formation and $R = 8.31$ J/(mol K) is universal gas constant.

Multiplying eq.(A.11) by density and Favre-averaging one has:

$$\overline{\rho}\widetilde{H} = \overline{\left(\dfrac{\Gamma}{(\Gamma - 1)}\right)} \cdot \overline{P} + \overline{\rho}\widetilde{Q} + \overline{\rho}\dfrac{\widetilde{U}^2}{2} \qquad (A.12)$$

where correlation <P'Γ'> and input of turbulent kinetic energy are neglected.

The values of $\Gamma/(\Gamma-1)$ and Q depend on reactive species mass fractions and temperature only. So, they can be calculated using flamelet solutions (A.7). To obtain their mean values, the averaging procedure of item A.4 was used. The value of $\widetilde{H}$ was obtained from the Favre-averaged energy conservation equation in its conventional form. As the result, eq.(A.12) gave the relation between mean values of density $\overline{\rho}$, pressure $\overline{P}$ and mean flow velocity $\widetilde{U}$. Here, only two parameters (Γ and Q) were needed from the flamelet library to close hydrodynamics equations. The particular solutions for Q and Γ at required valued of mixture fraction, scalar dissipation and pressure were obtained from the flamelet library by the linear interpolation between neighboring solutions in the same manner as it was done in *Bezgin et.al. (1996)*.

Appendix B Inflow Boundary Layers Simulation

The inflows, in the considered test cases, had boundary layers. So the inflow distributions for CFD were modeled taking into account this feature. The longitudinal velocity and eddy viscosity distributions in the incoming flows were derived from the experimental data on boundary layer thickness δ. The eddy viscosity distribution inside the boundary layer was approximated using modified Van-Driest relation:

$$\nu_t = 0.41 y U_\tau (1 - e^{-\frac{yU_\tau}{26\nu}})(1 - \frac{y}{\delta}) \cdot e^{-\frac{y}{\delta}}$$

where dynamics velocity U_τ was calculated using correlation for local skin friction factor c_f for compressible turbulent boundary layer at flat plate:

$$\frac{2U_\tau^2}{U_e^2} \equiv c_f = 0.023 \left(\frac{U_e \delta}{\nu}\right)^{0.2} \left(1 + 0.7 \frac{(k-1)}{2} M_e^2\right)^{-0.5} \frac{2}{(1 + \overline{T}_w)^{0.5}}$$

Here subscript "e" denotes parameters in core flow, $\overline{T}_w$ is the temperature factor, k is heat capacities ratio. The longitudinal velocity distribution in the boundary layer was obtained by integrating of the equation for the shear stress:

$$\overline{\tau}_{xy} = \overline{\rho}(\nu_t + \nu)\frac{\partial \widetilde{u}}{\partial y};$$

where the distribution for the shear stress inside the boundary layer was approximated as:

$$\overline{\tau}_{xy} = \overline{\rho} U_\tau^2 \left(1 - 3\left(\frac{y}{\delta}\right)^2 + 2\left(\frac{y}{\delta}\right)^3\right);$$

The turbulence kinetic energy distribution in the boundary layer was calculated from the approximate "equilibrium turbulence" relation:

$$\frac{\nu_t}{K}\left|\frac{\partial \widetilde{u}}{\partial y}\right| \approx 0.3;$$

The same procedure was used for $\widetilde{u}$, ν_t and K distributions calculations (if required) in the exit plane of the hydrogen injectors.

Appendix C Thermodynamics and Kinetics Reference Data

<div align="right">

Table C.1.

</div>

Reaction rates constants for hydrogen oxidation chemistry based on data by
Miller and Bowman (1989).

Reaction rate constant is presented in the form $K = AT^B \exp(-\dfrac{E}{RT})$.

Units used are Kelvins, seconds, mols and centimeters.

	Reaction	Forward rate		
		lg A	B	-E/R
1	H2 + O2 = OH + OH	13.23	0.00	-24044.0
2	OH + H2 = H2O + H	9.07	1.30	-1824.7
3	O + OH = O2 + H	14.60	-0.50	0.0
4	O + H2 = OH + H	4.70	2.67	-3165.3
5	H + O2 + M = HO2 + M	17.56	-0.72	0.0
6	OH + HO2 = H2O + OH	12.88	0.00	0.0
7	H + HO2 = OH + OH	14.15	0.00	-540.0
8	O + HO2 = O2 + OH	13.15	0.00	-540.0
9	OH + OH = O + H2O	8.78	1.30	0.0
10	H + H + M = H2 + M	18.00	-1.00	0.0
11	H + H + H2 = H2 + H2	16.96	-0.60	0.0
12	H + H + H2O = H2 + H2O	19.78	-1.25	0.0
13	H + OH + M = H2O + M	22.20	-2.00	0.0
14	H + O + M = OH + M	16.79	-0.60	0.0
15	O + O + M = O2 + M	13.28	0.00	899.8
16	H + HO2 = H2 + O2	13.10	0.00	0.0
17	HO2 + HO2 = H2O2 + O2	12.30	0.00	0.0
18	H2O2 + M = OH + OH + M	17.11	0.00	-22896.7
19	H2O2 + H = HO2 + H2	12.20	0.00	-1912.2
20	H2O2 + OH = H2O + HO2	13.00	0.00	-905.8
21	HO2 + NO = NO2 + OH	12.32	0.00	241.0
22	NO2 + H = NO + OH	14.54	0.00	-754.8
23	NO2 + O = NO + O2	13.00	0.00	-301.9
24	NO2 + M = NO + O + M	16.04	0.00	-33212.7
25	HNO + M = H + NO + M	16.18	0.00	-24496.9
26	HNO + OH = NO + H2O	13.56	0.00	0.0
27	HNO + H = H2 + NO	12.70	0.00	0.0
28	N + NO = N2 + O	12.51	0.30	0.0
29	N + O2 = NO + O	9.81	1.00	-3160.2
30	N + OH = NO + H	13.58	0.00	0.0

The third-body efficiencies are as follows: for reaction (5), H2O = 18.6, H2 =2.6 and N2 = 1.3; for reaction (10), H2 = 0.0 and H2O = 0.0; for reactions (13) and (14), H2O = 5.0; and for reaction (25), H2O = 10.0, O2 = 2.0, N2 = 2.0 and H2 = 2.0.

Table C.2.

Reaction rates constants for hydrogen oxidation chemistry based on data by
Jachimowski (1988).

Reaction rate constant is presented in the form $K = AT^B \exp(-\frac{E}{RT})$.
Units used are Kelvins, seconds, moles and centimeters.

	Reaction	Forward rate		
		lg A	B	-E/R
1	H2 + O2 = OH + OH	13.23	0.00	-24154.7
2	H + O2 = OH + O	14.41	0.00	-8454.1
3	O + H2 = OH + H	10.26	1.00	-4478.7
4	OH + H2 = H2O + H	13.34	0.00	-2591.6
5	OH + OH = H2O + O	12.80	0.00	-548.5
6	H + OH + M = H2O + M	22.34	-2.00	0.0
7	H + H + M = H2 + M	17.81	-1.00	0.0
8	H + O + M = OH + M	16.78	-0.60	0.0
9	H + O2 + M = HO2 +M	15.32	0.00	503.2
10	HO2 + H = H2 + O2	13.11	0.00	0.0
11	HO2 + H = OH + OH	14.15	0.00	-543.5
12	HO2 + H = H2O + O	13.00	0.00	-543.5
13	HO2 + O = O2 + OH	13.18	0.00	-478.1
14	HO2 + OH = H2O + O2	12.90	0.00	0.0
15	HO2 + HO2 = H2O2 + O2	12.30	0.00	0.0
16	H + H2O2 = H2 + HO2	12.15	0.00	-1811.6
17	O + H2O2 = OH + HO2	13.15	0.00	-4227.1
18	OH + H2O2 = H2O + HO2	12.79	0.00	-719.6
19	H2O2 + M = OH + OH +M	17.08	0.00	-22896.7
20	O + O + M = O2 + M	17.78	0.00	905.8
21	N + N + M = N2 + M	17.45	-0.75	0.0
22	N + O2 = NO + O	9.81	1.00	-4176.8
23	N + NO = N2 + O	13.20	0.00	0.0
24	N + OH = NO + H	11.80	0.50	0.0
25	H + NO + M = HNO + M	15.73	0.00	301.9
26	H + HNO = NO + H2	12.68	0.00	0.0
27	O + HNO = NO + OH	11.70	0.50	0.0
28	OH + HNO = NO + H2O	13.56	0.00	0.0
29	HO2 + HNO = NO + H2O2	12.30	0.00	0.0
30	HO2 + NO = NO2 + OH	12.53	0.00	130.8
31	H + NO2 = NO + OH	14.54	0.00	-754.8
32	O + NO2 = NO + O2	13.00	0.00	-301.9
33	NO2 + M = NO + O + M	16.06	0.00	-33212.7

The third-body efficiencies relative to N2 = 1.0 are as follows: for reaction (6), H2O = 6.0; for reaction (7), H2 = 2.0 and H2O = 6.0; for reaction (8), H2O = 5.0; for reaction (9), H2 = 2.0 and H2O = 16.0; and reaction (19), H2O = 15.0.

Table C.3

Polynomial coefficients for thermodynamical properties approximation from Alemasov, et.al. (1971).

Enthalphy $H = A_I + \sum_{i=1}^{7} A_i x^i$ (J/mol), entrophy $S = A_S + 10^{-3} A_I \ln x + \sum_{i=2}^{7} \frac{i}{i-1} A_i x^{i-1}$ $\left(\dfrac{J}{mol \cdot K}\right)$, $x = \dfrac{T}{1000}$

T is temperature in Kelvins, μ is molar weight in kg/mol.

	μ	A_S	A_I	A_1	A_2	A_3	A_4	A_5	A_6	A_7
O	0.016	1.8908422E+02	2.4275916E+05	2.2410764E+04	-1.7265002E+04	1.0305618E+03	-3.6058405E+02	7.2900697E+01	-7.6554363E+00	3.2357642E-01
O_2	0.032	2.2737469E+02	-7.8338353E+03	2.3363288E+04	1.1344190E+04	-5.6862959E+03	1.8430891E+03	-3.4538653E+02	3.4370091E+01	-1.4099905E+00
H	0.001	1.3986962E+02	2.1190009E+05	2.0818472E+04	-2.9523678E+01	1.9433405E+01	-6.8227195E+00	1.3074247E+00	-1.2887342E-01	5.1061121E-03
H_2	0.002	1.7071521E+02	-9.0186617E+03	3.1295524E+04	-4.7428008E+03	4.4791623E+03	-1.5709183E+03	2.9222022E+02	-2.8095988E+01	1.0976161E+00
OH	0.017	2.2486857E+02	3.0253603E+04	3.1781619E+04	-5.5713986E+03	5.5738683E+03	-2.1234197E+03	4.2335948E+02	-4.3227566E+01	1.7813063E+00
HO_2	0.033	2.4864170E+02	-6.9643738E+03	2.5088917E+04	1.9809408E+04	-8.3743023E+03	2.5338444E+03	-4.7406450E+02	4.7873608E+01	-1.9867593E+00
H_2O	0.018	2.2449392E+02	-2.5140681E+05	3.0849677E+04	2.1103526E+04	4.2017770E+03	-2.0165908E+03	4.2895533E+02	-4.4758303E+01	1.8616812E+00
H_2O_2	0.034	2.5037094E+02	-1.4648530E+05	2.7103555E+04	3.0929810E+04	-1.2428987E+04	3.4142397E+03	-5.8455816E+02	5.5567894E+01	-2.2223348E+00
N	0.014	1.7885623E+02	4.6670509E+05	2.0996093E+04	-3.8634725E+02	3.4972979E+02	-1.6133129E+02	3.7320547E+01	-3.8260814E+00	1.4528543E-01
N_2	0.028	2.2372830E+02	-8.3007961E+03	2.7351826E+04	1.3058227E+04	2.1442408E+03	-1.2906443E+03	3.1852362E+02	-3.7324427E+01	1.7050206E+00
NO	0.030	2.3850112E+02	8.3177913E+04	2.5678096E+04	6.0005054E+03	-1.3533171E+03	2.6666536E+01	4.9234895E+01	-8.8796781E+00	4.9125222E-01
NO_2	0.046	2.4887553E+02	2.5224126E+04	2.1664397E+04	3.2081751E+04	-1.6310527E+04	4.9918396E+03	-8.7953888E+02	8.3125988E+01	-3.3624189E+00
HNO	0.031	2.4421107E+02	9.3047636E+04	2.5921977E+04	1.3301262E+04	-1.9041572E+04	2.7630678E+03	-8.7314766E+01	1.4844476E+01	-8.6075814E+01

FIGURES

air

fuel

flame

FUEL LEAN SIDE ($z<z_s$)

$\vec{n}$

$z=z_s$

δ_{ch}

$z=z_s-dz$

$z=z_s+dz$ FUEL RICH SIDE ($z>z_s$)

$\delta_{ch} \ll L_t$

(L_t is turbulence integral length scale)

JOINT PDF MODEL

$$\mathcal{P}(T,C_1,...,C_J)=$$
$$\mathcal{P}(z)\mathcal{P}(N)\delta(T-T(z,N))\prod_{\alpha=1}^{J}\delta(C_\alpha-C_\alpha(z,N))$$

Analitical solution of eq. for $\mathcal{P}(z)$

$\mathcal{P}(z)=(1-\gamma)\delta(z)+\gamma\ \mathcal{P}_t(z)$

$\mathcal{P}_t(z)=\mathcal{P}_t(z,\tilde{z},\sigma^2)$

$\mathcal{P}_t(z)\Rightarrow$Airy/Gaussian

FLAMELET EQS.

$$N\frac{d^2C_\alpha}{dz^2}+R_\alpha=0 \qquad \alpha=1,...,J$$

$$\frac{d^2H}{dz^2}=0$$

$C_\alpha=C_\alpha(z,N,...)$
$T=T(z,N,...)$
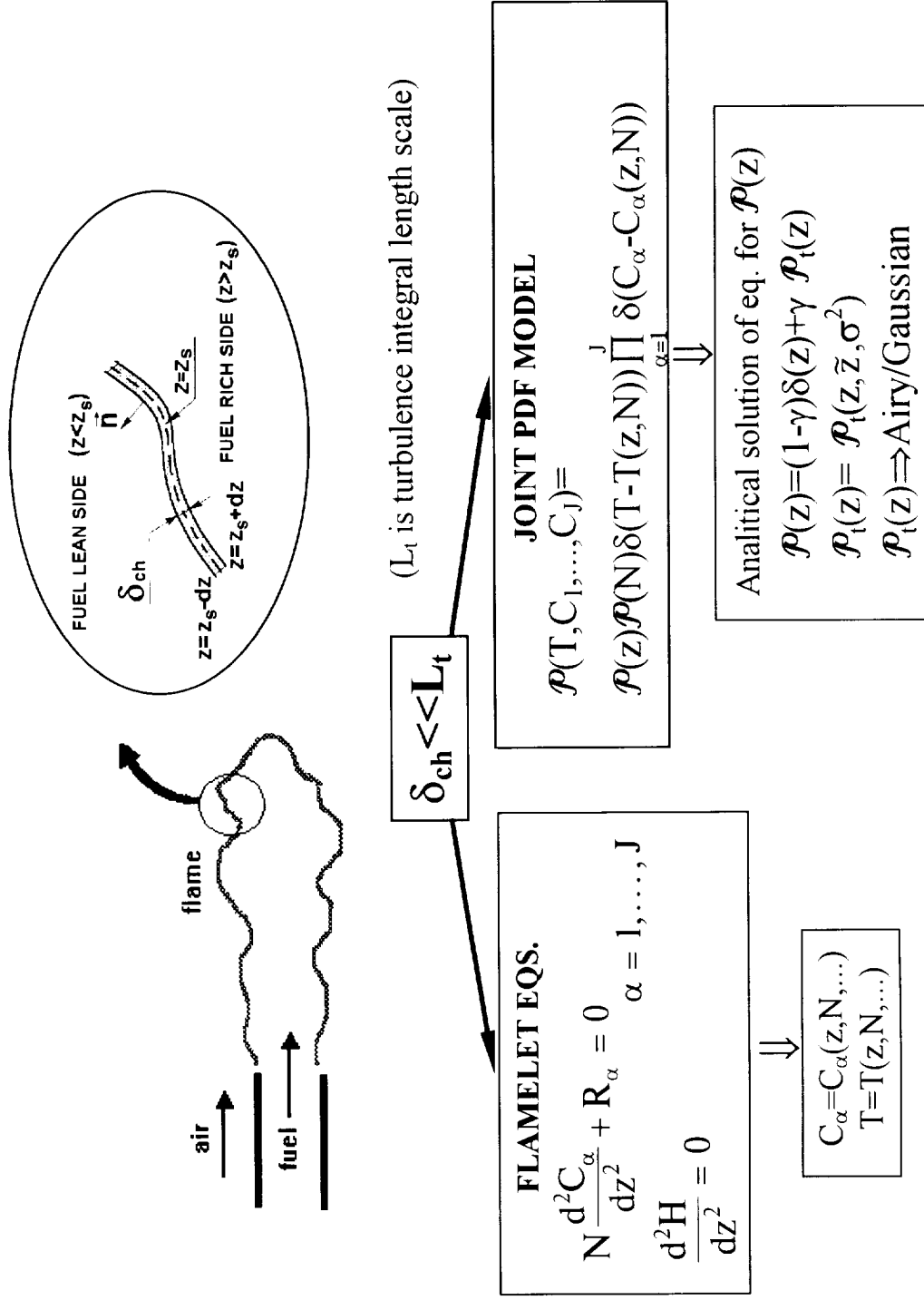
Fig.1. Schematic of the flamelet approach.

- *FOUR PARAMETRIC DEPENDENCE* $C\alpha=(z,N,P,U^2/2,\text{boundary conditions})$
  $\Downarrow$
  $(U-U_a)/(U_f-U_a) \approx z^{\beta}$
  $\Downarrow$

FL LIBRARY $\Leftarrow$ $C\alpha=(z,N,P,\text{boundary conditions})$

- *INCORPORATION TO CFD SOLVER*

FL LIBRARY $C_\alpha=C_\alpha(z,N,P)$ → AVERAGING $\Rightarrow$ $\overline{\Gamma},\overline{Q}$ → CFD SOLVER

$$\overline{h} = \left(\frac{\overline{\Gamma}}{\overline{\Gamma}-1}\right)\frac{\overline{P}}{\overline{\rho}}+\overline{Q}$$

$\overline{z},\sigma^2,\overline{N},\overline{P}$

- *IGNITION DELAY DISTANCE*

air
fuel
MIXING (FL is valid)
SELF-IGNITION REGION (FL is not valid)
FLAME FRONT (FL is valid)

- *FLAMELET MODEL FORMALIZATION*

air
fuel
MIXING (FL is valid)
$\overline{N} < N_{cr}$
FLAME FRONT (FL is valid)
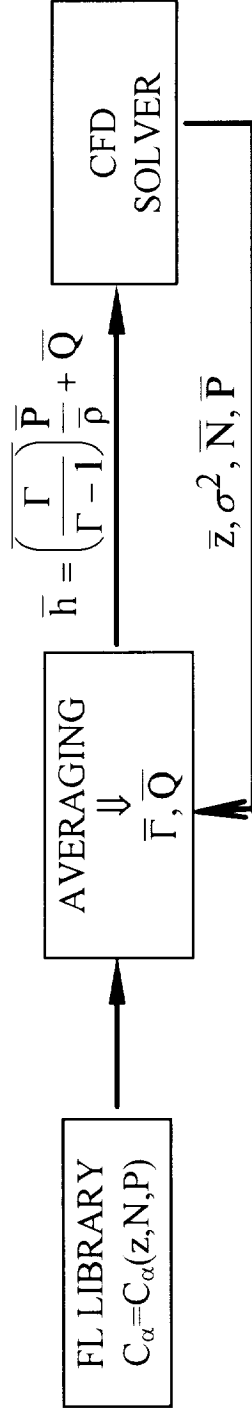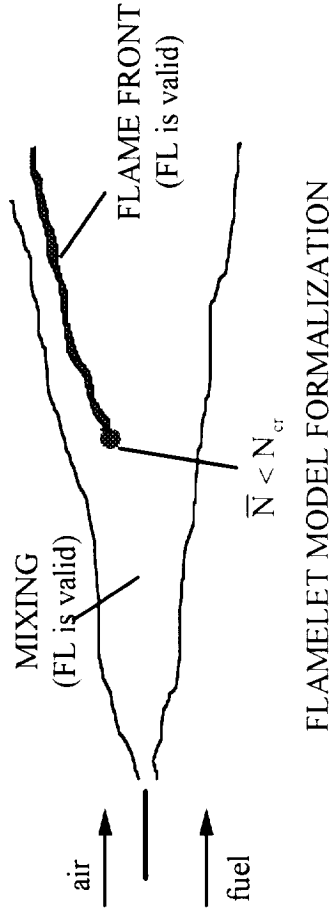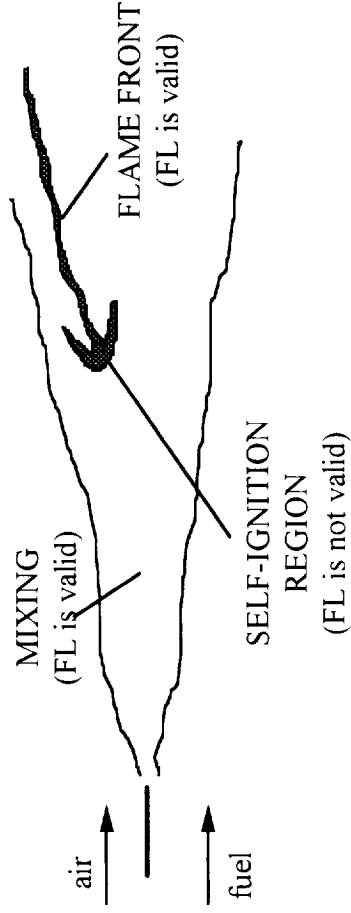
Fig.2. Features of the FL application to supersonic flames.
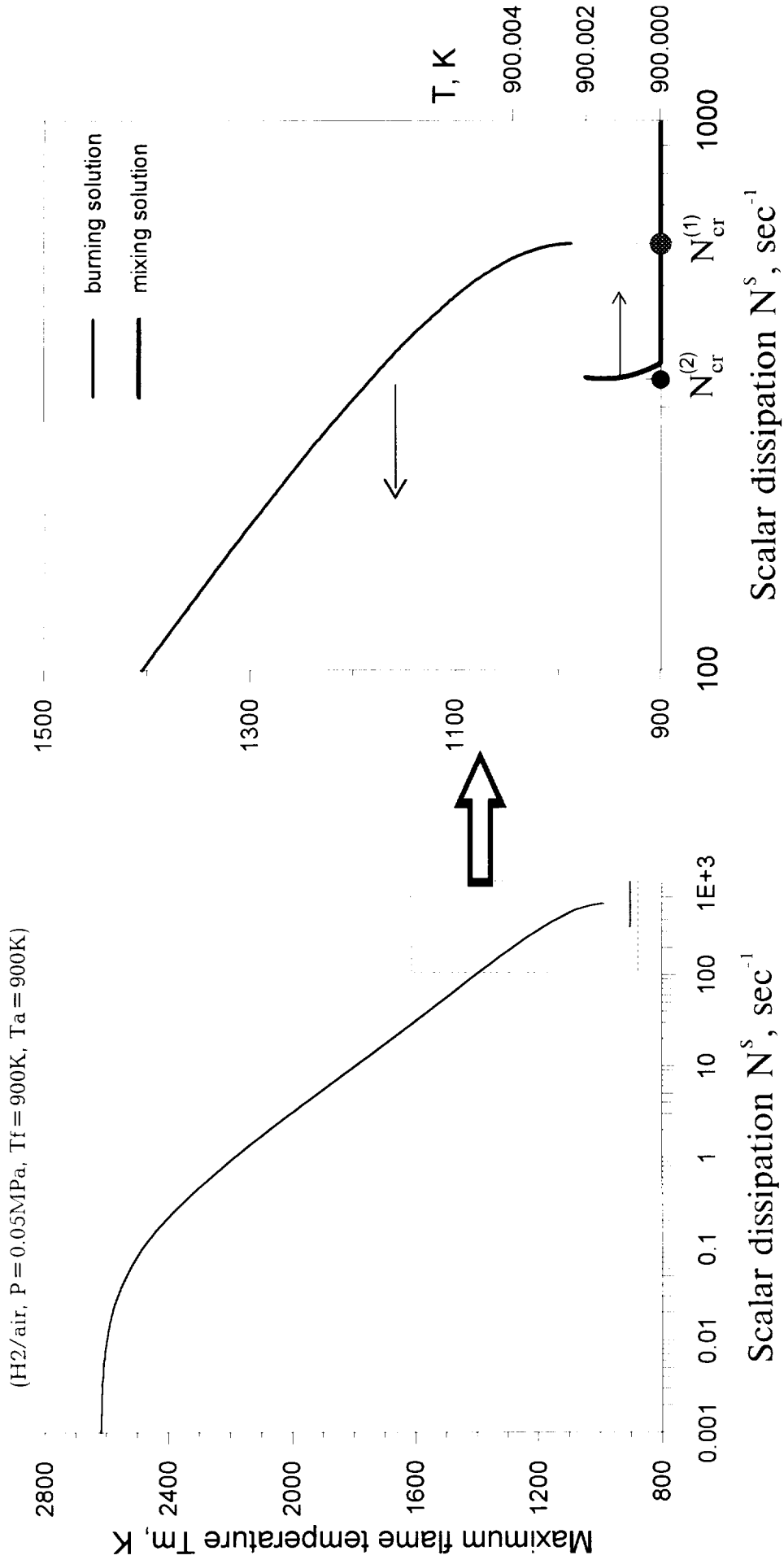
Fig.3. Ignition/extinction behaviour of flamelet model.

a) Beach experiment

b) Burrows-Kurkov experiment
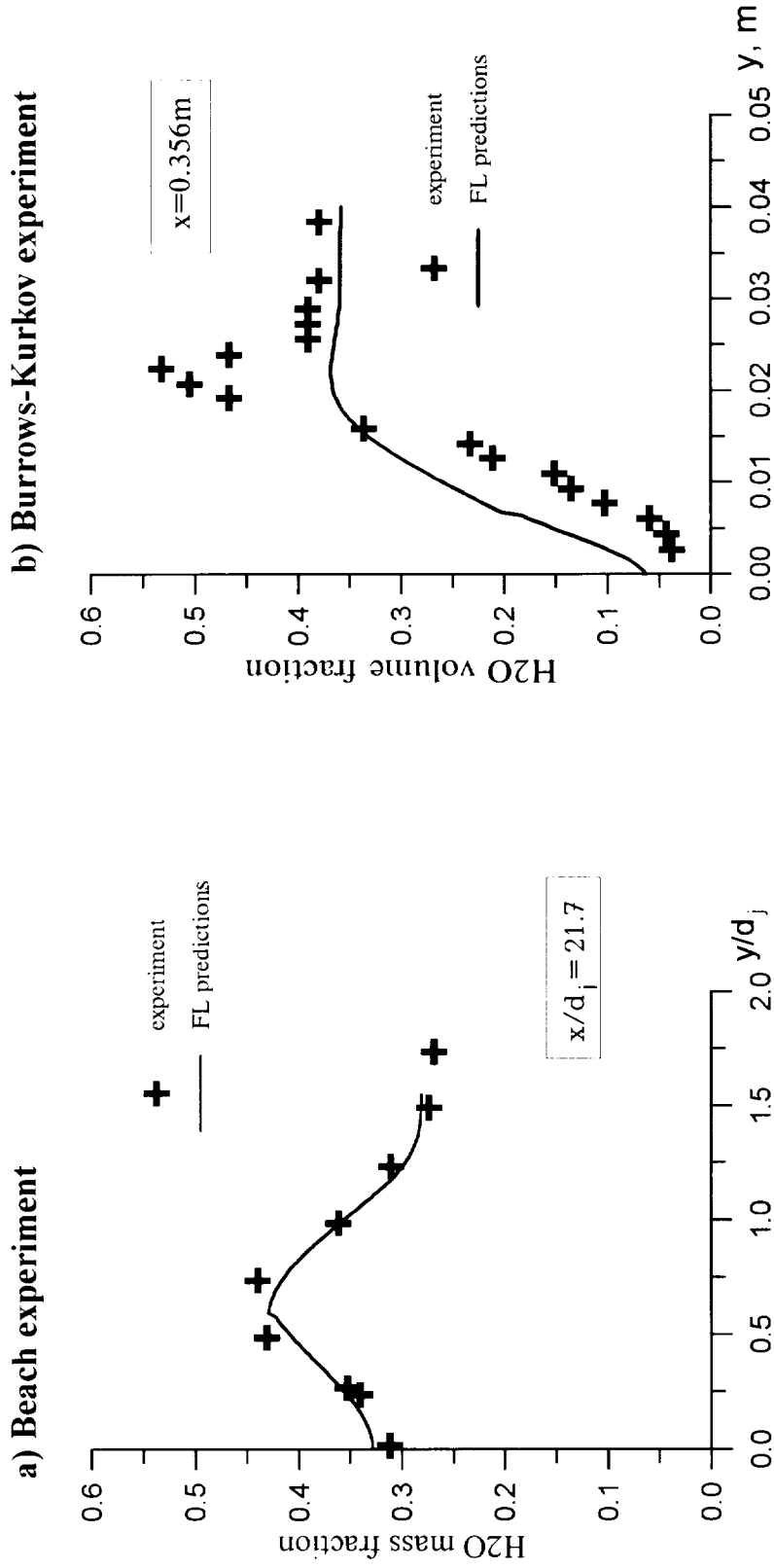
Fig.4. Accuracy of previous FL predictions.
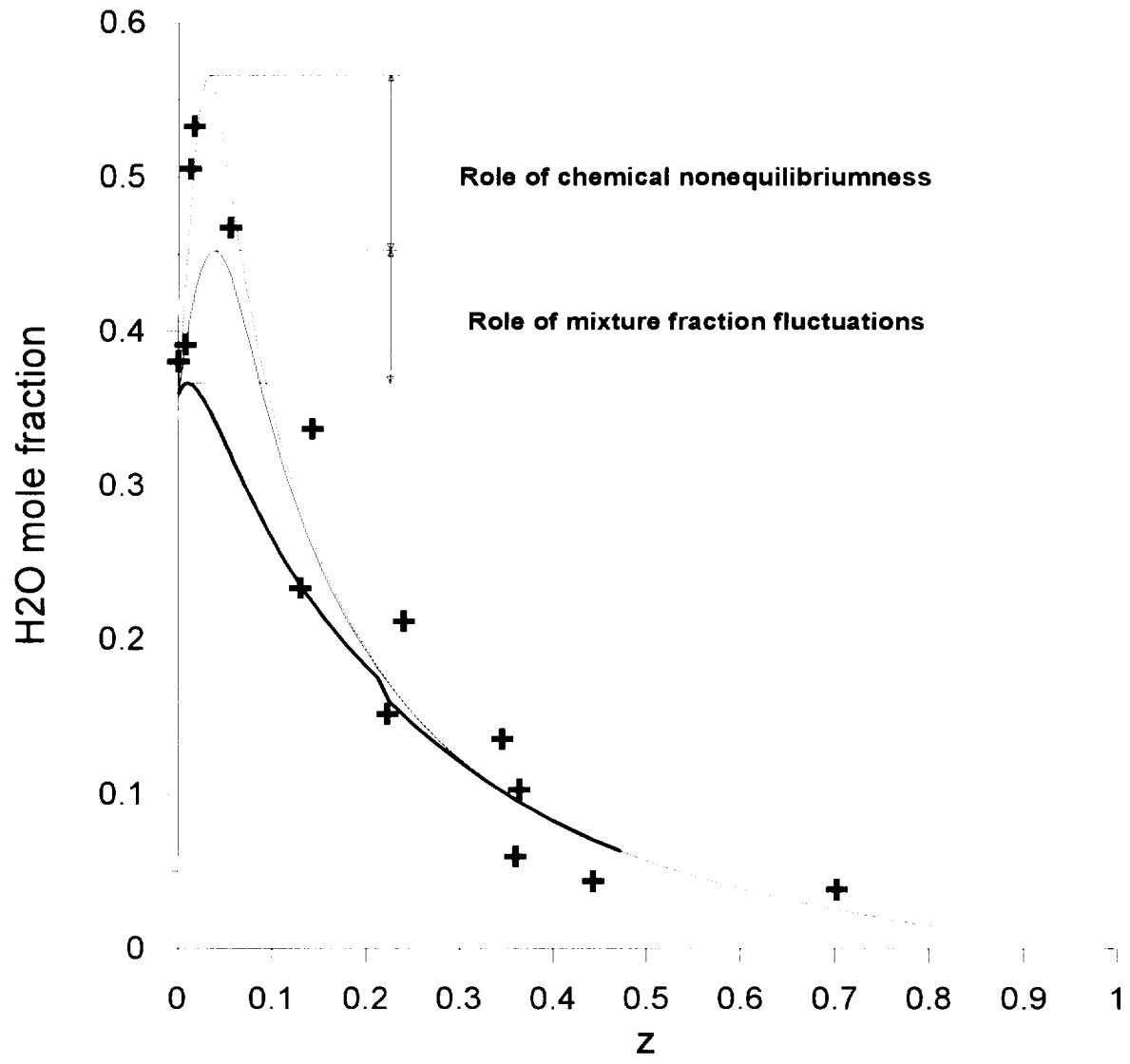
Fig.5. Relative role of the chemical nonequilibriumness/mixture fraction fluctuations
in previous FL approach predictions budget.

——————— Flamelet averaged solution.

·—————· Flamelet instantaneous solution.

············· Equilibrium chemistry limit

✚ Experimental data

Burrows-Kurkov test case.
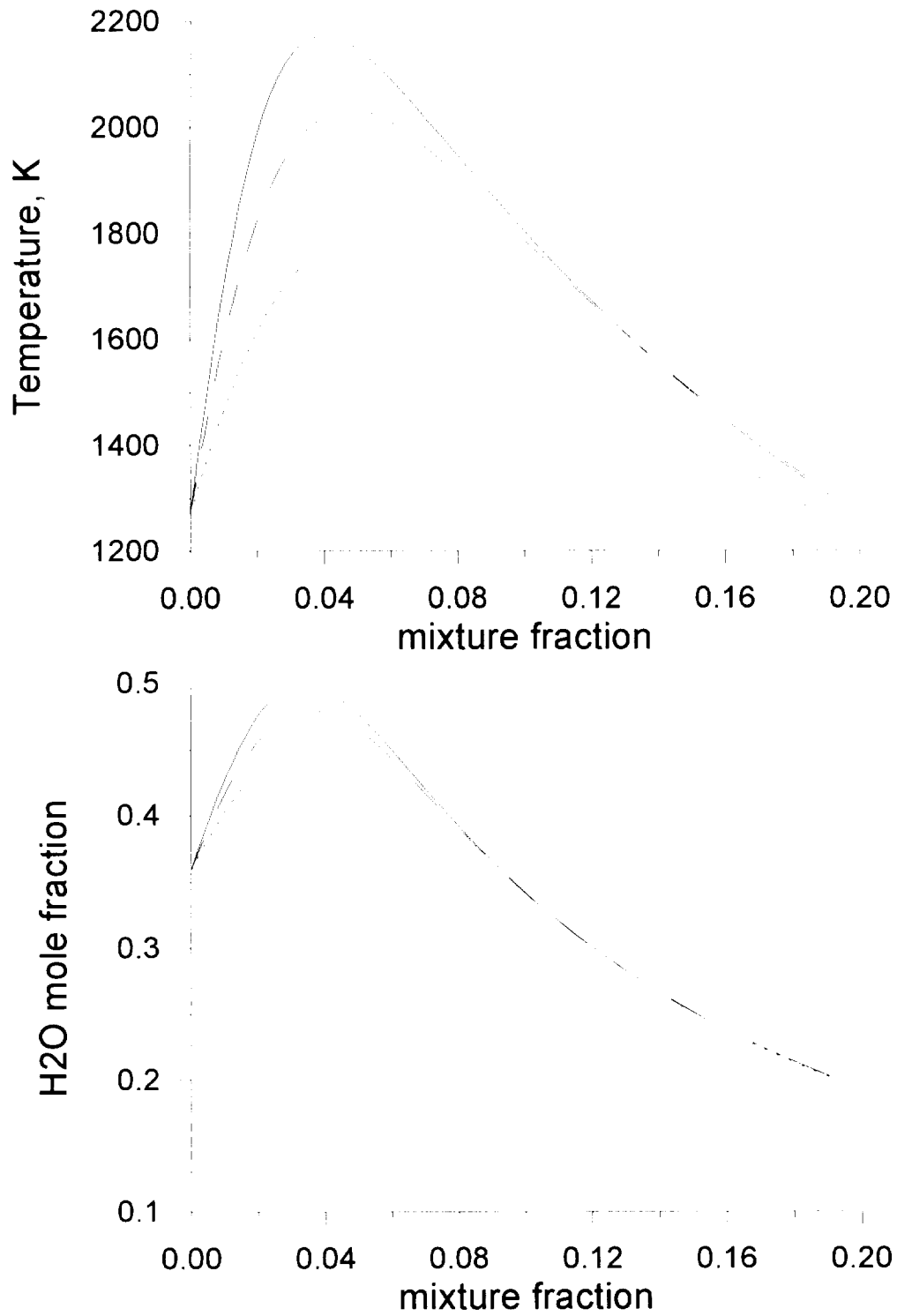
Fig.6. Tests of detailed chemistry model.

Miller & Bowman scheme (ignoring third body efficiences)

Miller & Bowman scheme (selective third body efficiences)

Jachimowski scheme

Conditions of Burrows-Kurkov test case.

$N^s = 30 \text{ sec}^{-1}$

Fig.7. Scheme and conditions of Burrows and Kurkov experiment.
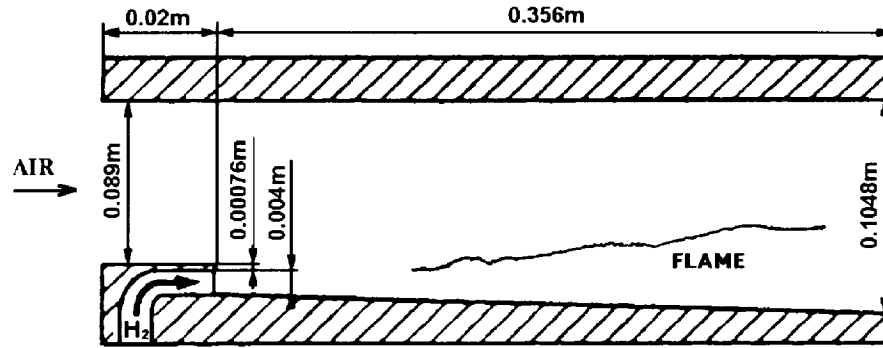
	Hydrogen jet	Air stream
Mach number, M	1.00	2.44
Temperature, T, K	254	1270
Velocity, U, m/s	1216	1764
Pressure, P, MPa	0.1	0.1
Mass fractions:		
C_{H2}	1.000	0
C_{O2}	0	0.258
C_{N2}	0	0.486
C_{H2O}	0	0.256
C_{OH}	0	*1.0e-5*[*)]
C_{NO}	0	*2.8e-4*

*) Expected values are *italic*. They were obtained from equilibrium calculations.
Species with mass fraction less than 10^{-5} are not shown.
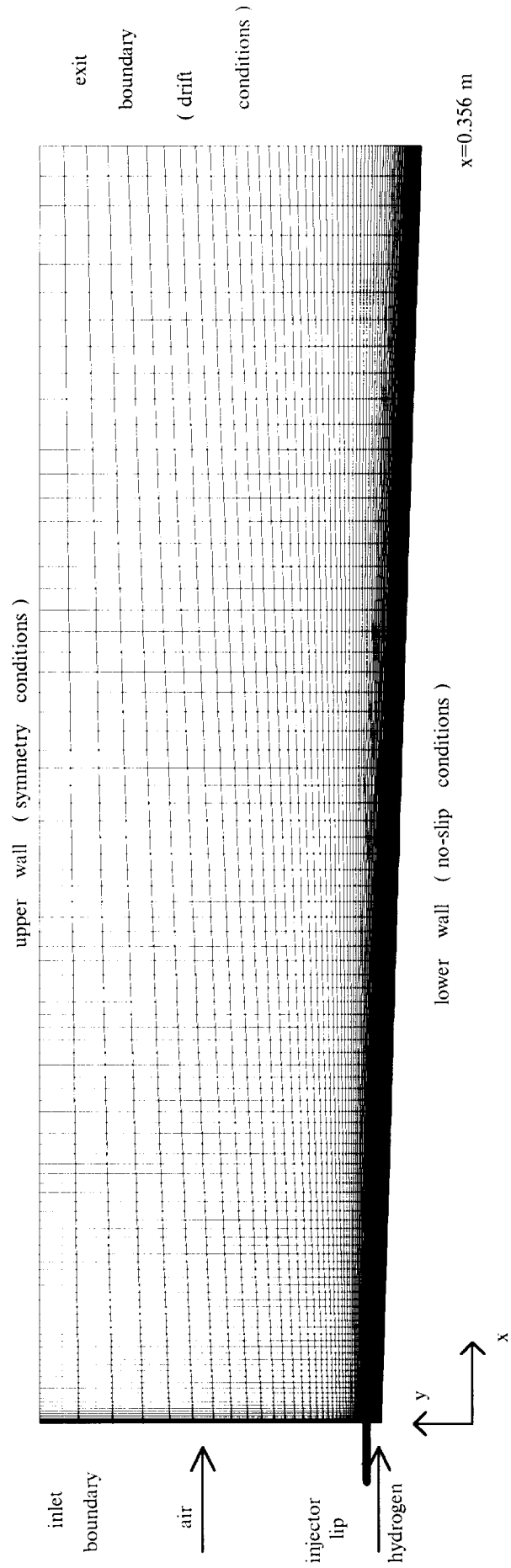
Fig.8. Computational domain together with grid (100x90 cells)

Burrows - Kurkov Test Case
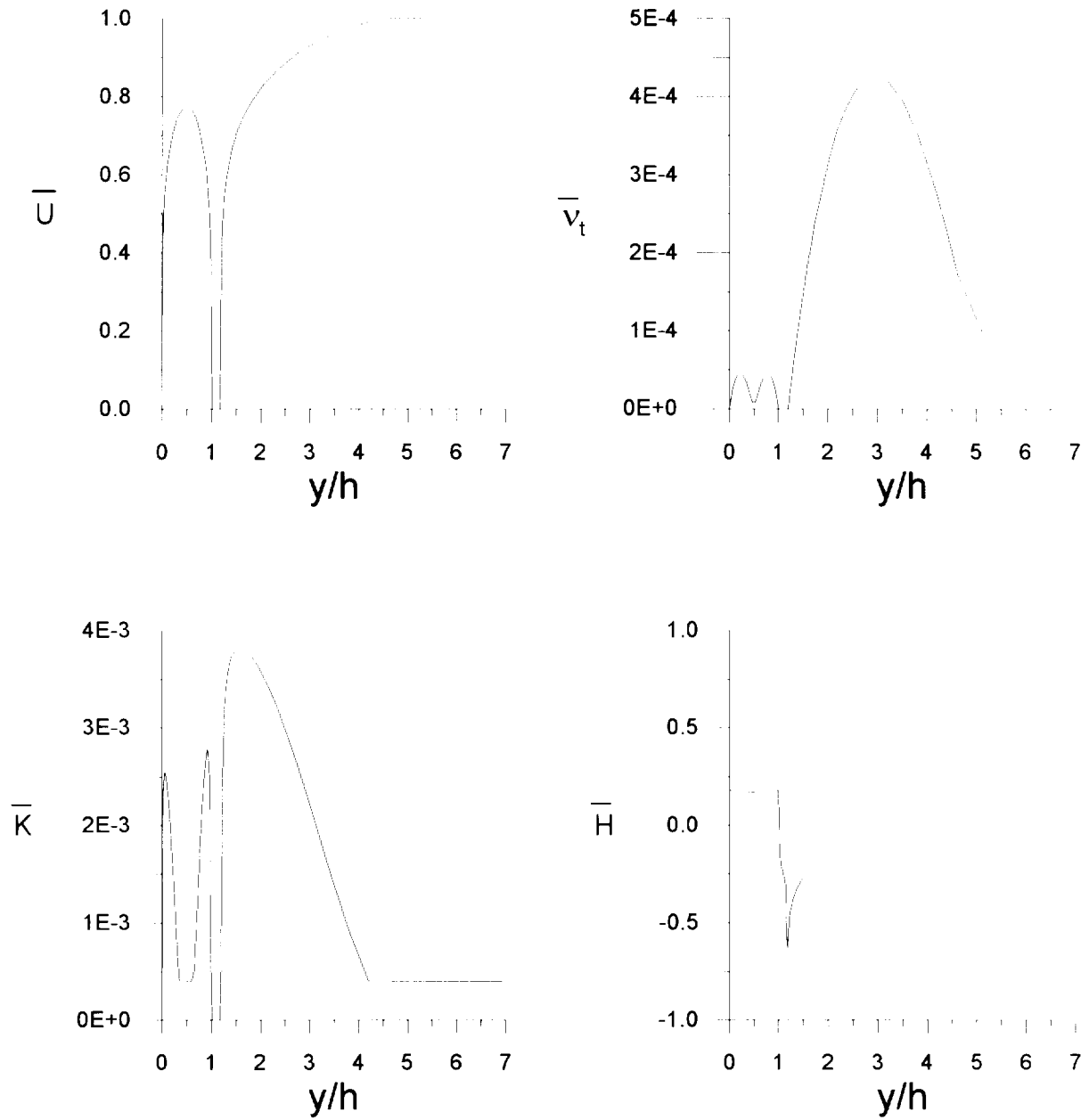
Fig.9. Inflow parameters

Burrows-Kurkov test case

2.700

2.567	
2.362	
2.138	
1.913	
1.688	
1.463	
1.238	
1.019	
0.788	
0.563	
0.338	
0.119	

0.000

x, cm
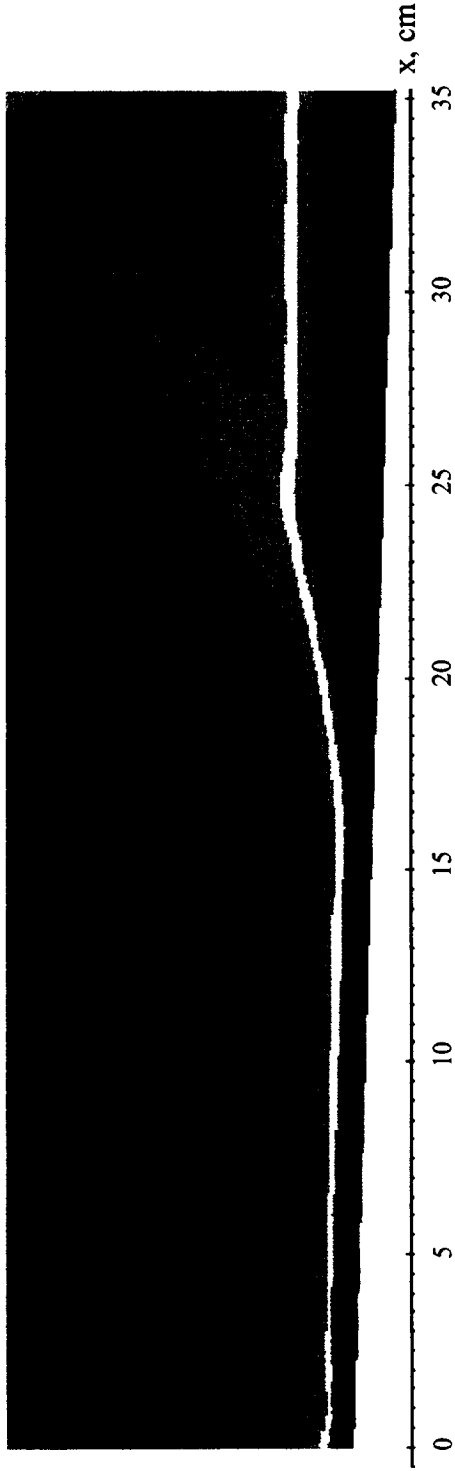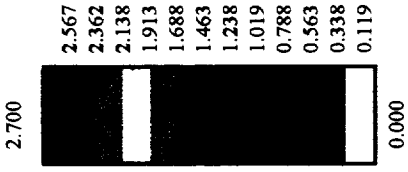
Fig.10. Mach number contours

Burrous-Kurkov test case
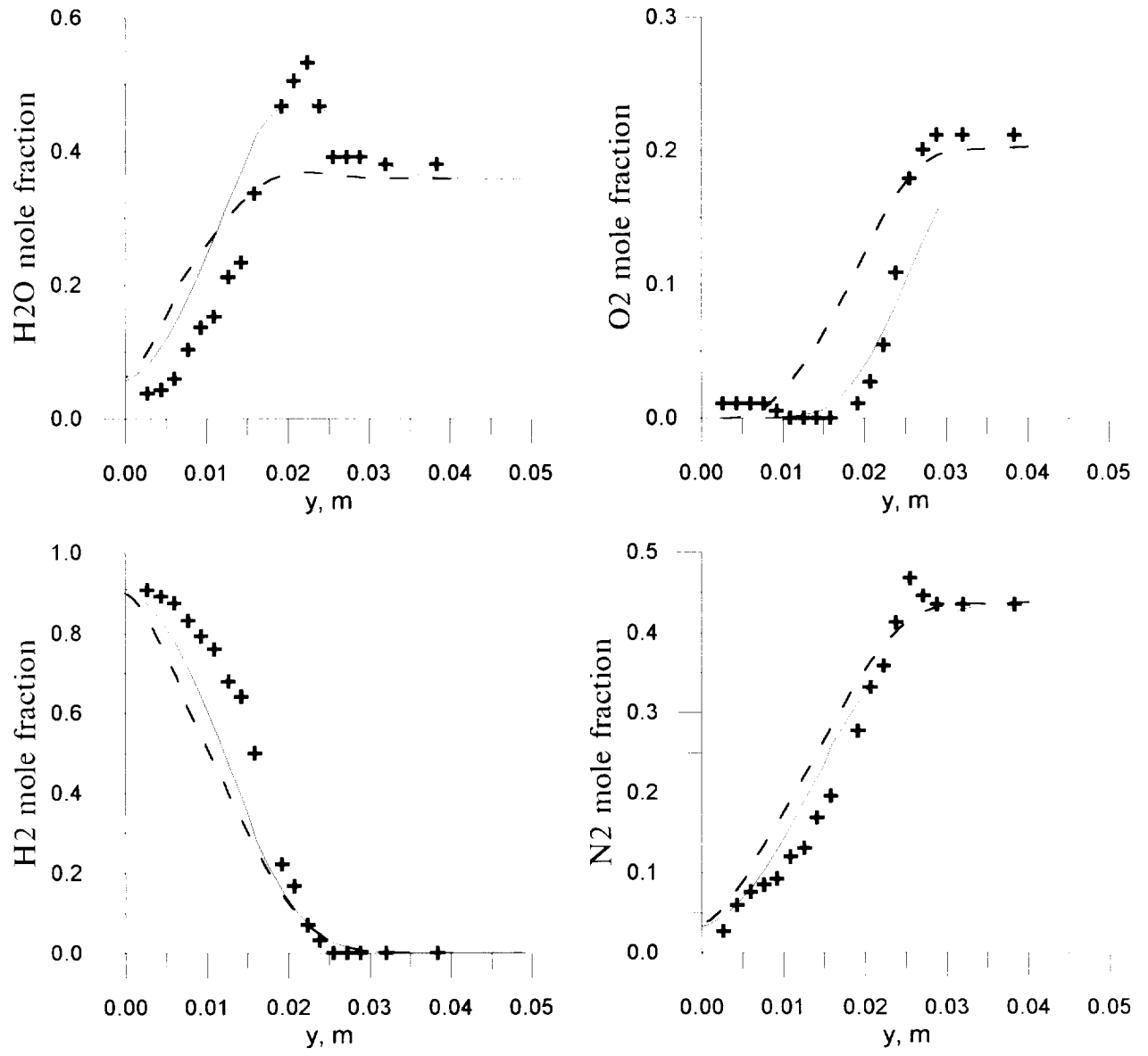
Fig.11. Comparison of FL predictions with experimental data.
x=0.356 m.

———————— current predictions

— — — previous results

✚ experimental data

Burrows-Kurkov test case.
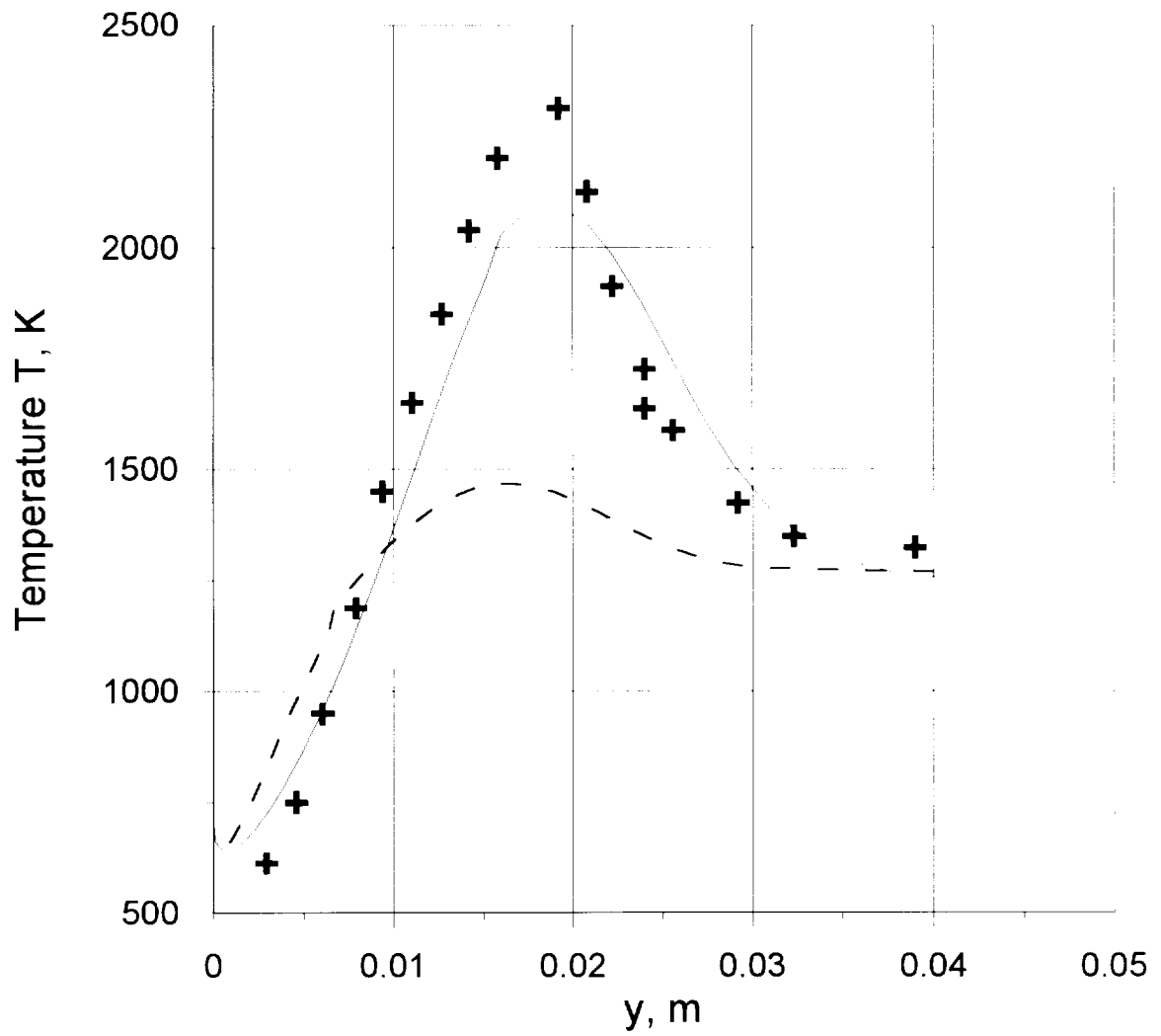
Fig.12. Static temperature profile.
x=0.356 m.

.... current predictions

— — — previous results

+ Experimental data

Burrows-Kurkov test case.

CURRENT PREDICTIONS

PREVIOUS RESULTS

Role of chemical nonequilibriumness

Role of mixture fraction fluctuations

Role of chemical nonequilibriumness

Role of mixture fraction fluctuations

H2O mean mole fraction

Z
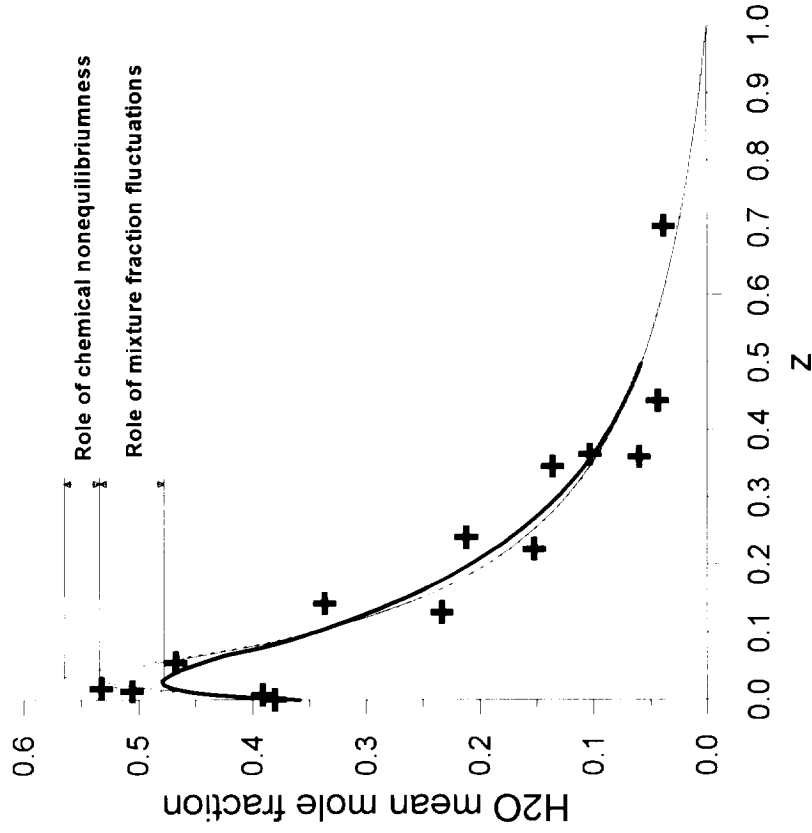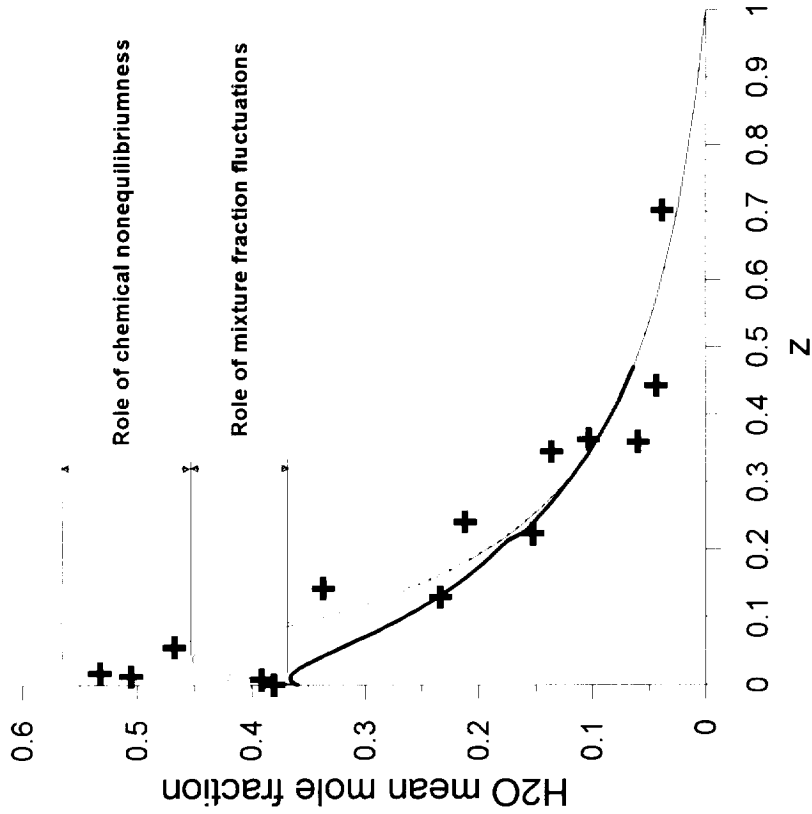
Fig.13. Relative role of the chemical nonequilibriumness/mixture fraction fluctuations
in FL approach predictions budget.
x=0.356 m.

——— Flamelet averaged solution.

·········· Flamelet instantaneous solution.

— — Equilibrium chemistry limit

+ Experimental data

Burrows-Kurkov test case.
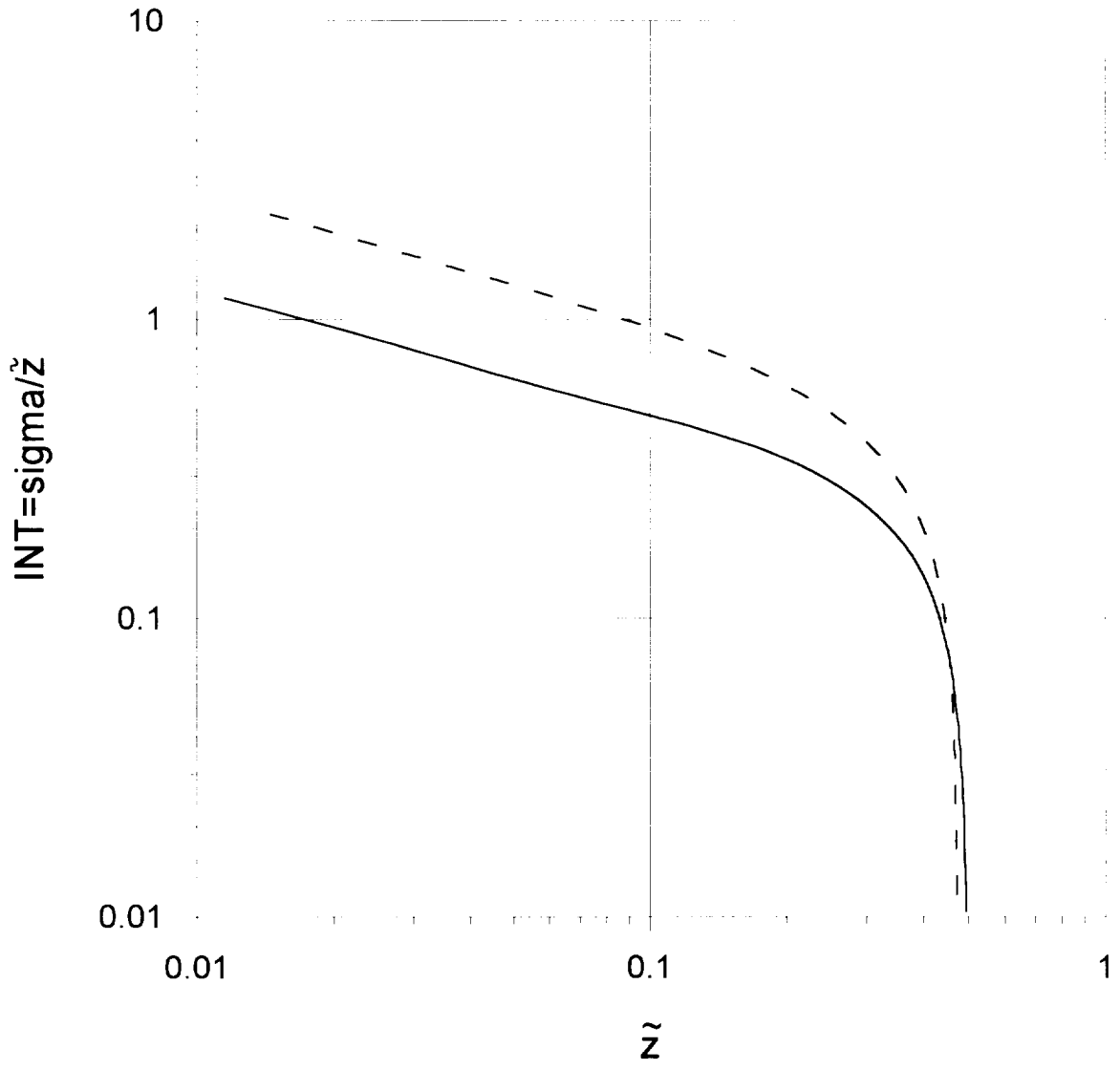
Fig.14. Mixture fraction fluctuations intensity v.s. mean mixture fraction $\tilde{z}$.
x=0.356 m cross section.

——————— current modeling

— — — previous results

Burrows-Kurkov test case.

Cut from computational region

a) Mean mixture fraction:

.001

old calculations

current calculations

b) Mixture fraction variance:

.010

.010

old calculations

.010

current calculations

c) Turbulent kinetic energy:

.001

.001

.001

old calculations

.001

current calculations
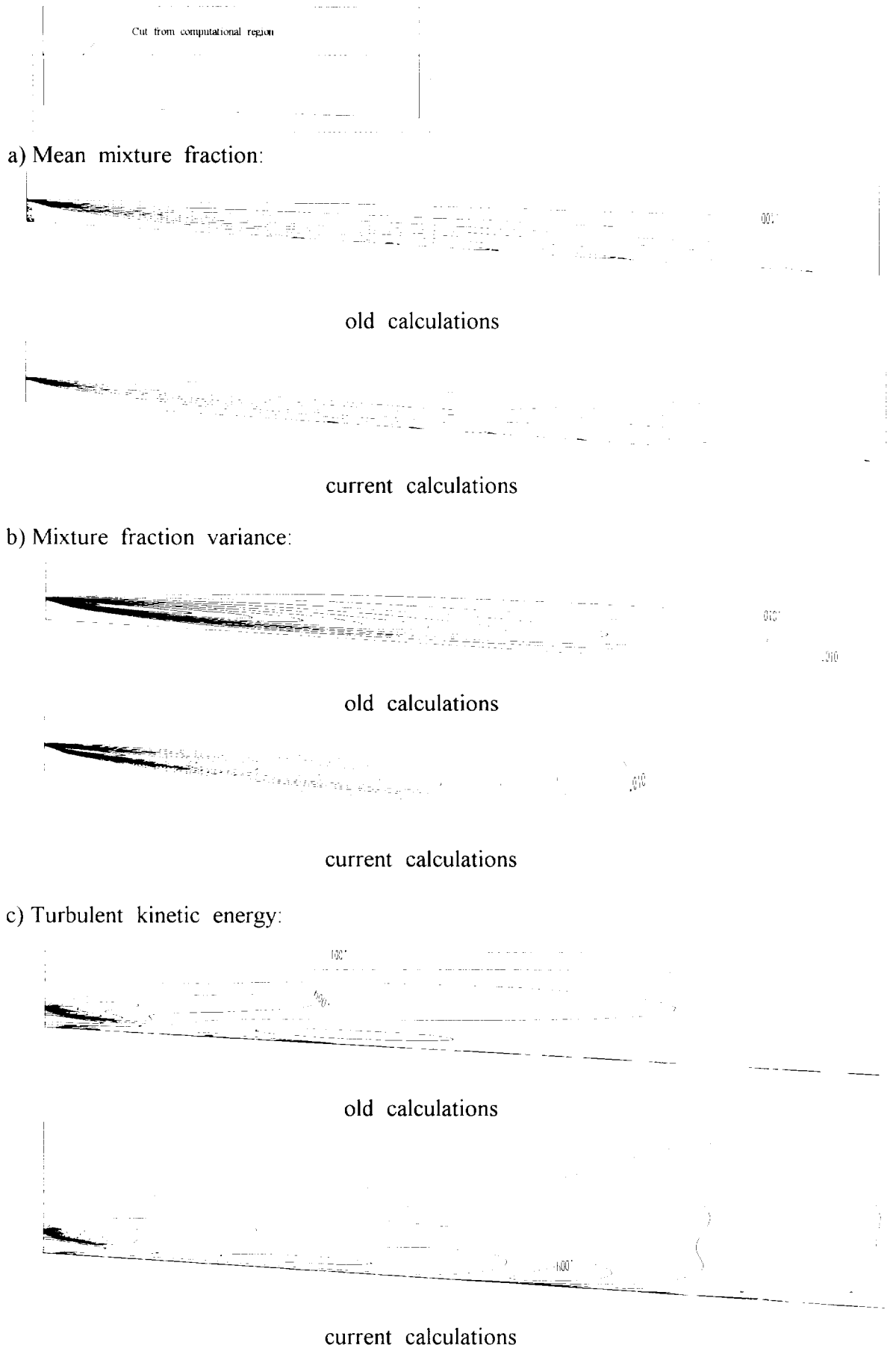
Fig. 15. Turbulence characteristics

Burrous-Kurkov test case
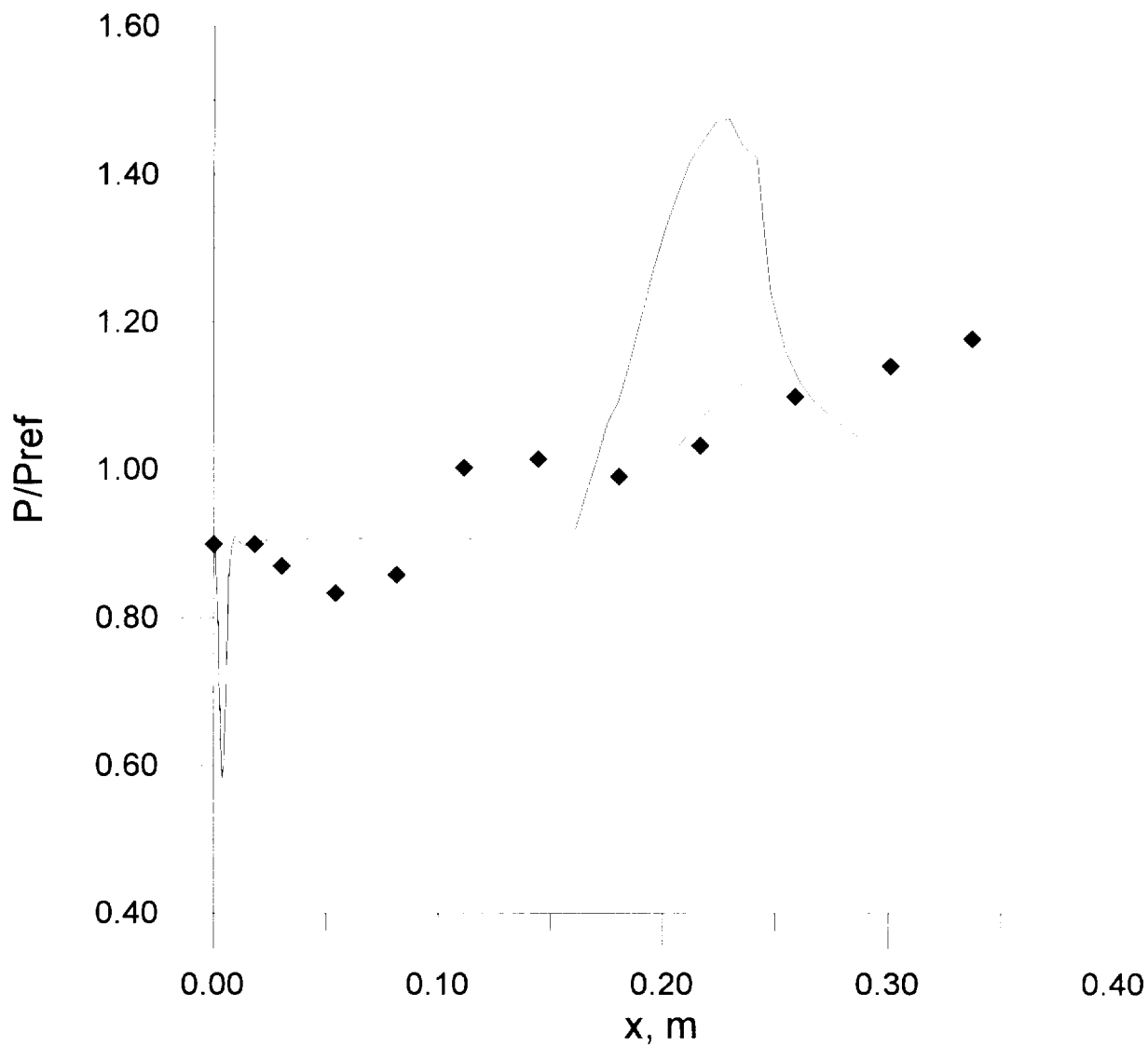
Fig.16. Wall pressure distributions

◆ experimental data

FL approach with small smoothing

FL approach with large smoothing

Burrows-Kurkov test case

D = 0.0653 m
d_j = 0.009525 m
Injector lip thickness = 0.0015 m
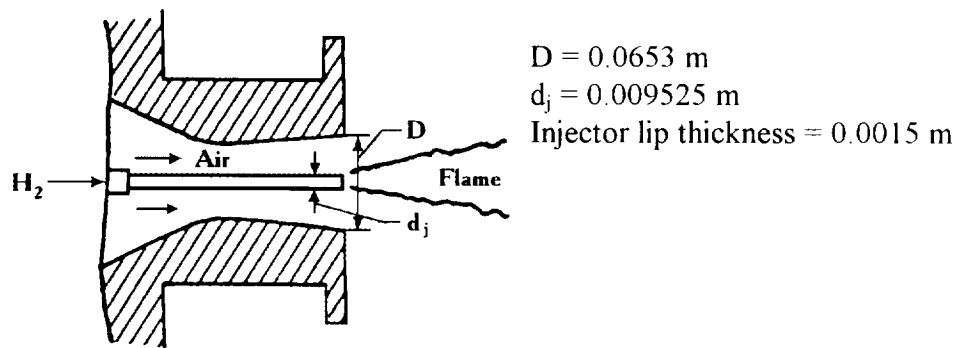
	Hydrogen jet	Free stream
Mach number, M	2.00	1.90
Temperature, T, K	251	1495
Velocity, U, m/s	2432	1510
Pressure, P, MPa	0.1	0.1
Mass fractions:		
C_{H2}	1.000	0
C_{O2}	0	0.241
C_{N2}	0	0.478
C_{H2O}	0	0.281
C_{OH}	*0*	*1.0e-4*[*]
C_{NO}	*0*	*1.0e-3*

Fig. 17. Scheme and conditions of Beach et al. coaxial experiment.

*) Expected values are *italic*. They were obtained from equilibrium calculations.
Species with mass fraction less than 10^{-5} are not shown.
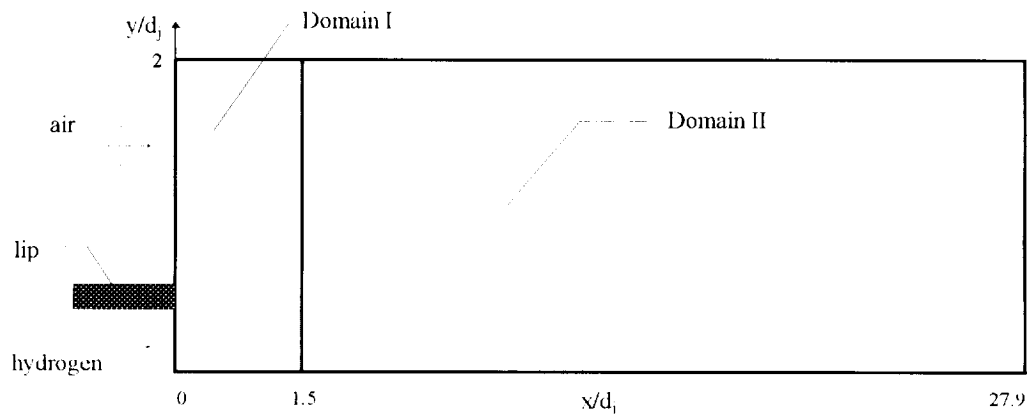
Fig. 18. Schematic of computational domain

Beach test case
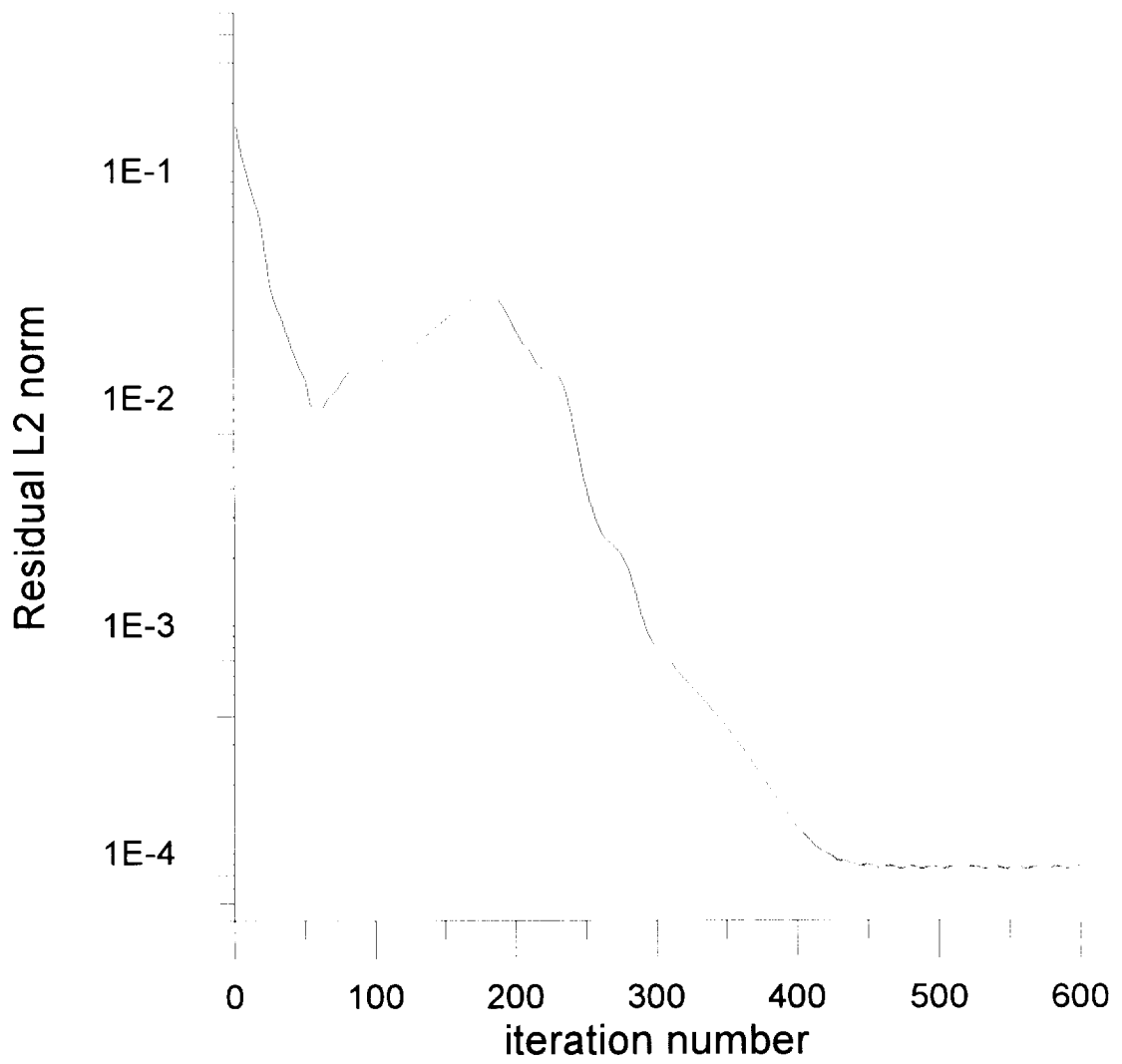
Fig. 19. L2 norm behavior.

Beach test case

y/d₁

x/dⱼ
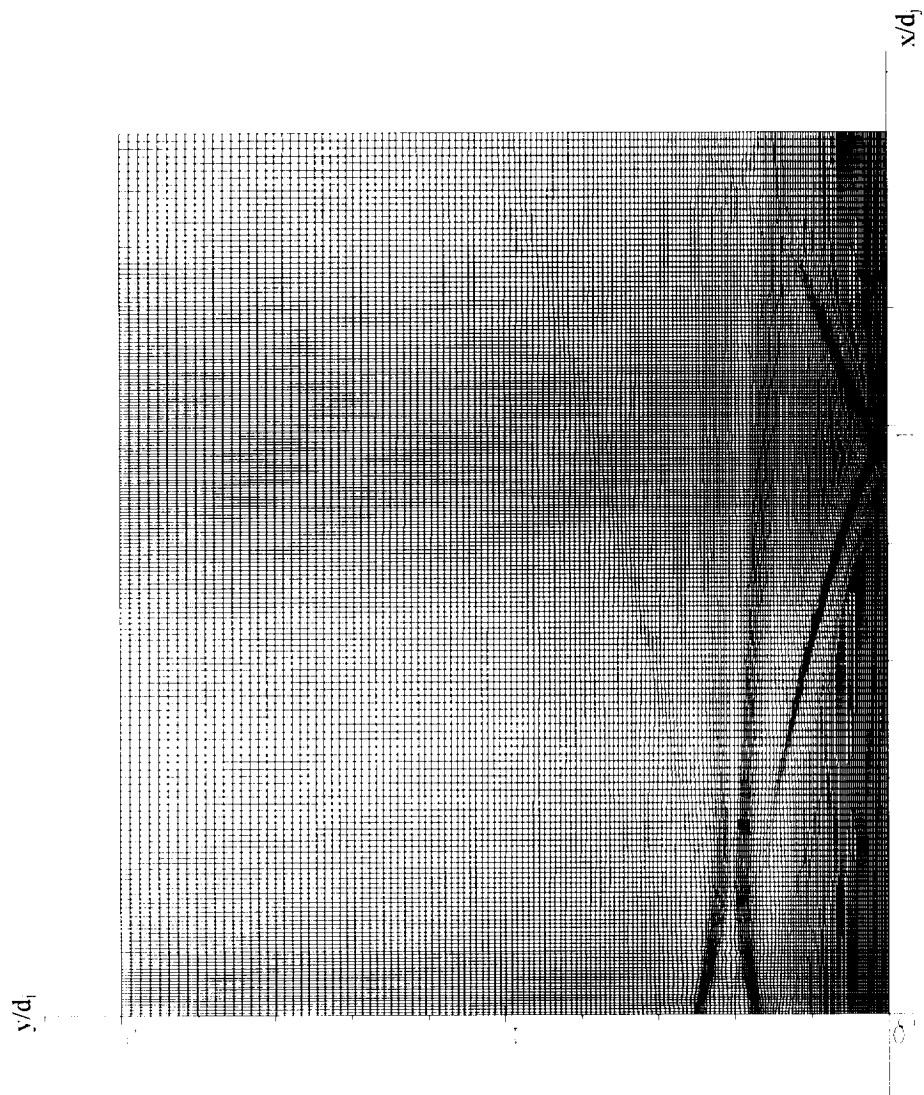
Fig.20. Adaptive grid for Domain I (200x170 cells)

Beach test case

x/d$_j$

y/d$_j$
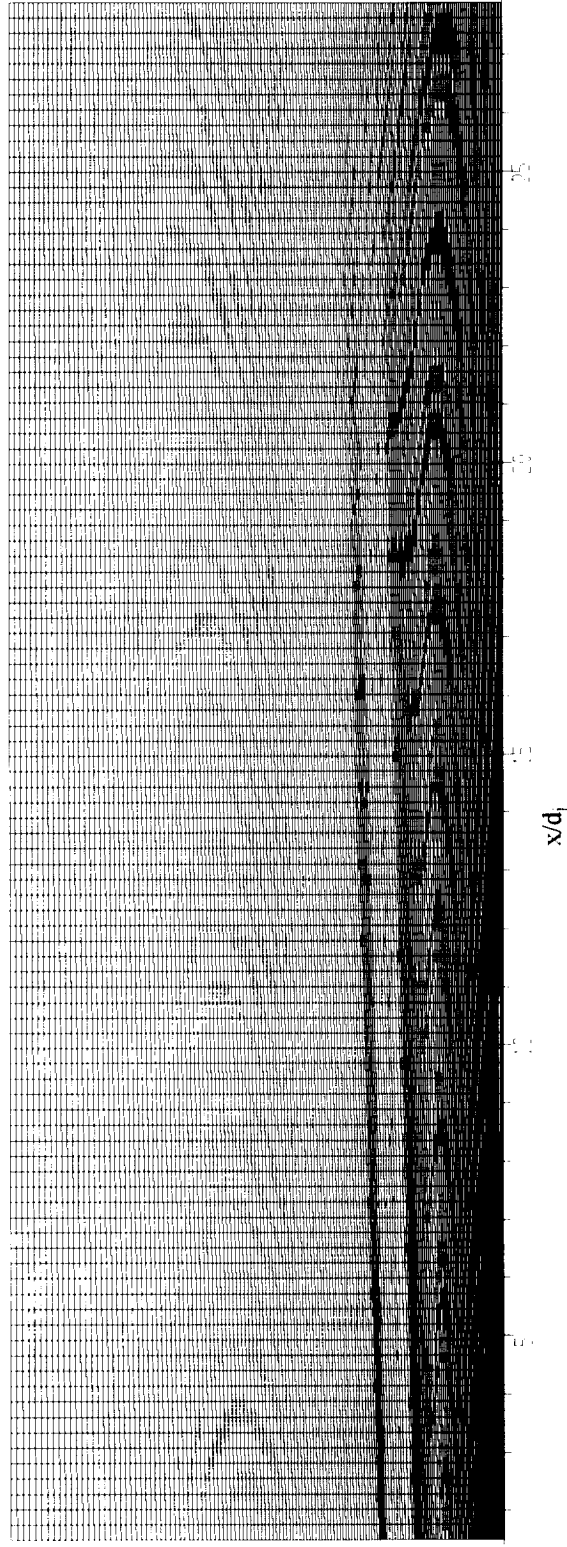
Fig.21. Adaptive grid for Domain II (100x170 cells)

Beach test case

y/d$_i$

2.200

2.129
1.987
1.846
1.704
1.562
1.421
1.279
1.137
.996
.854
.712
.571

.500

x/d$_j$

Mach number contours

y/d$_i$

.170
.160
.150
.140
.135

.170
.160
.260 .250 .240 .230

x/d$_j$
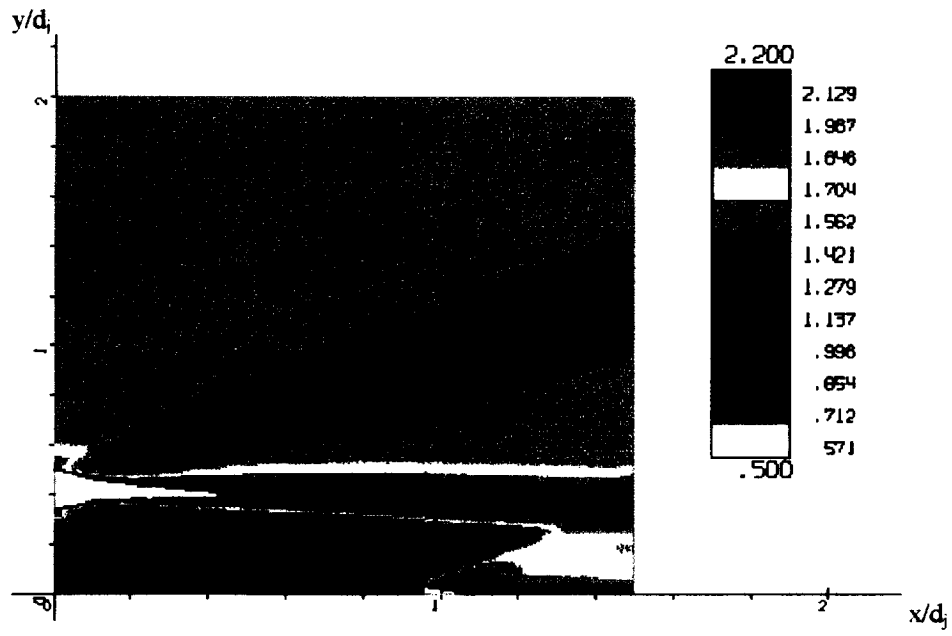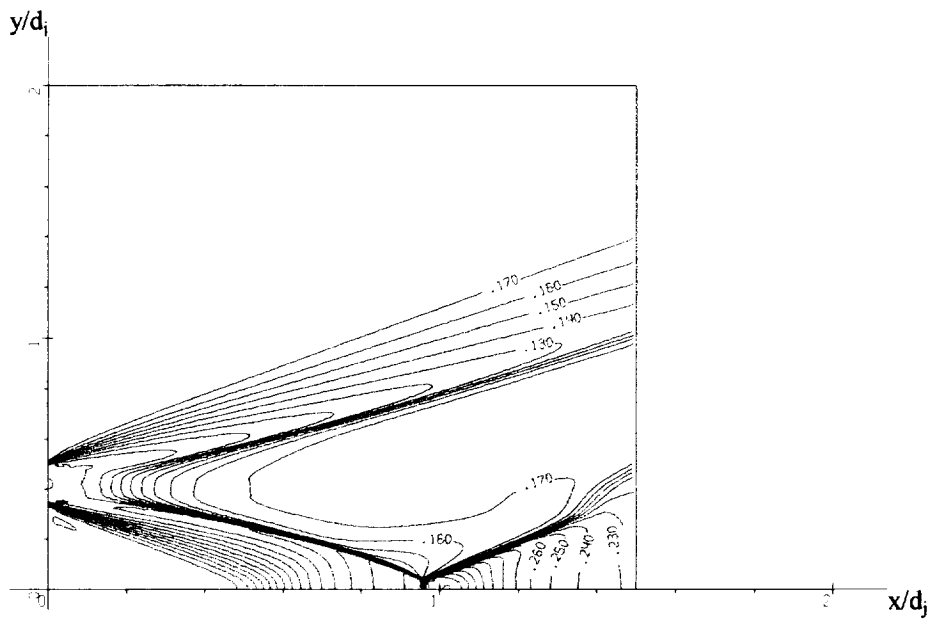
Pressure contours

Fig.22. Flow fields near injector
(Domain I in Fig.18)

Beach test case
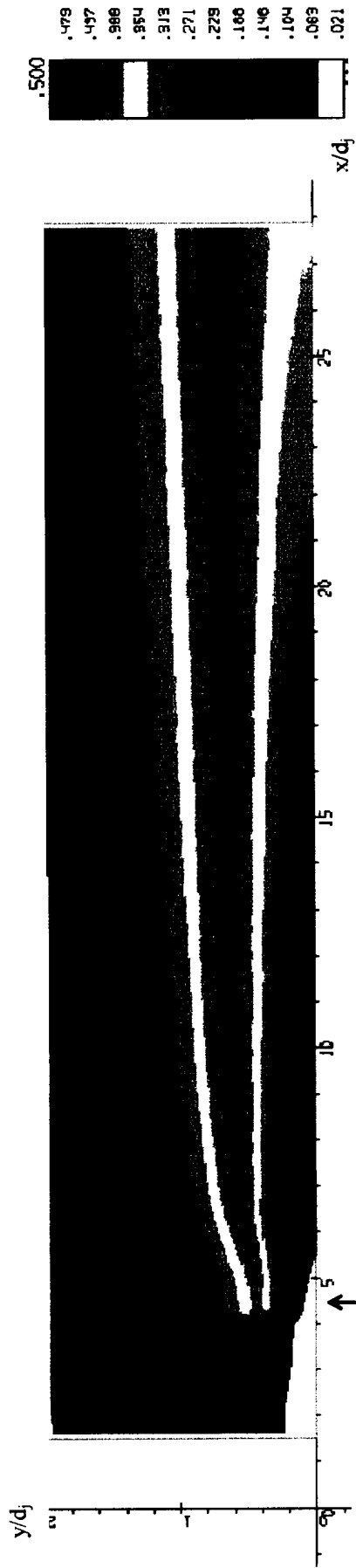
Fig.23. Mean H2O mass fraction contours

self ignition point
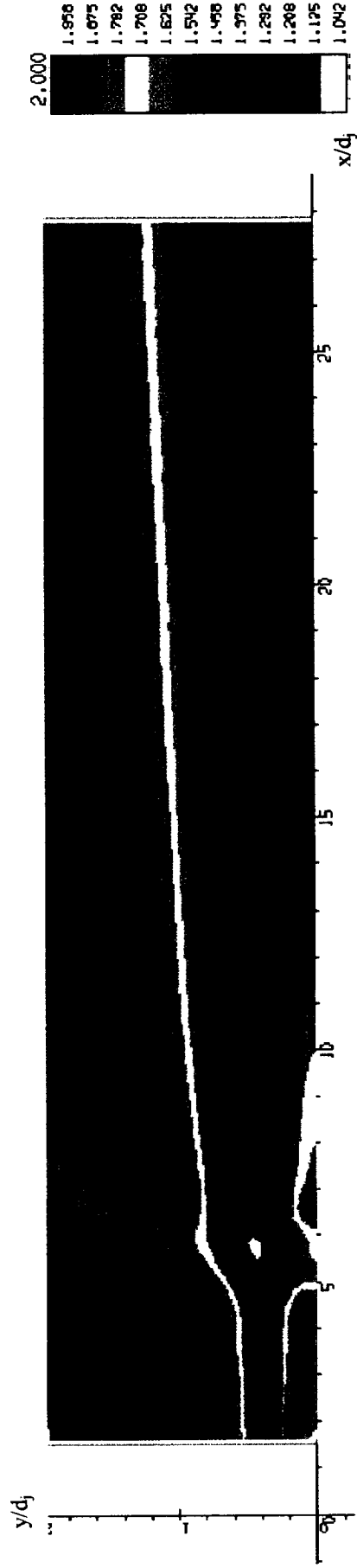
Fig.24. Mach number contours

Beach test case
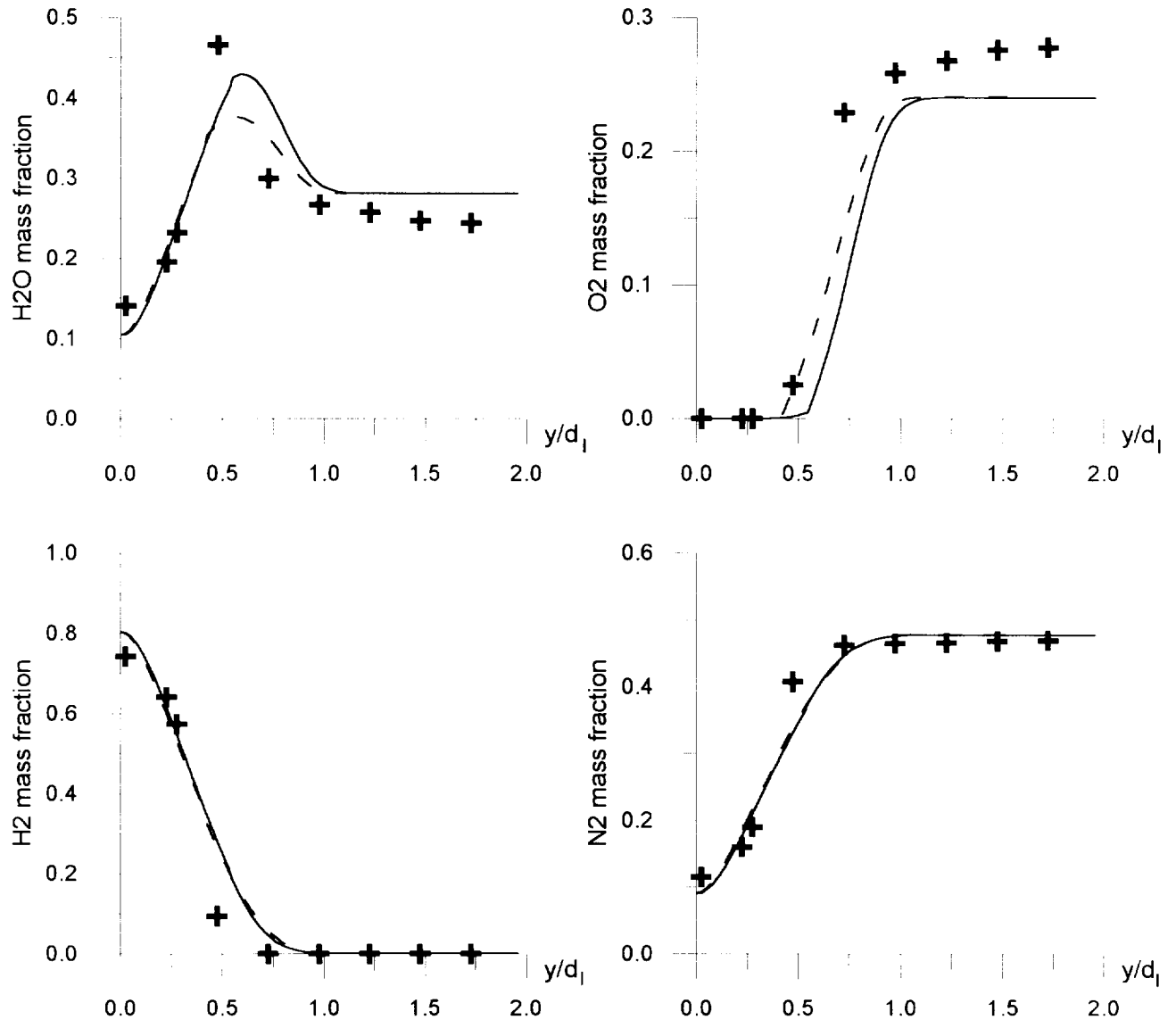
Fig.25a. Comparison of FL predictions with experimental data.

——————— current predictions

— — — previous results

➕ experimental data of Beach et al.

$x/d_I = 8.26$
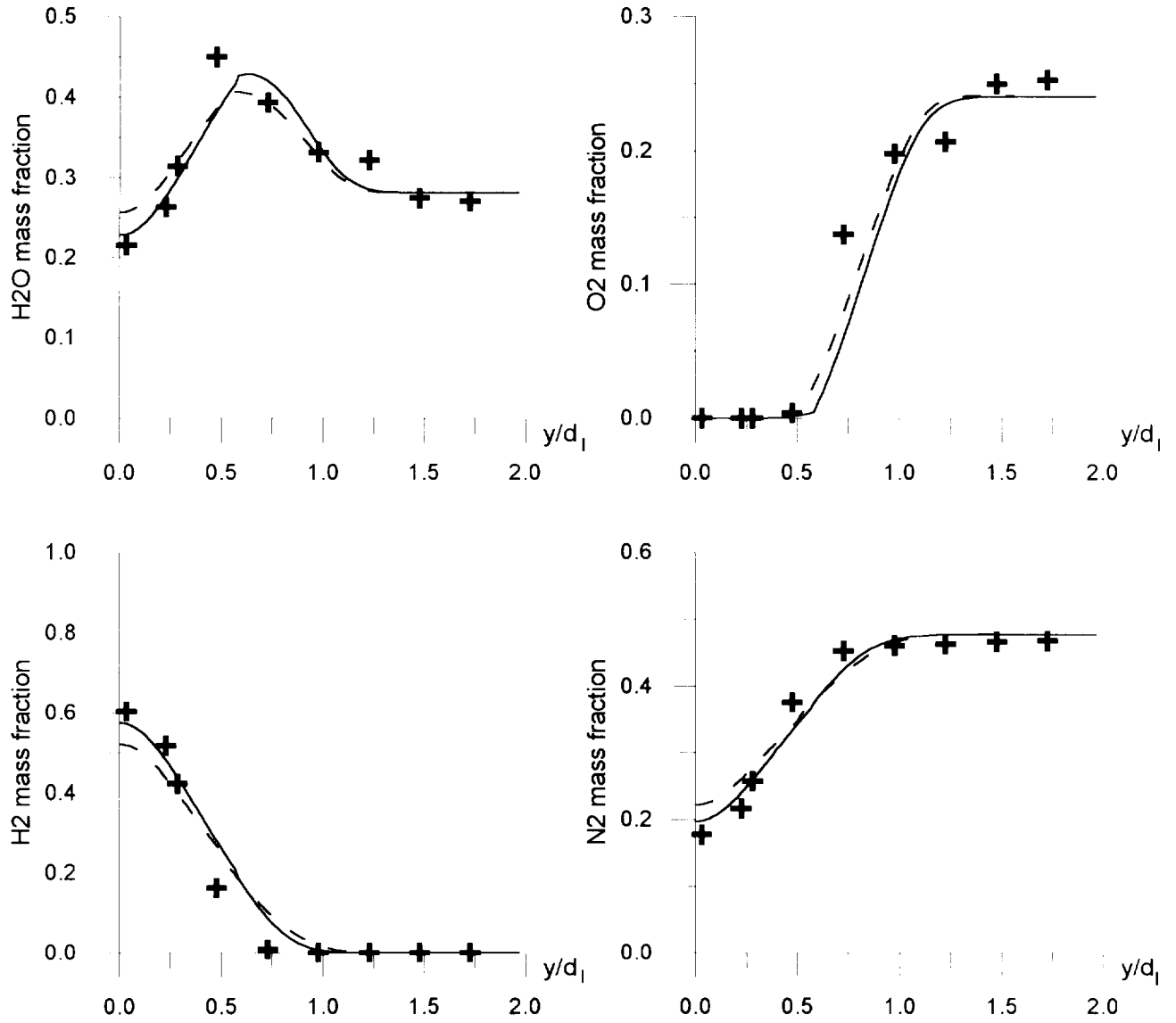
Fig.25b. Comparison of FL predictions with experimental data.

——————— current predictions

— — · previous results

➕ experimental data of Beach et al.

$x/d_1 = 15.5$
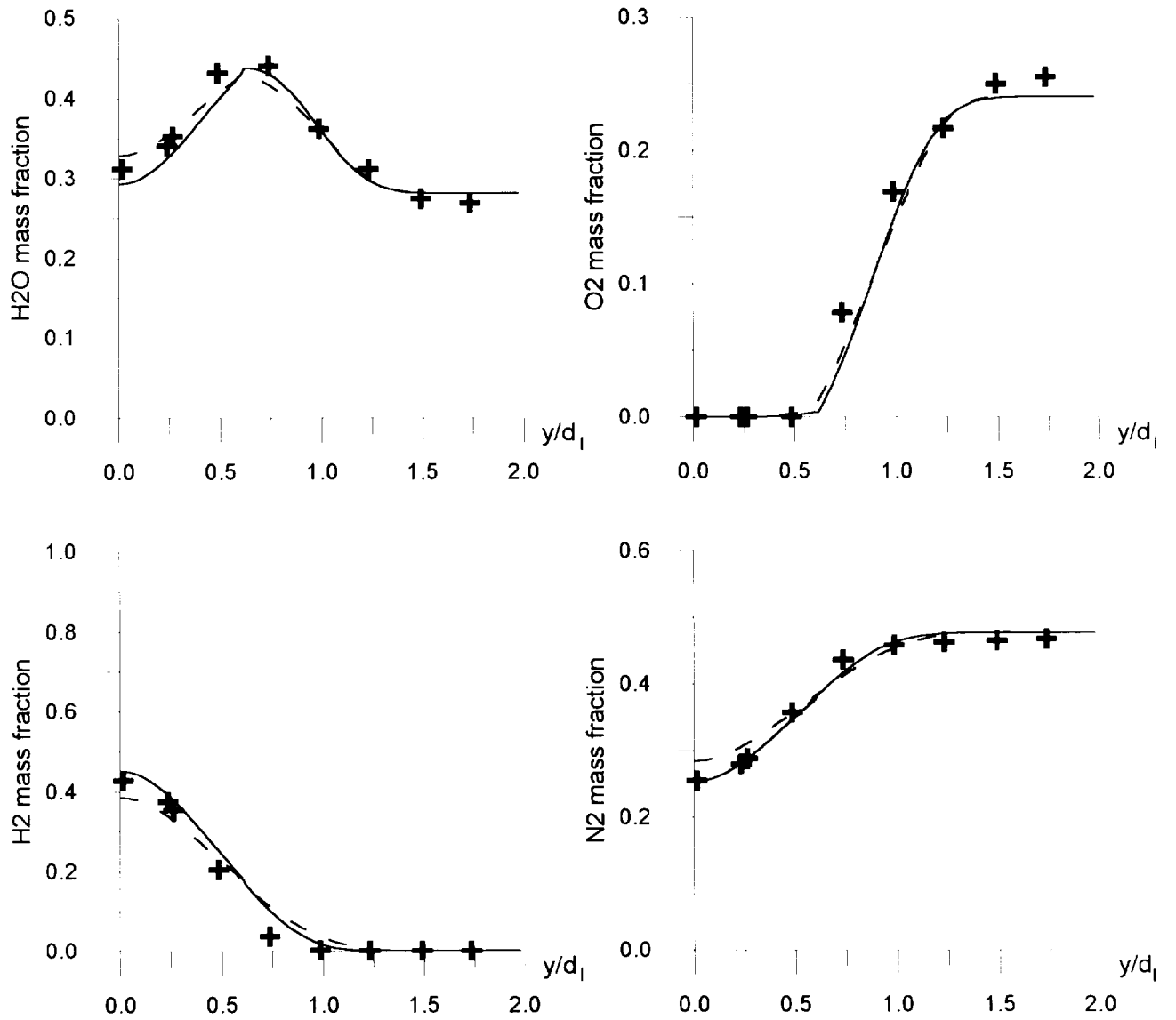
Fig.25c. Comparison of FL predictions with experimental data.

—————— current predictions

— — · previous results

✚ experimental data of Beach et al.

$x/d_l = 21.7$

Fig.25d. Comparison of FL predictions with experimental data.

——————— current predictions

— — · previous results

✚ experimental data of Beach et al.

$x/d_l = 27.9$

D = 0.01778 m
Injector internal diameter d = 0.00236 m
Injector lip thickness = 0.000725 m
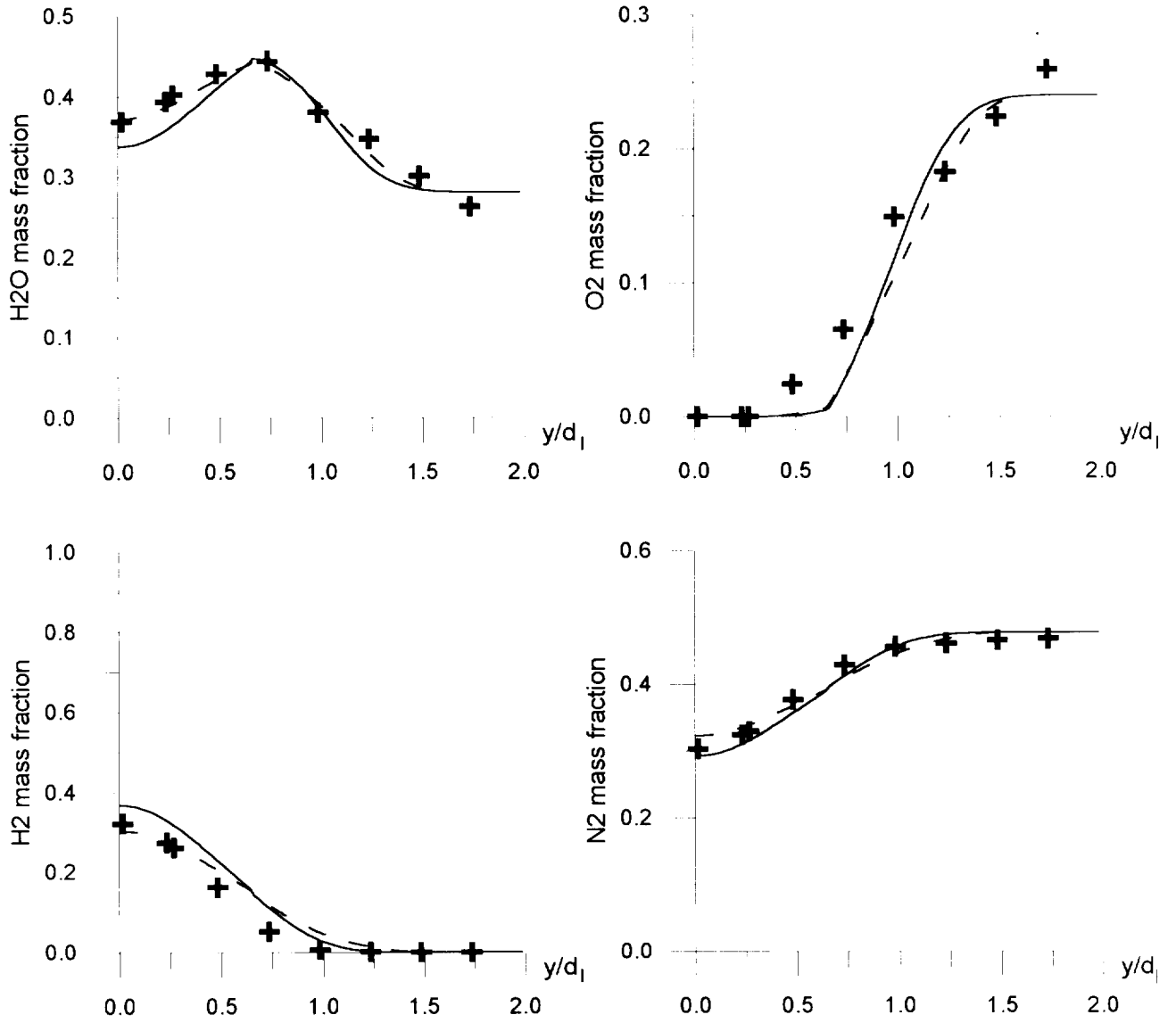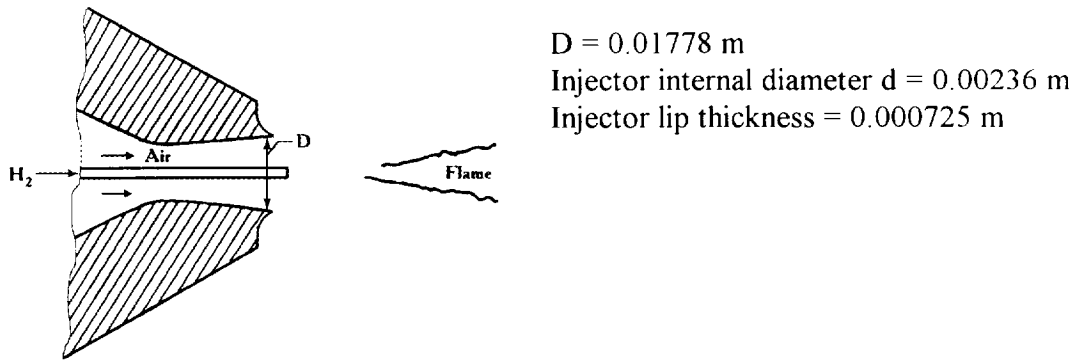
	Hydrogen jet	Free stream	Ambient air
Mach number, M	1.0	2.0	0
Temperature, T, K	545	1250	300
Velocity, U, m/s	1780	1420	0
Pressure, P, MPa	0.112	0.107	0.1013
Mass fractions:			
C_{H2}	1.000	0	0
C_{O2}	0	0.245	0.233
C_{N2}	0	0.58	*0.767[*]*
C_{H2O}	0	0.175	*0.*
C_{OH}	0	*6.65e-4*	0

Fig.26. Scheme and conditions of Cheng et al. coaxial experiment.
*) Expected values are *italic*.
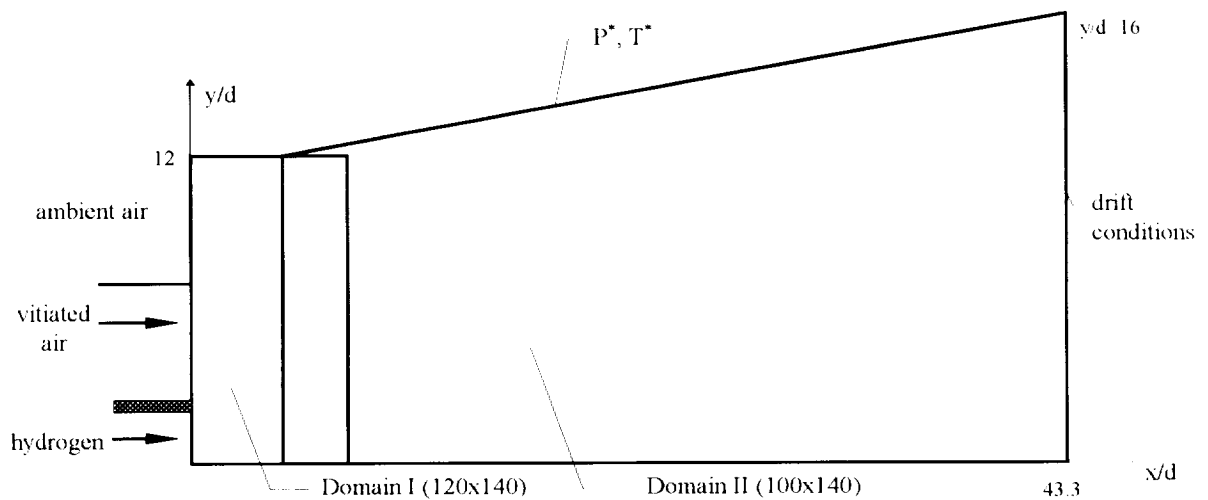
Fig.27. Schematic of computational domain.

Cheng et.al. test case
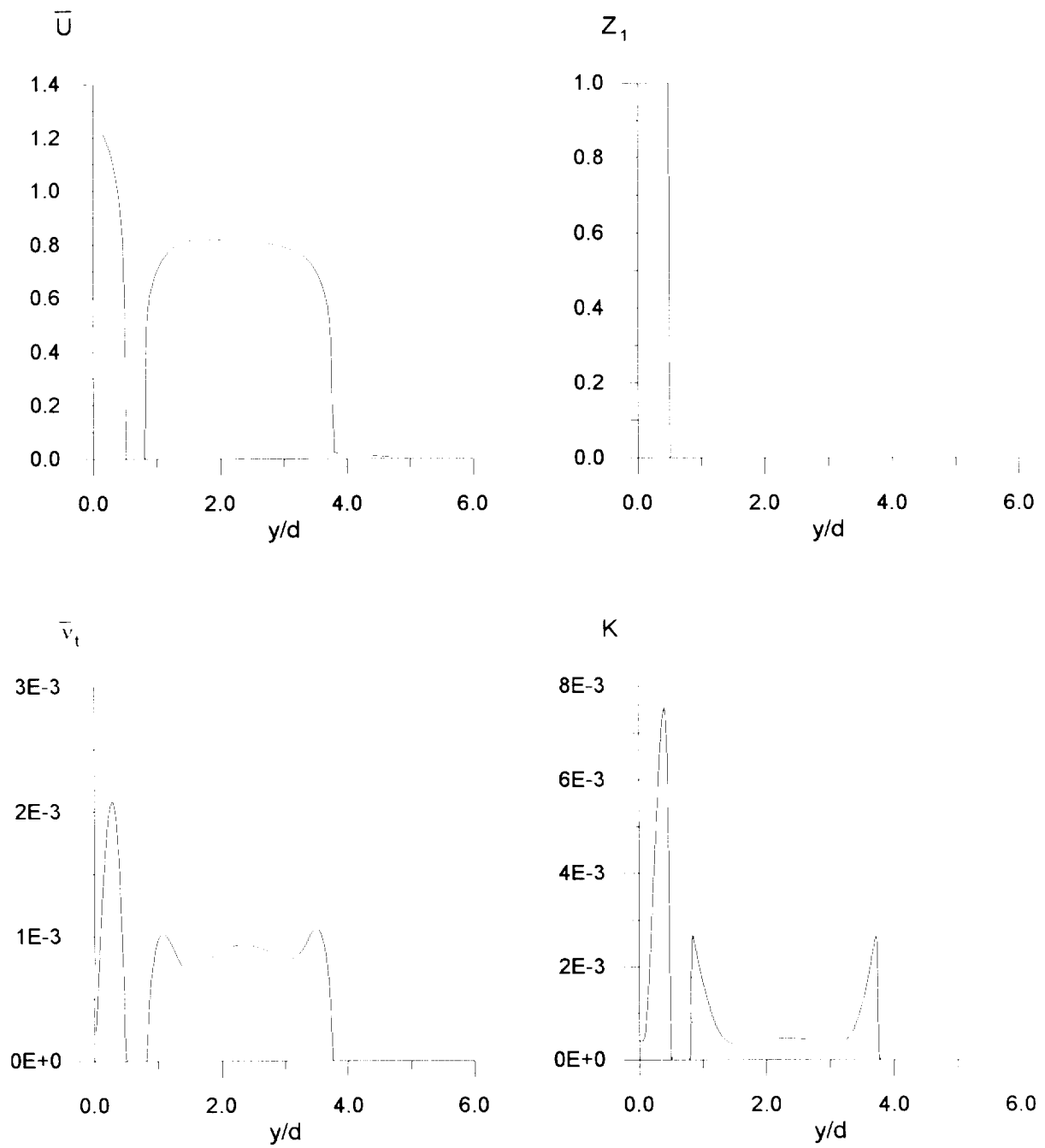
Fig.28.   Inflow parameters distributions

Cheng et.al. test case

x/d

Pressure contours

| 2.108 |
| 1.925 |
| 1.742 |
| 1.558 |
| 1.375 |
| 1.192 |
| 1.008 |
| .825 |
| .642 |
| .458 |
| .275 |
| .092 |

2.200

.000

x/d
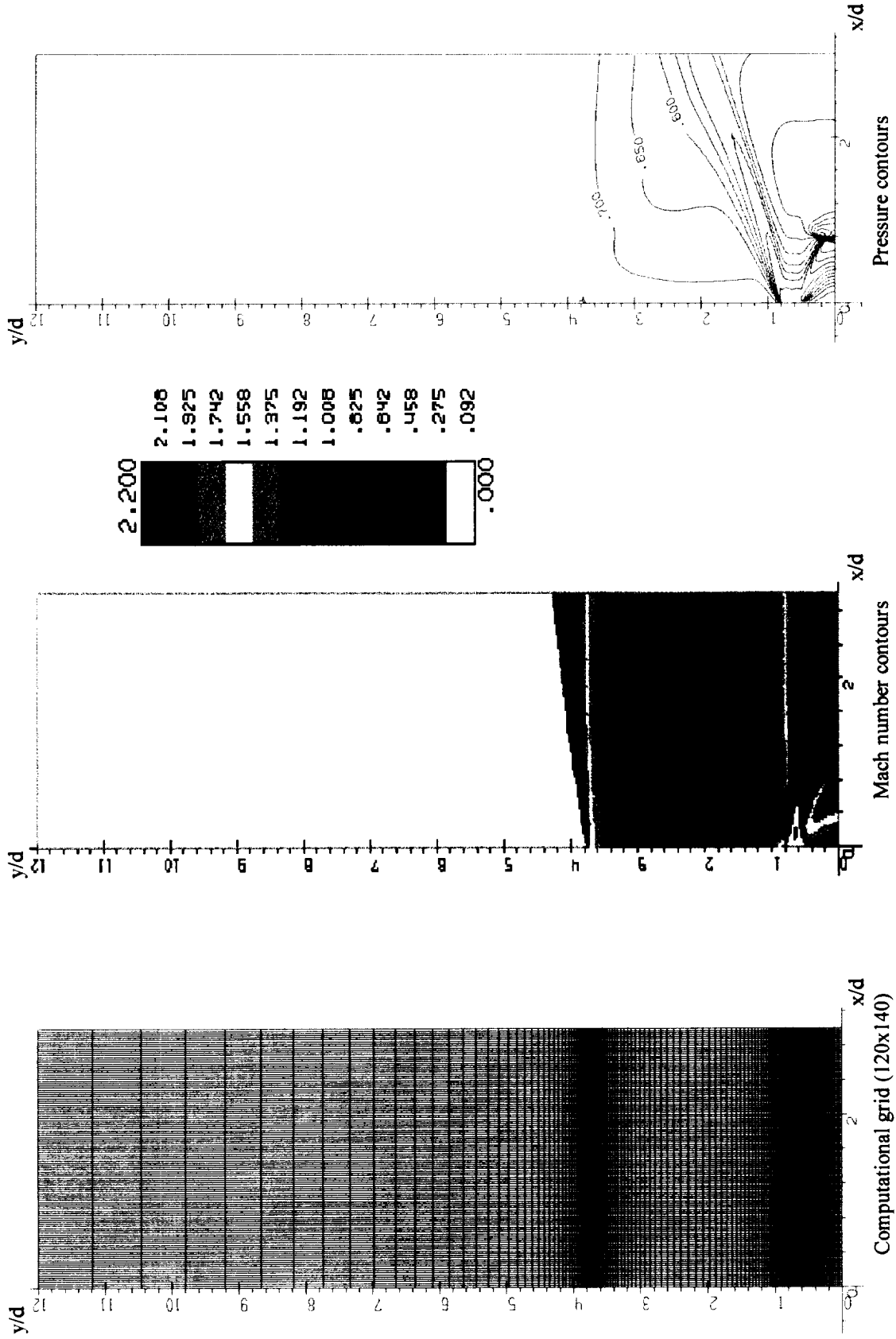
Mach number contours
Fig.29. Grid and flow pattern near injector (Domain I)
Cheng et.al. test case

x/d

Computational grid (120x140)
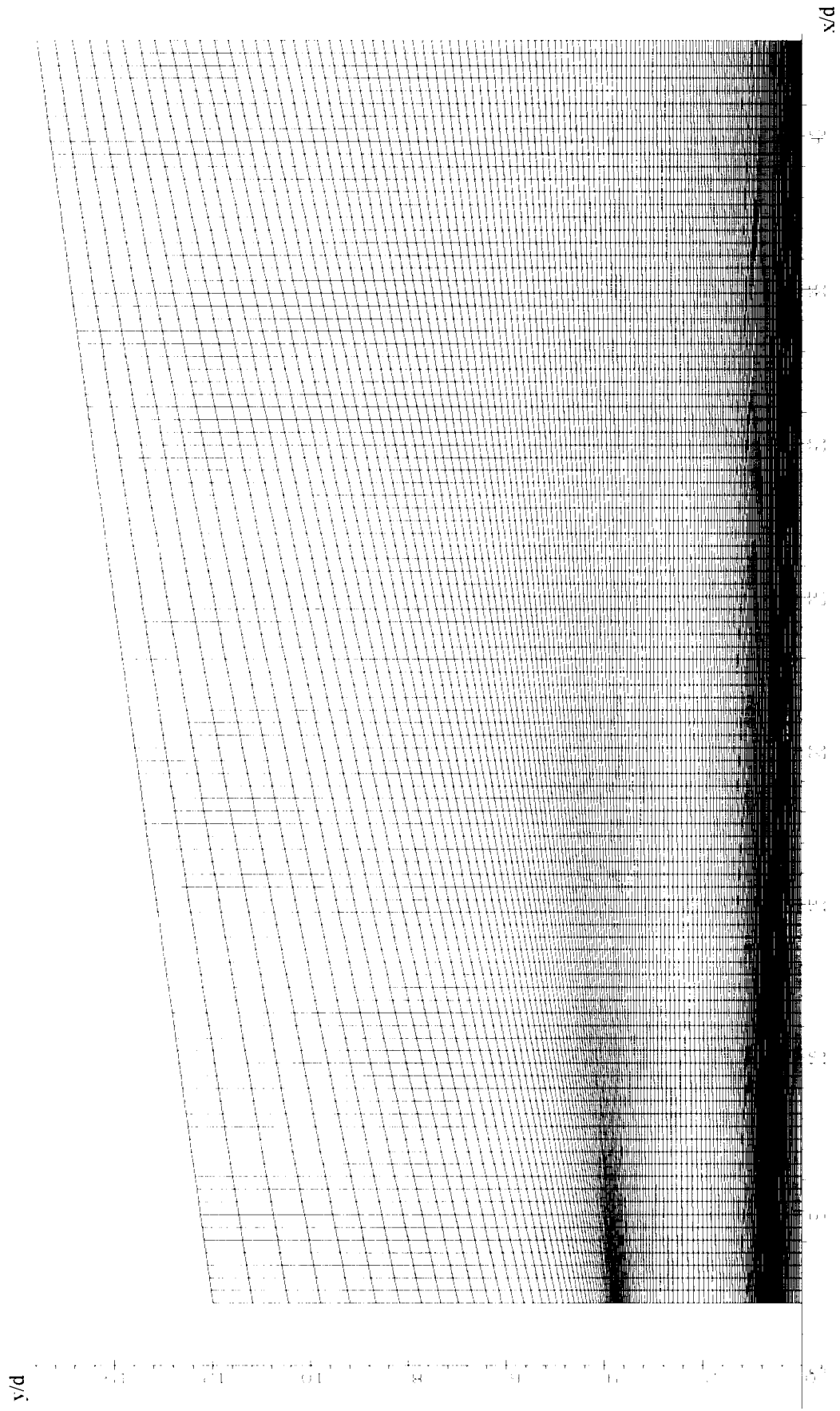
Fig.30. Computational grid (100x140) for Domain II

Cheng et.al. test case
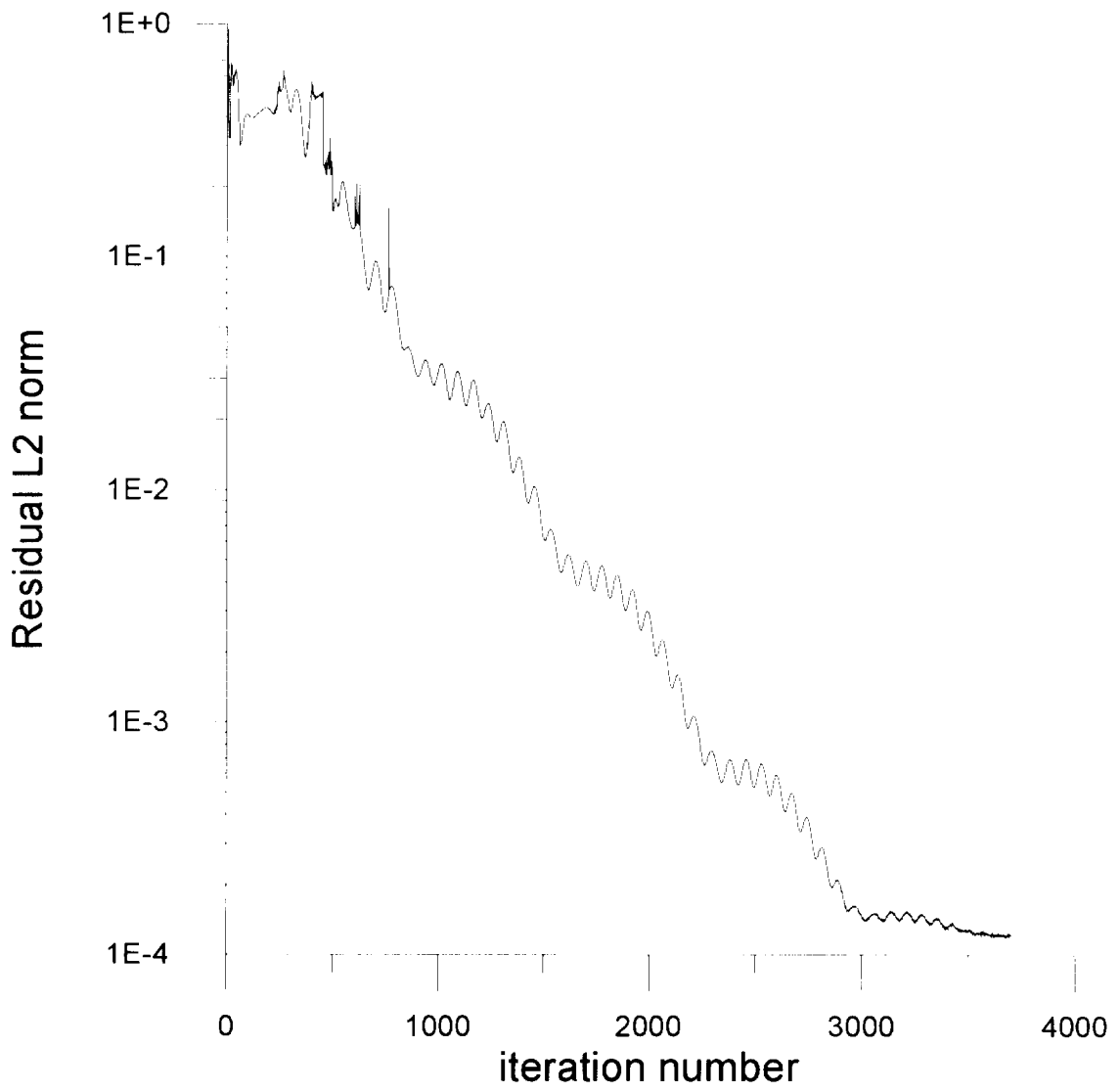
Fig.31. Convergence history

Cheng et.al. test case
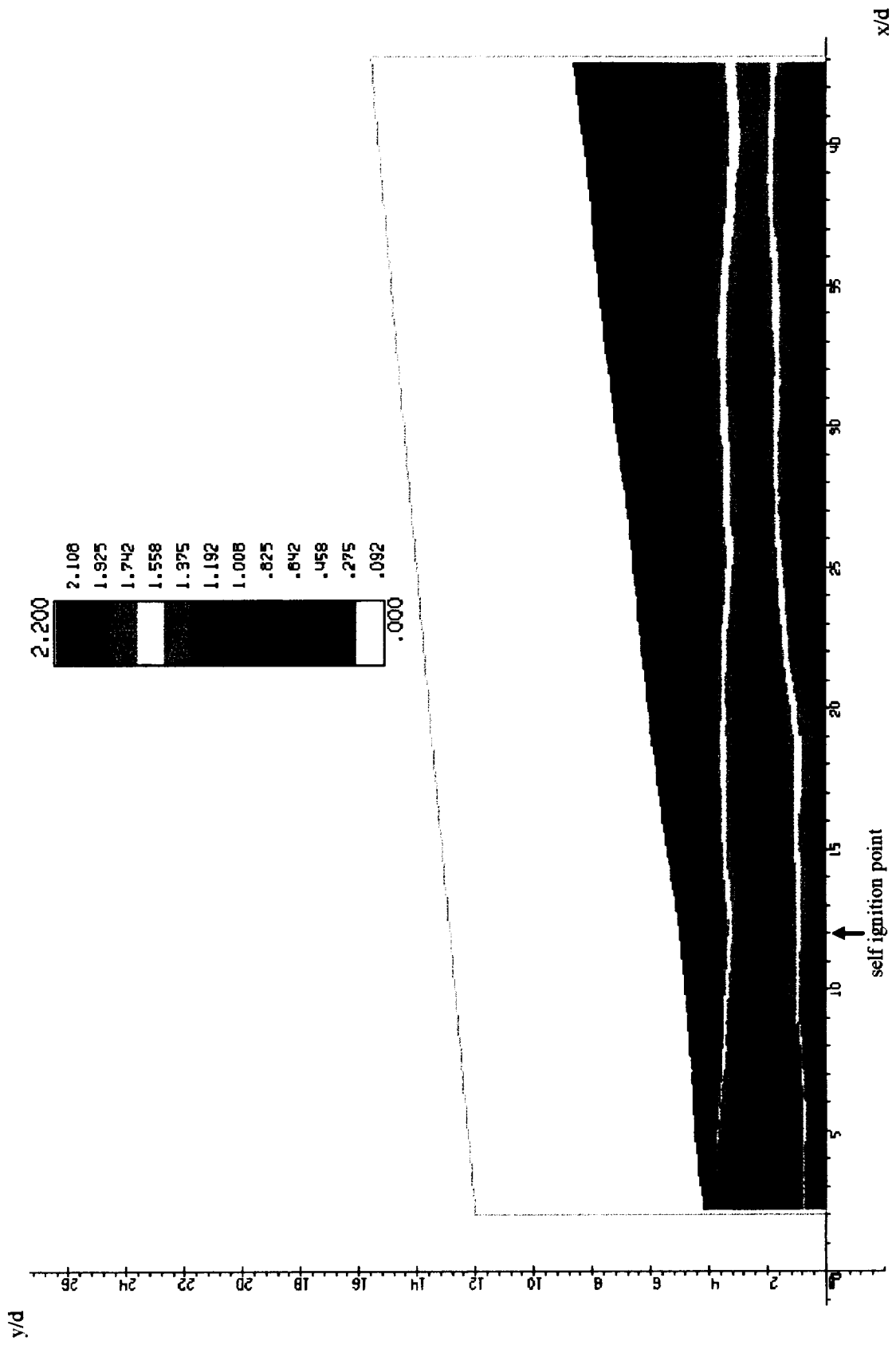
Fig.32. Mach number contours

Cheng et.al. test case
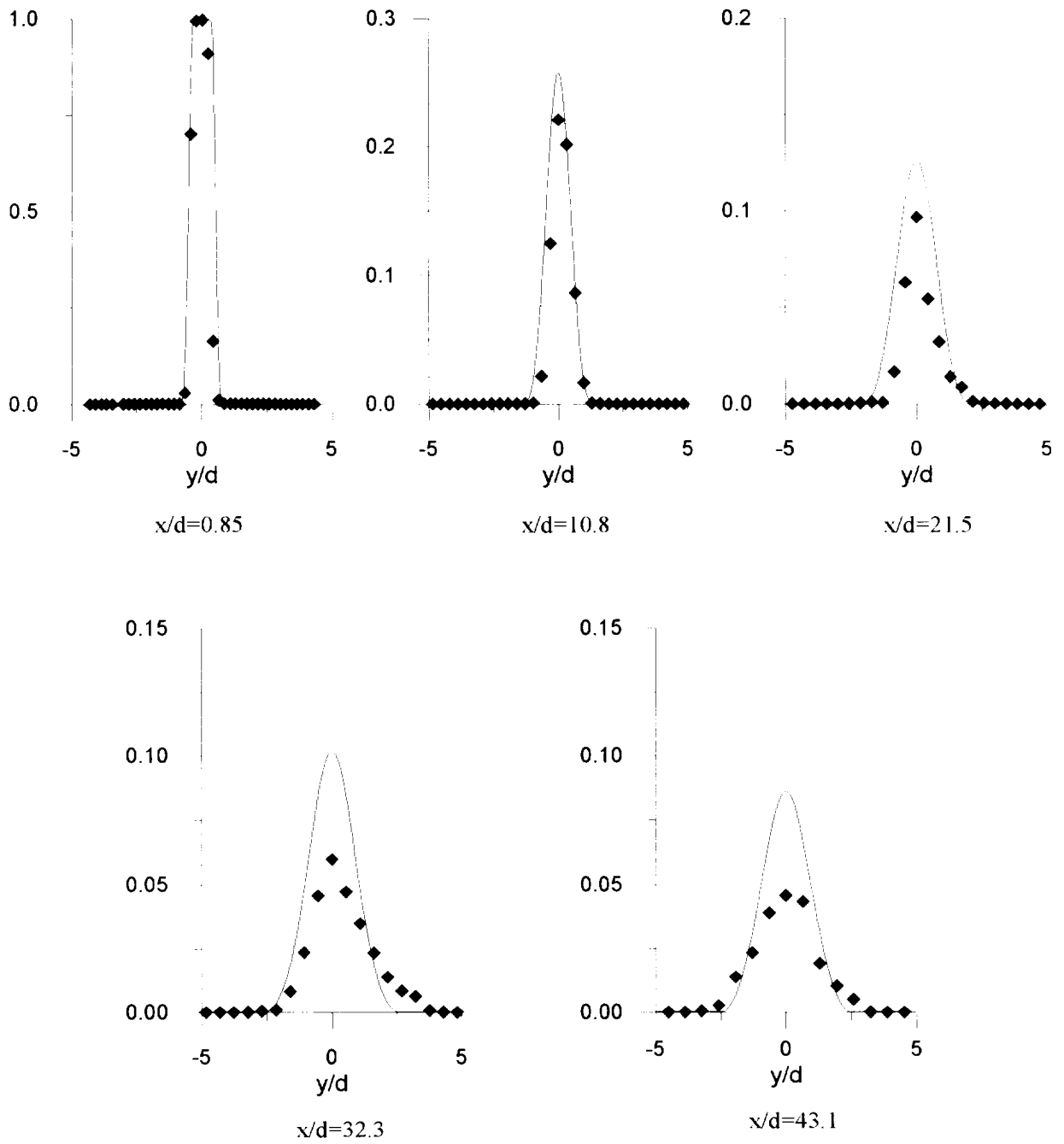
Fig.33a. Mean mixture fraction

◆   experimental data

⸺⸺⸺   FL approach

Cheng et.al. test case
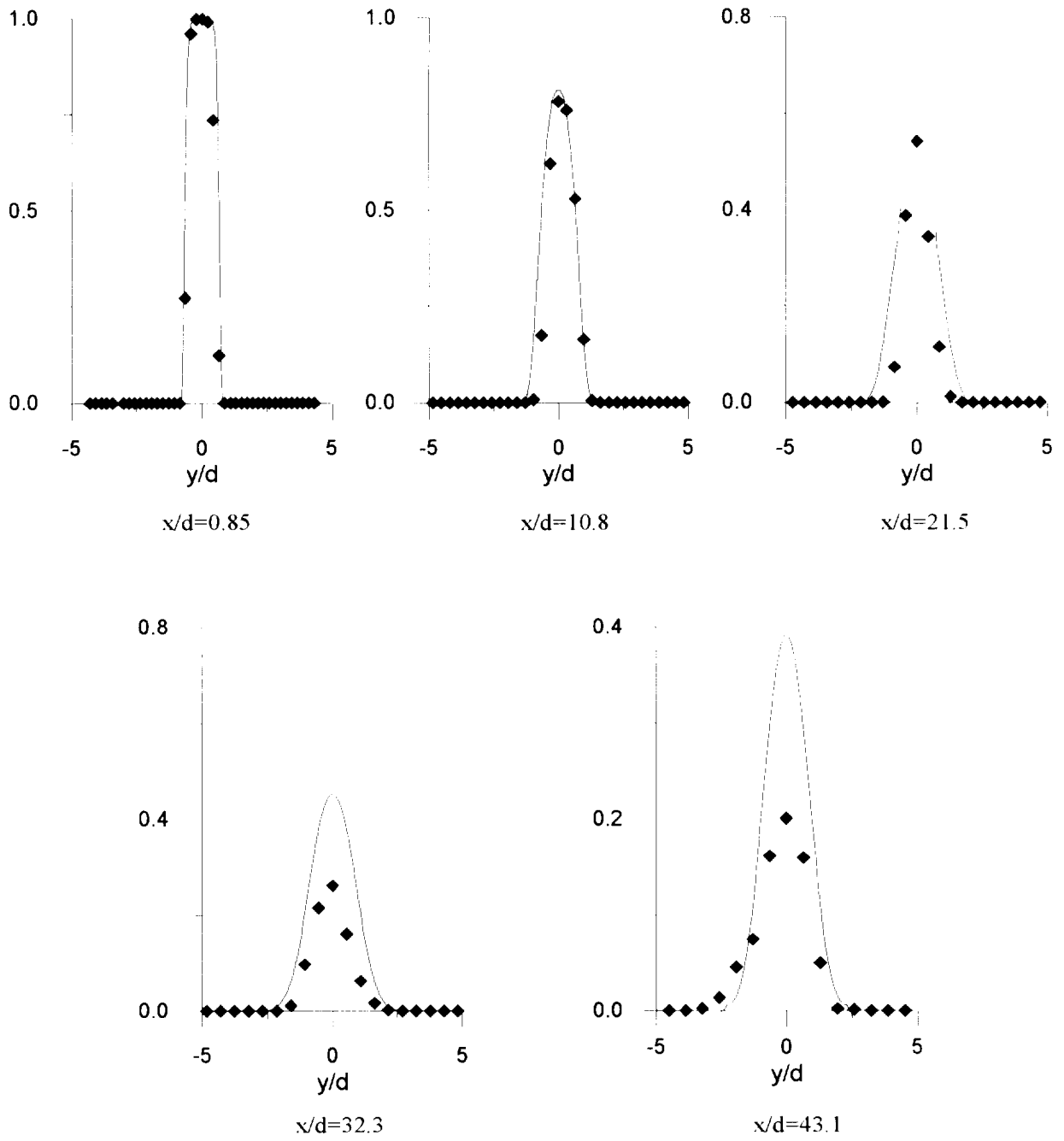
Fig.33b. Mean H2 mole fraction

◆   experimental data

FL approach

Cheng et.al. test case
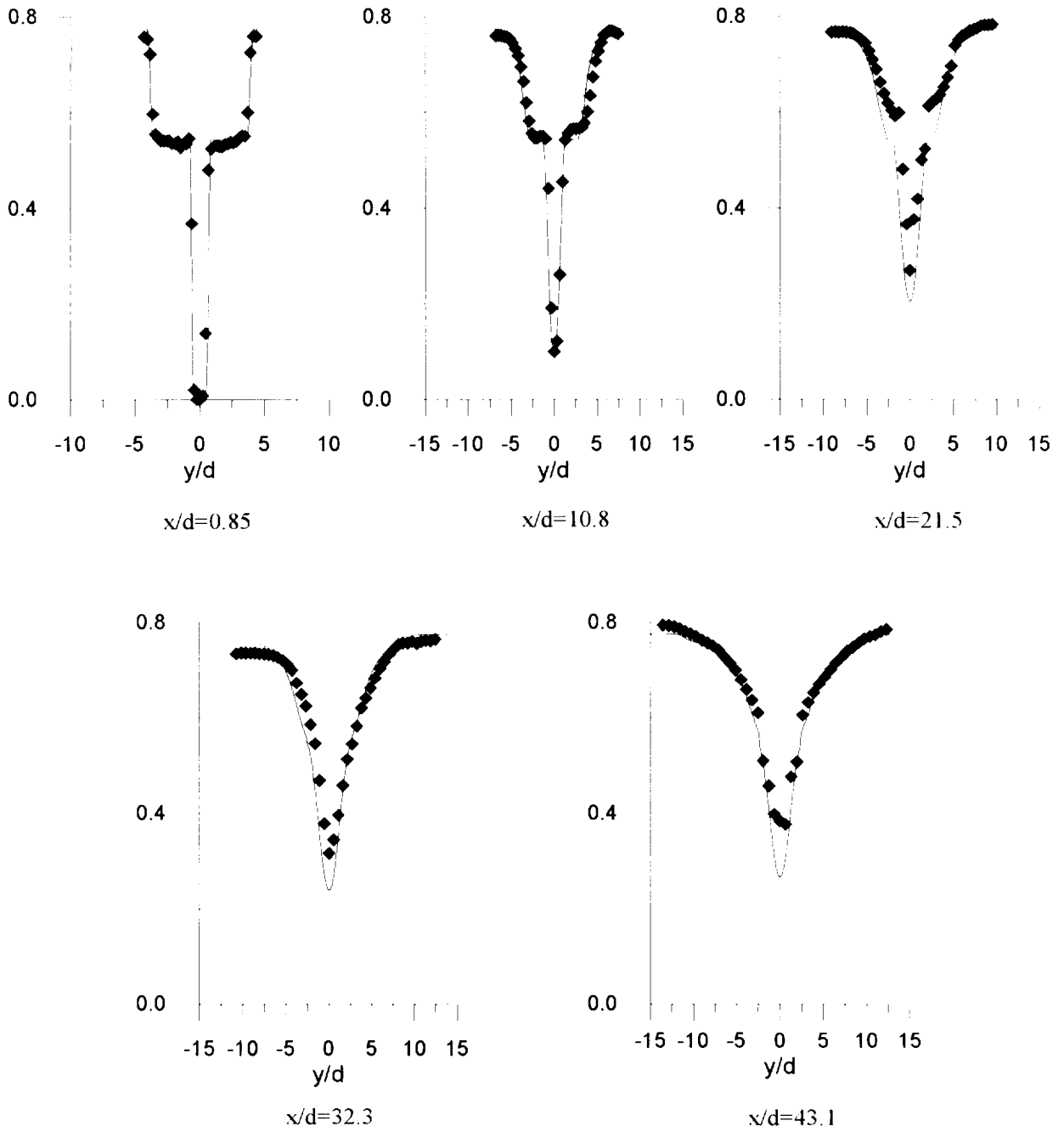
Fig.33c. Mean N2 mole fraction

◆   experimental data

⋯⋯⋯   FL approach

Cheng et.al. test case
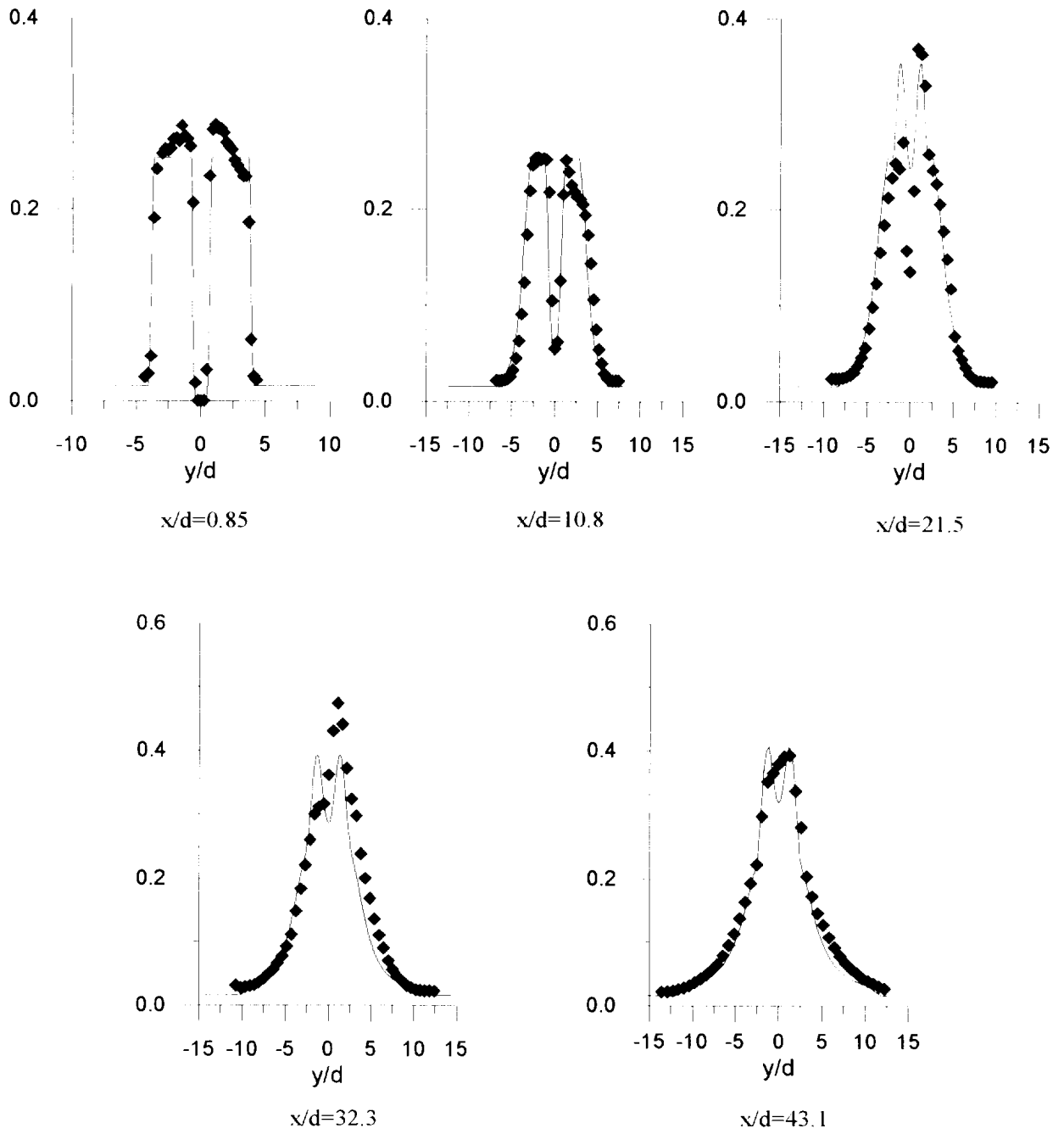
Fig.33d. Mean H2O mole fraction

◆   experimental data

⋯⋯   FL approach

Cheng et.al. test case
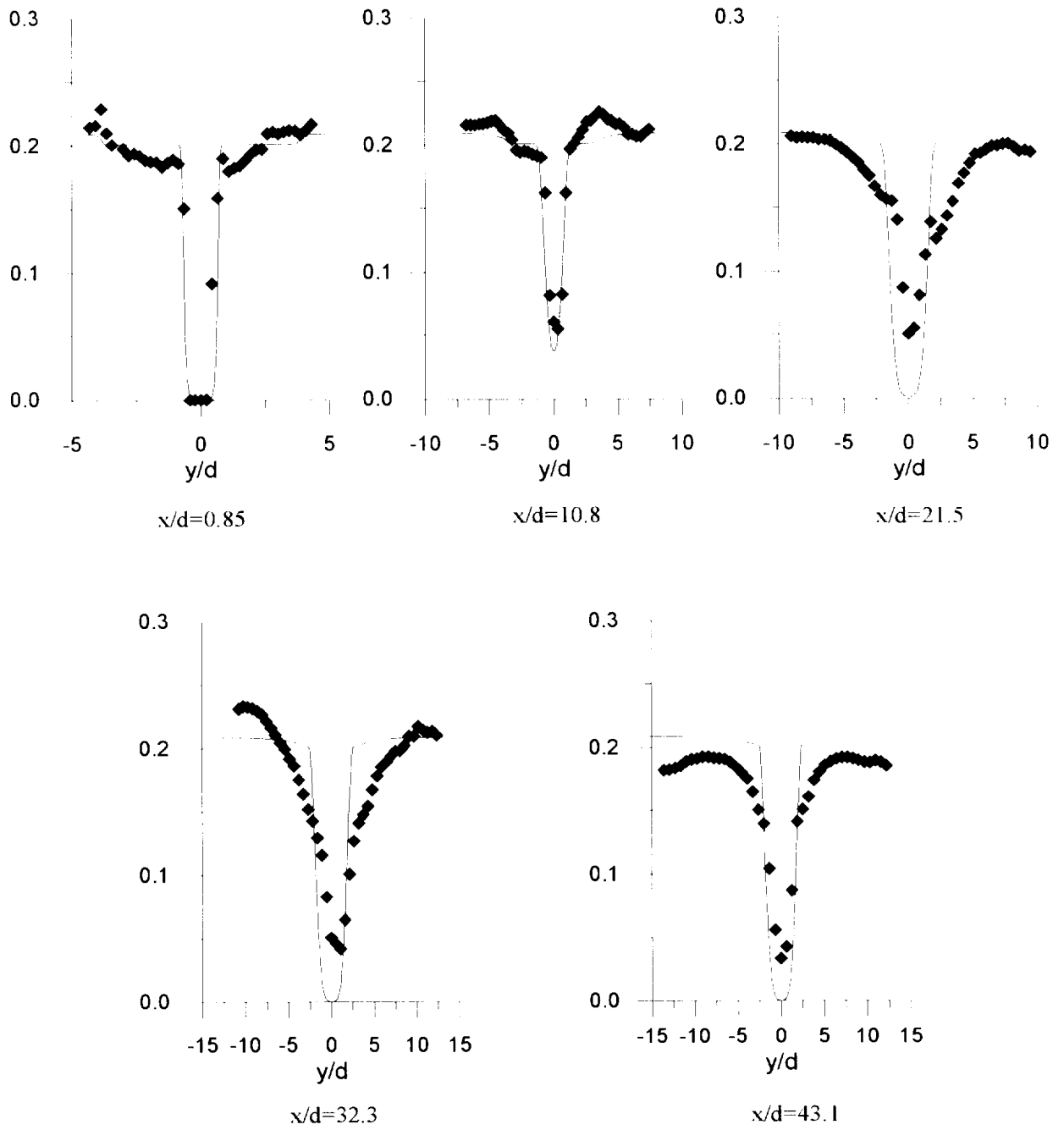
Fig.33e. Mean O2 mole fraction

◆   experimental data

‑‑‑‑‑   FL approach

Cheng et.al. test case
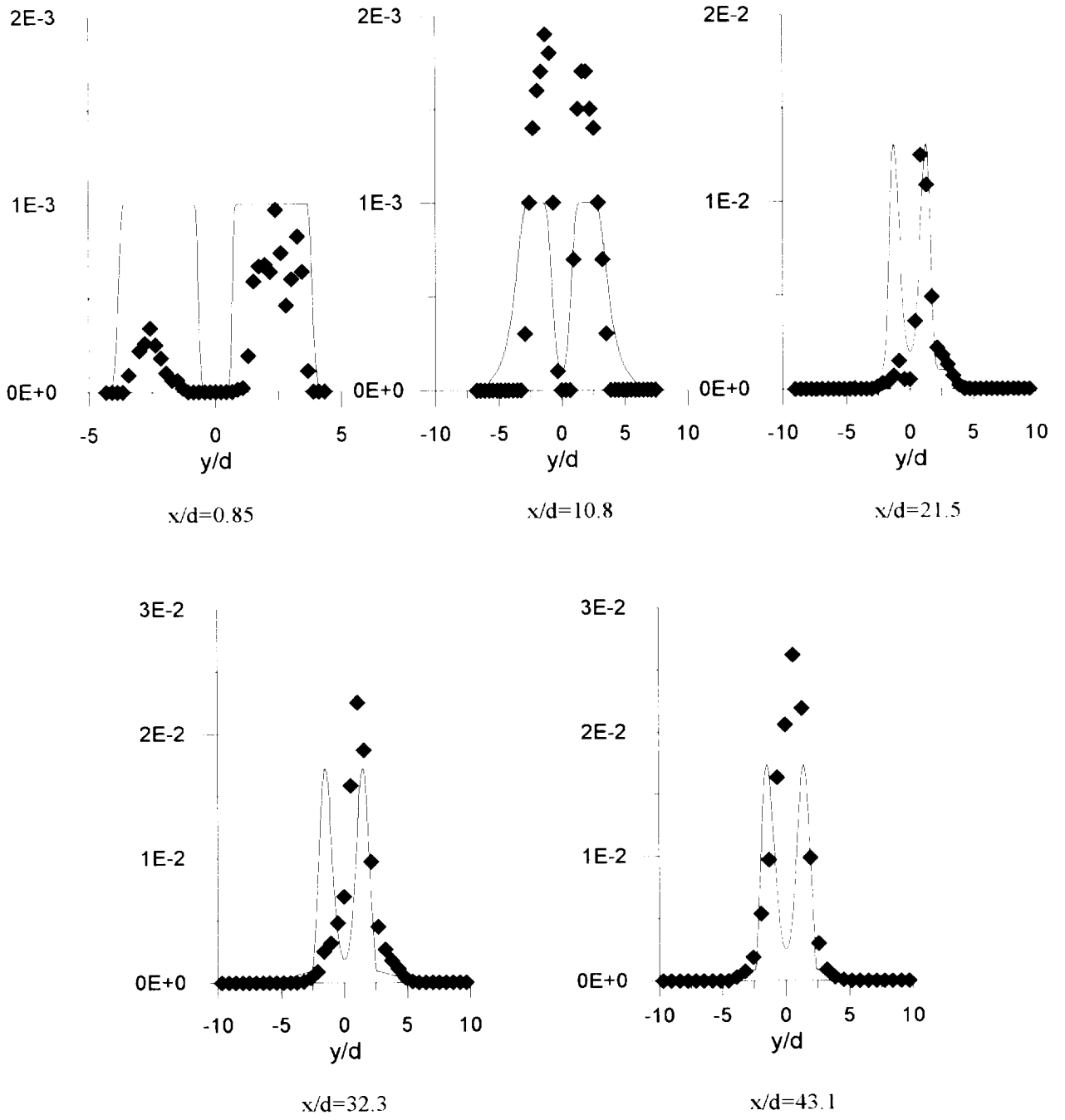
Fig.33f. Mean OH mole fraction

◆   experimental data

·······   FL approach

Cheng et.al. test case
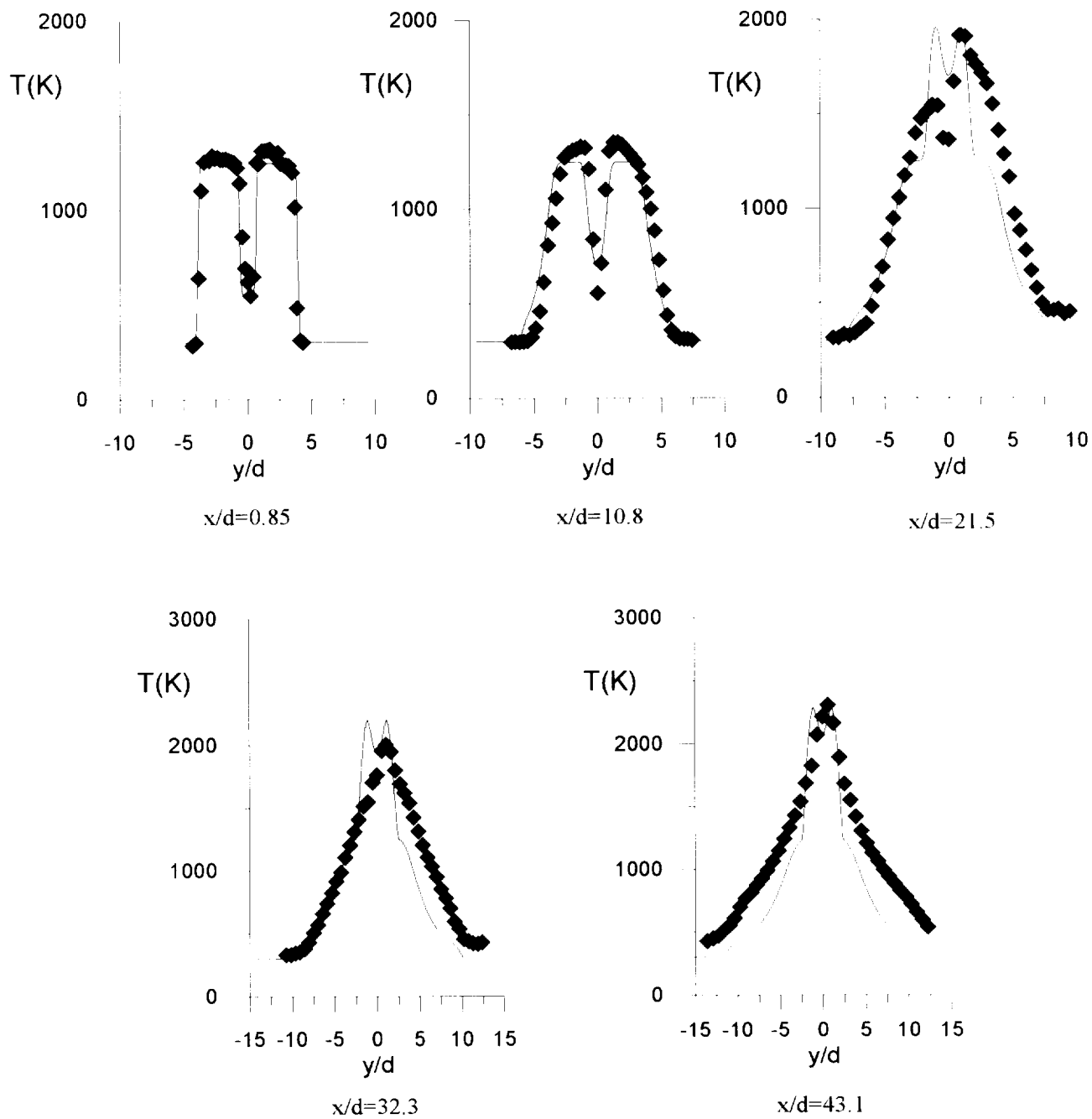
Fig.34. Mean temperature profiles.

◆   experimental data

———   FL approach

Cheng et.al. test case
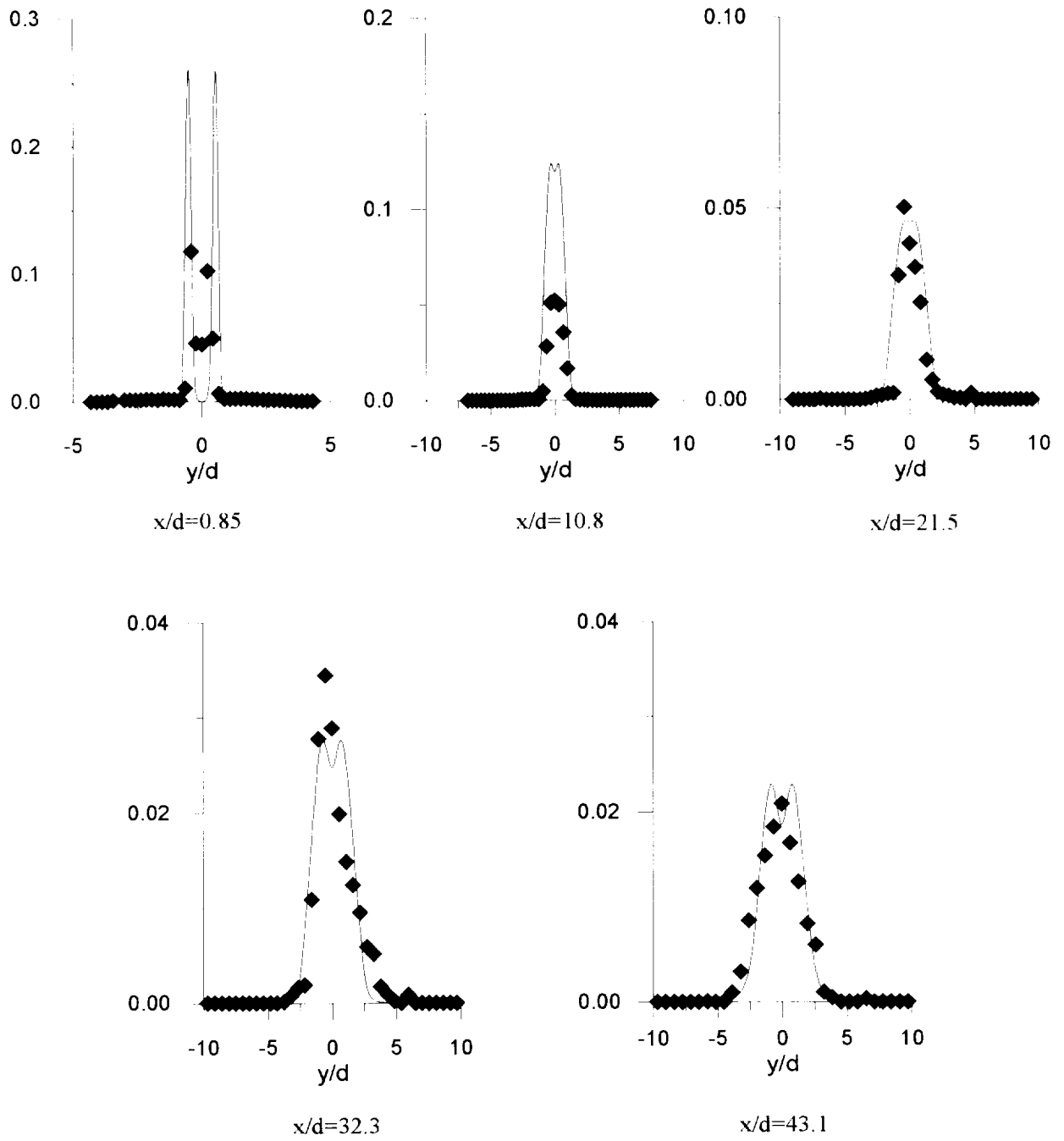
Fig.35. RMS mixture fraction

◆ experimental data

FL approach

Cheng et.al. test case
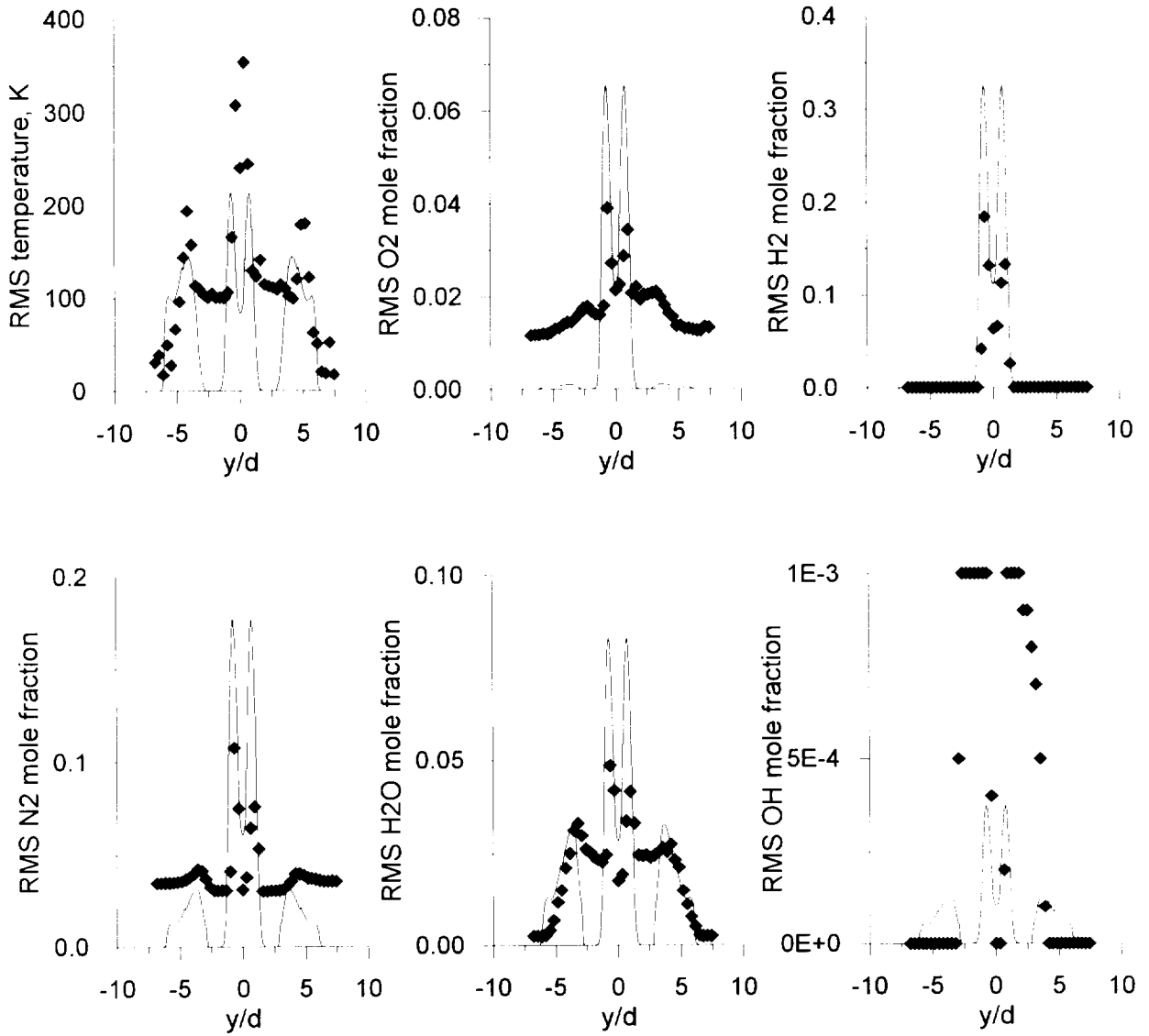
Fig.36. Temperature and species RMS profiles
at axial location x/d=10.8 .

FL approach

◆   experimental data

Cheng et al. test case.
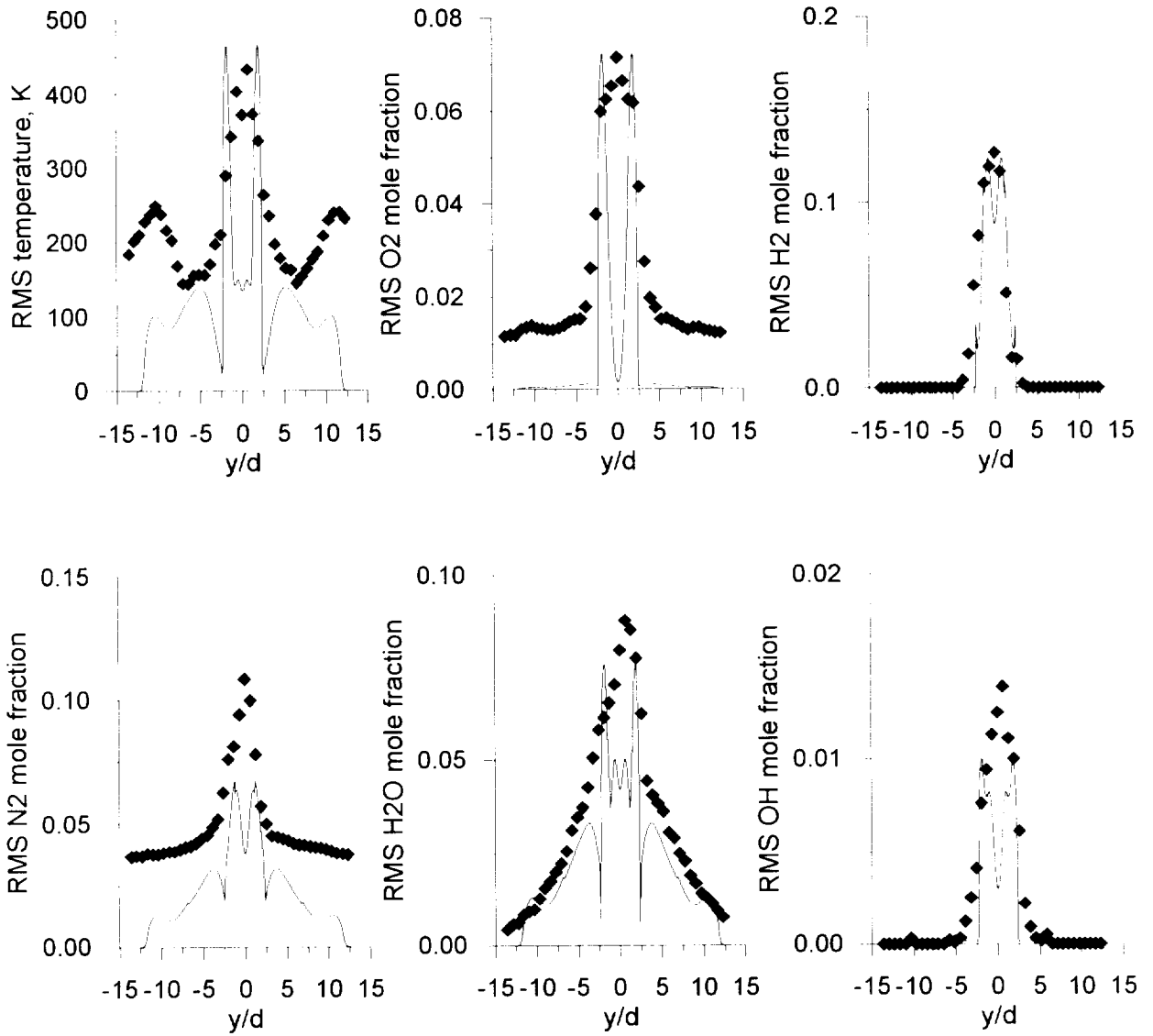
Fig.37. Temperature and species RMS profiles
at axial location x/d=43.1 .

...... FL approach

◆   experimental data

Cheng et al. test case.
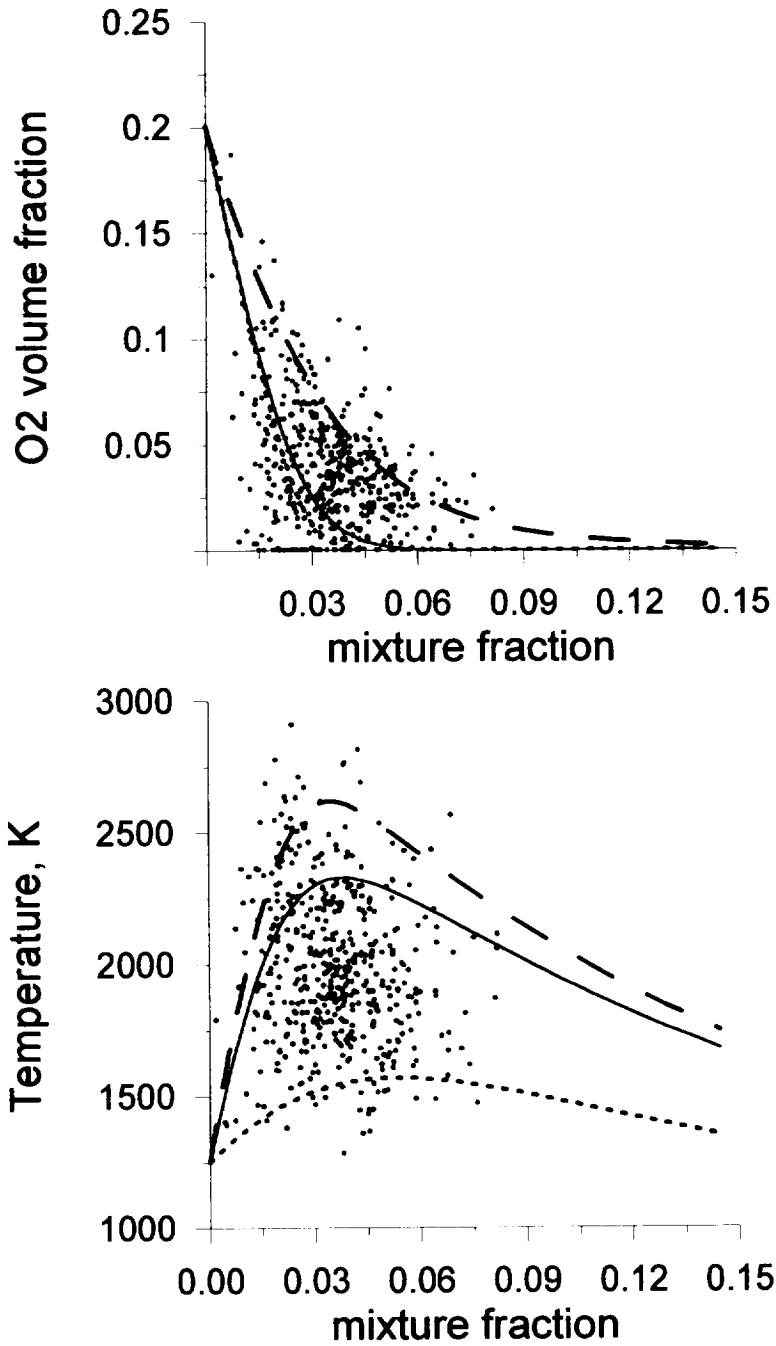
Fig.38a. Estimation of upper and lower prediction
limits for flamelet model.
Cheng et. al. test case.
x/d=32.3, y/d=1.1.

●　　　　experimental data

————　　conditionally averaged flamelet solution

— — —　upper predicted limit

· · · · · · · ·　lower predicted limit
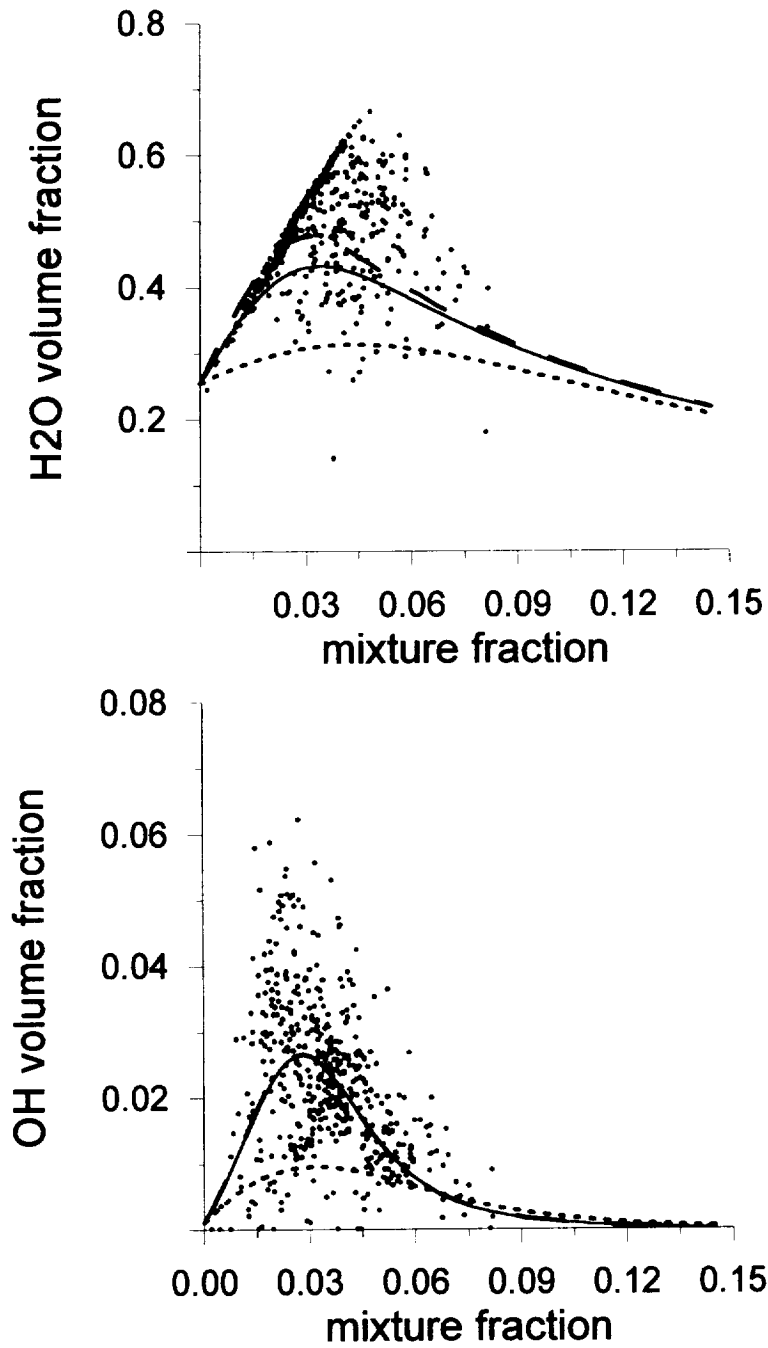
Fig. 38b. Estimation of upper and lower prediction
limits for flamelet model.
Cheng et. al. test case.
x/d=32.3, y/d=1.1.

●   experimental data

———   conditionally averaged flamelet solution

— —   upper predicted limit

·······   lower predicted limit
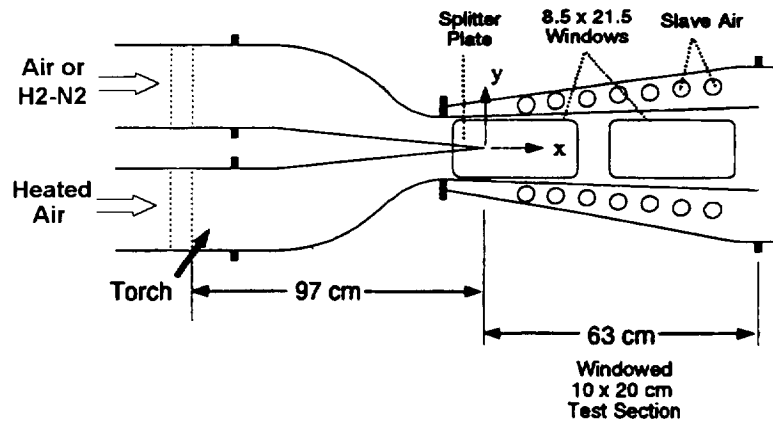
	NON-REACTING	REACTING
Air side speed, U1, m/s	394	390
Fuel side speed, U2, m/s	134	137
Air side Mach number	0.72	0.71
Fuel side Mach number	0.39	0.30
Aie side total temperature, K	824	817
Fuel side total temperature, K	303	348
Mass fractions:		
air stream O2	*0.233*[*]	*0.233*
air stream N2	*0.767*	*0.767*
fuel stream O2	*0.233*	0
fuel stream N2	*0.767*	0.969
fuel stream H2	0	0.031

Fig.39. Scheme and conditions of Chang et al. experiment.
*) Expected values are *italic*.
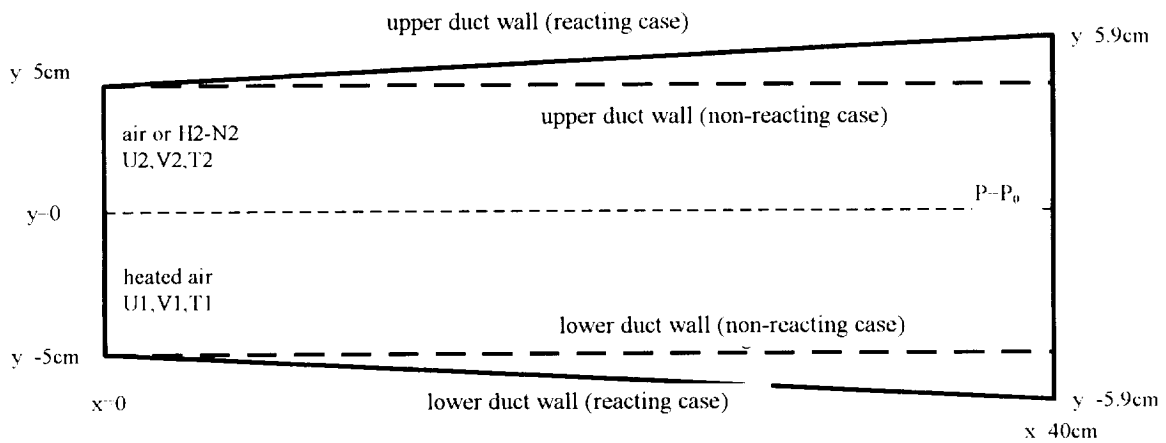
Fig.40. Scheme of the computational domain.
Chang et al. test case.
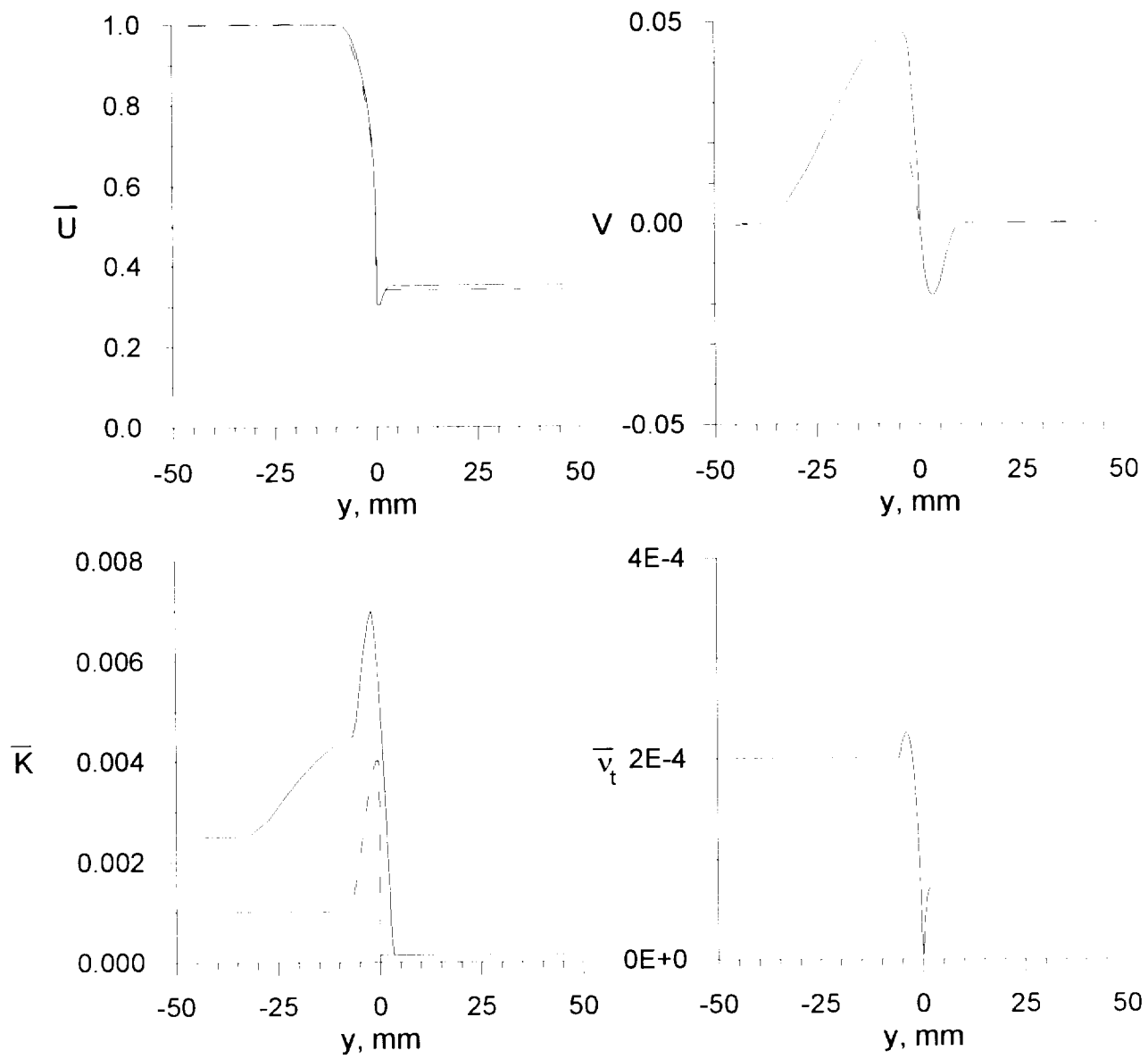
Fig.41. Inlet profiles.

——— reacting case

— — non-reacting case

Chang et al. test case.

REACTING CASE
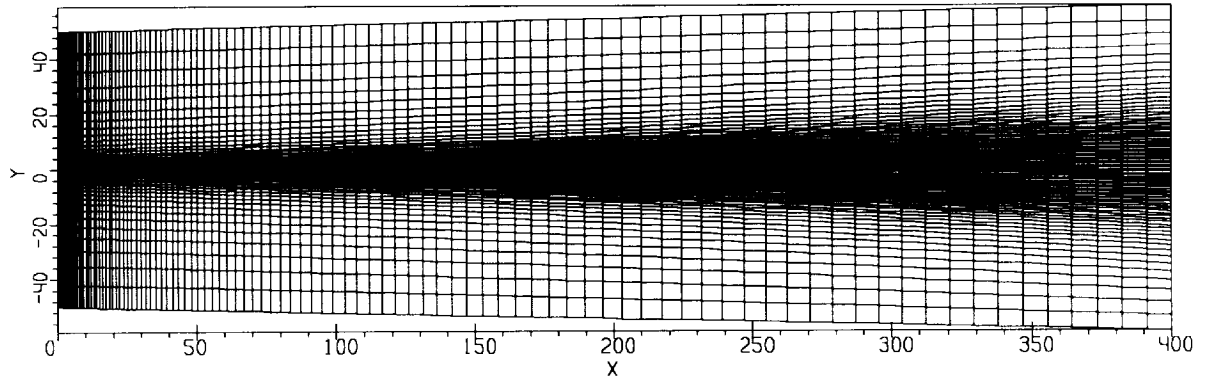
NON-REACTING CASE
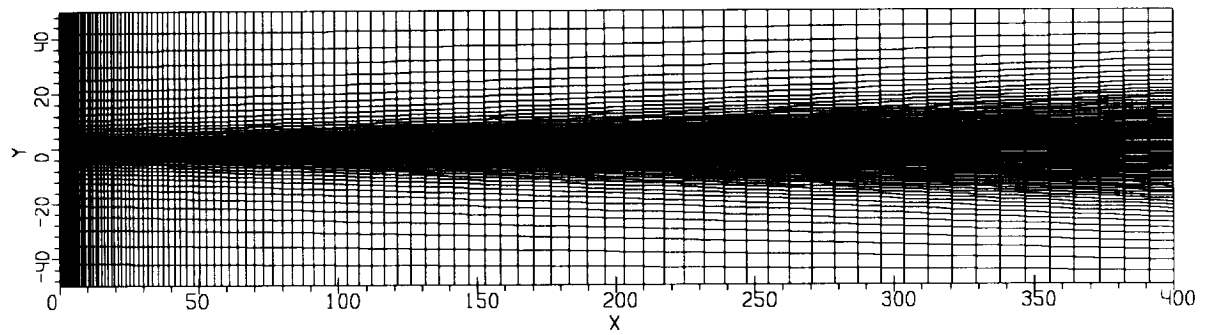
Fig.42. Computational grid (100x80).
Chang et al. test case.
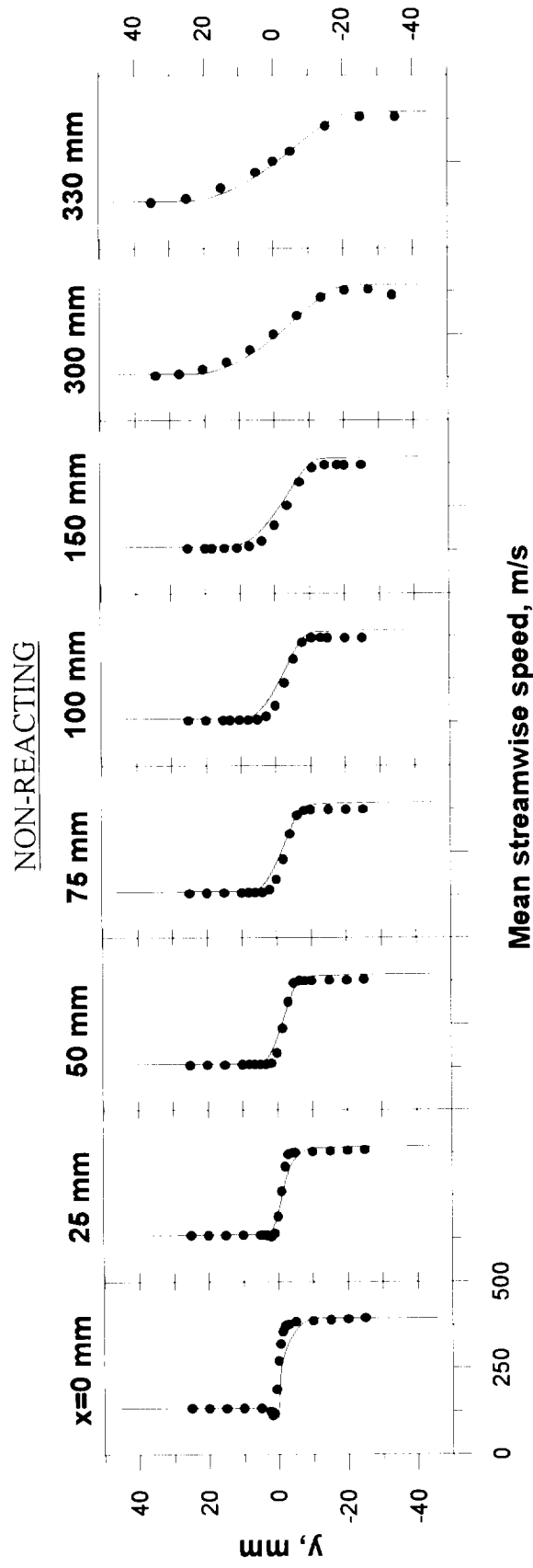
Fig. 43. Mean streamwise velocity profiles. Non-reacting case.

Chang et al. test case.

NON-REACTING

Mean cross-stream speed, m/s
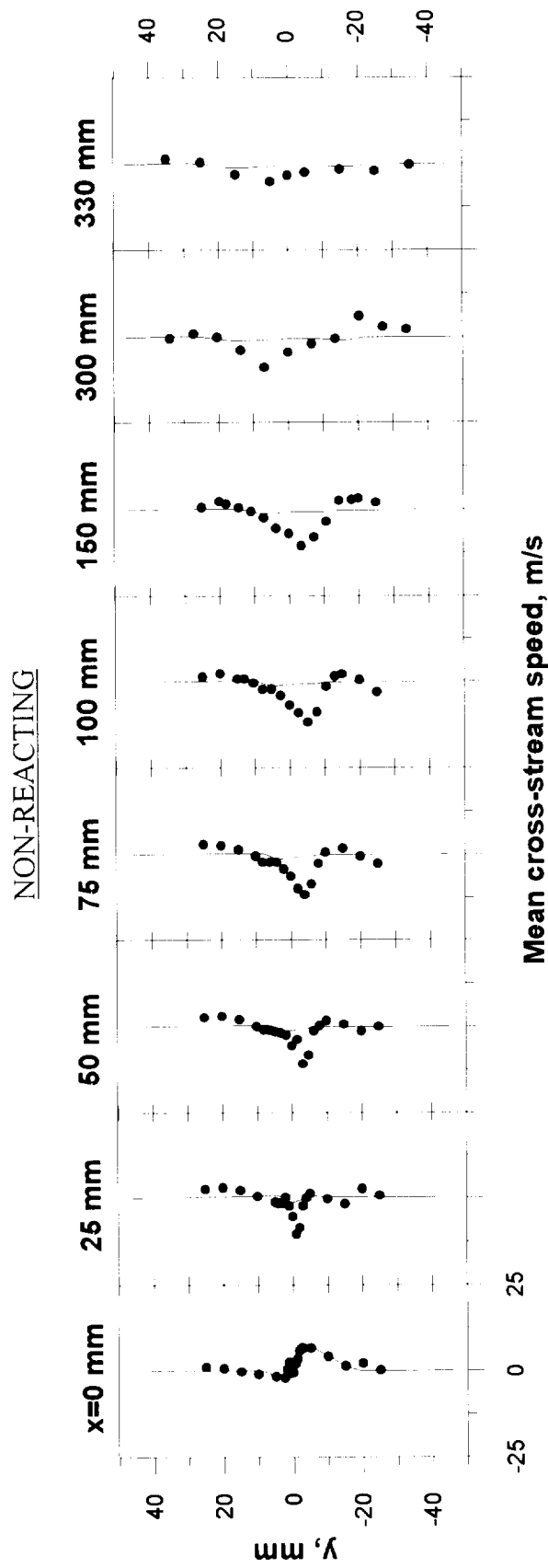
Fig. 44. Mean cross-stream velocity profiles. Non-reacting case.

Chang et al. test case.
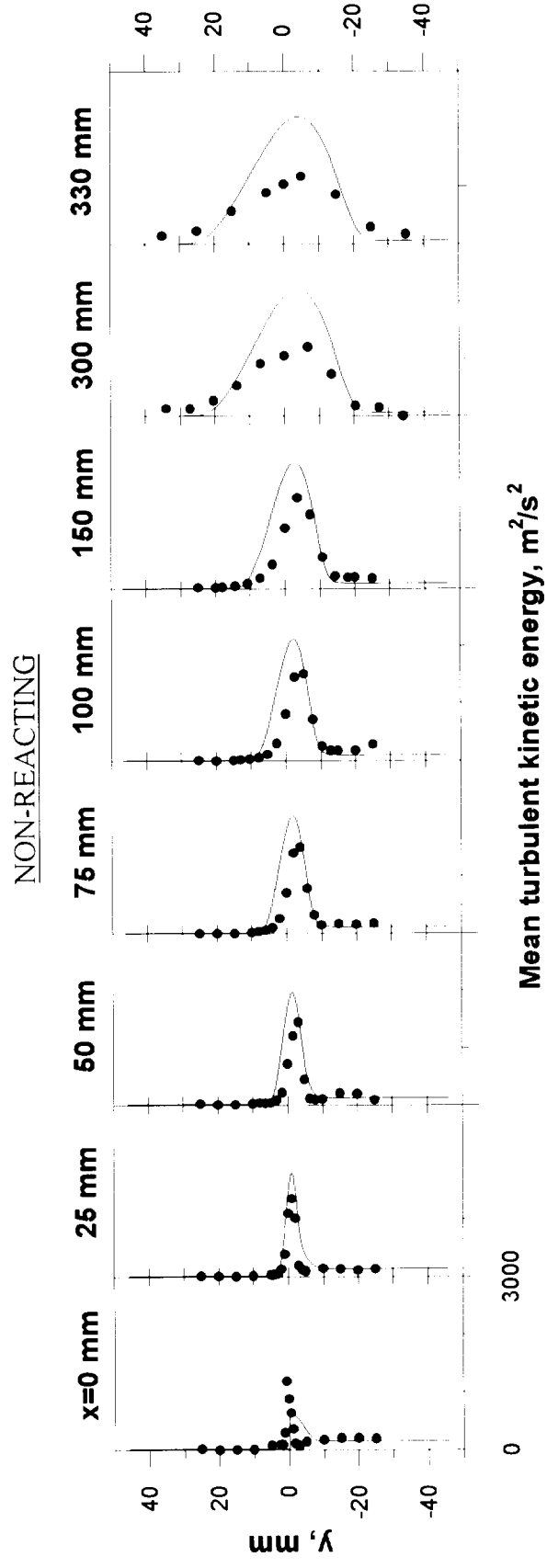
Fig.45. Profiles of turbulent kinetic energy. Non-reacting case.

Chang et al. test case.
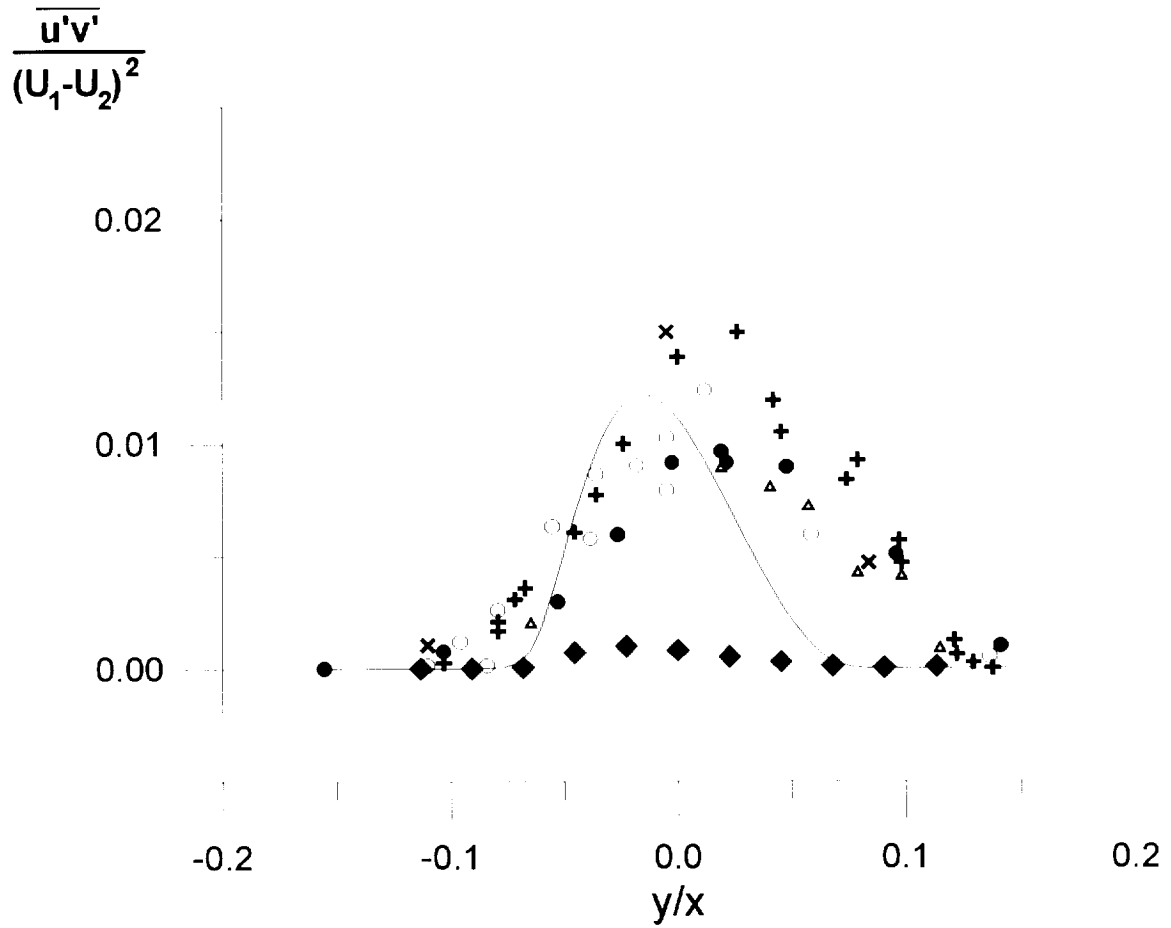
Fig.46. Comparison of calculated normalized Reynolds Stress
with experimental data.

------- calulations, Chang et al. test case, non-reacting, x=300mm

Experimental Data:

◆   Chang et al.,1996, non-reacting, x=300mm

●   Wignanski and Fiedler, 1968

+   Sanyach and Mathilu, 1969

✗   x=50 mm ⎫

( )   x=100 mm ⎬ data by Secundov*

△   x=200 mm ⎭

*Details of Secundov's experiment can be found in Abramovich et al., 1984.
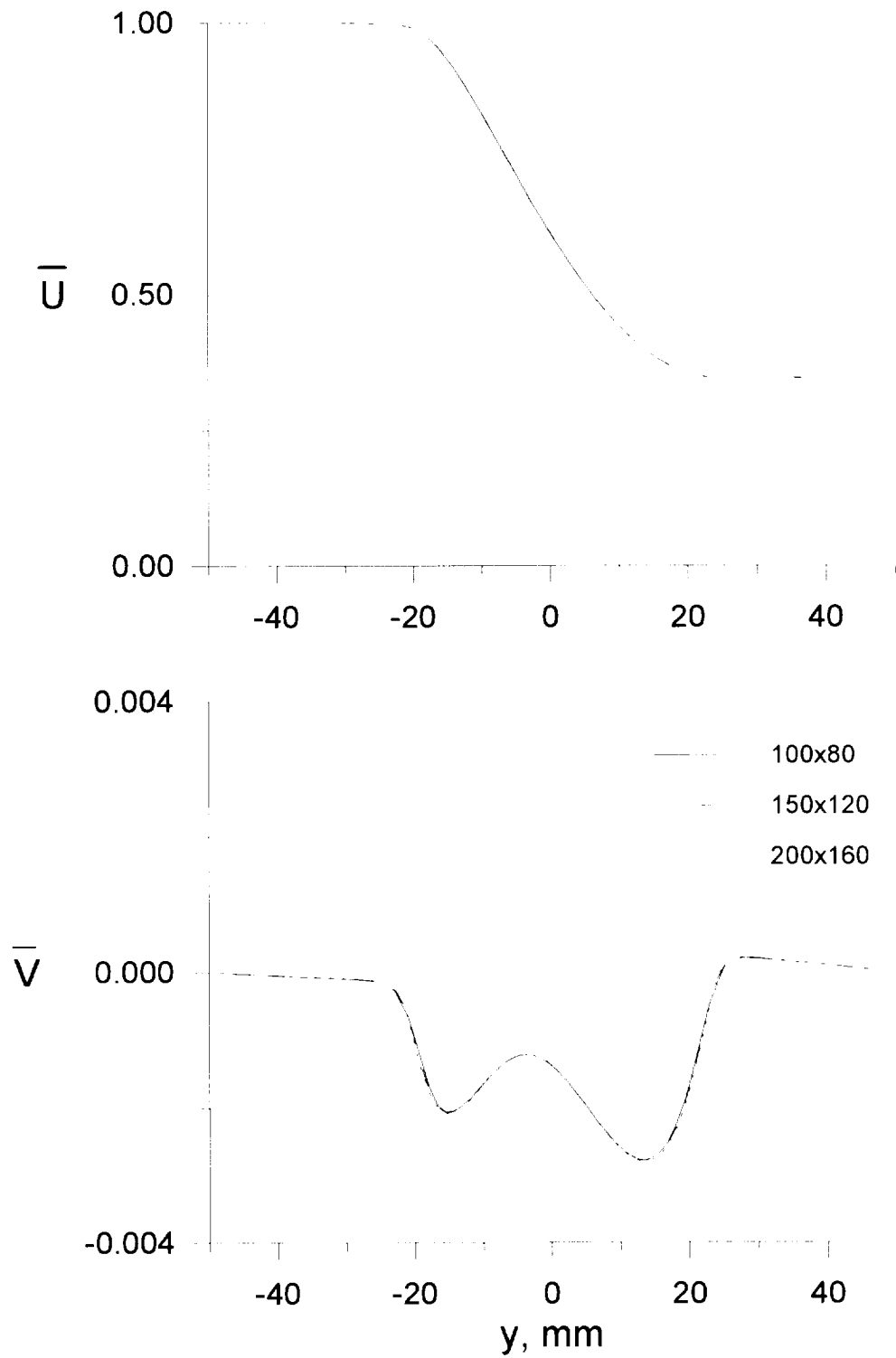
Fig.47a. Influence of discretization on calculated velocity components.
Non-reacting case. x=300 mm.
$\overline{U}=u/u_a$, $\overline{V}=v/u_a$.

Chang et al. test case.
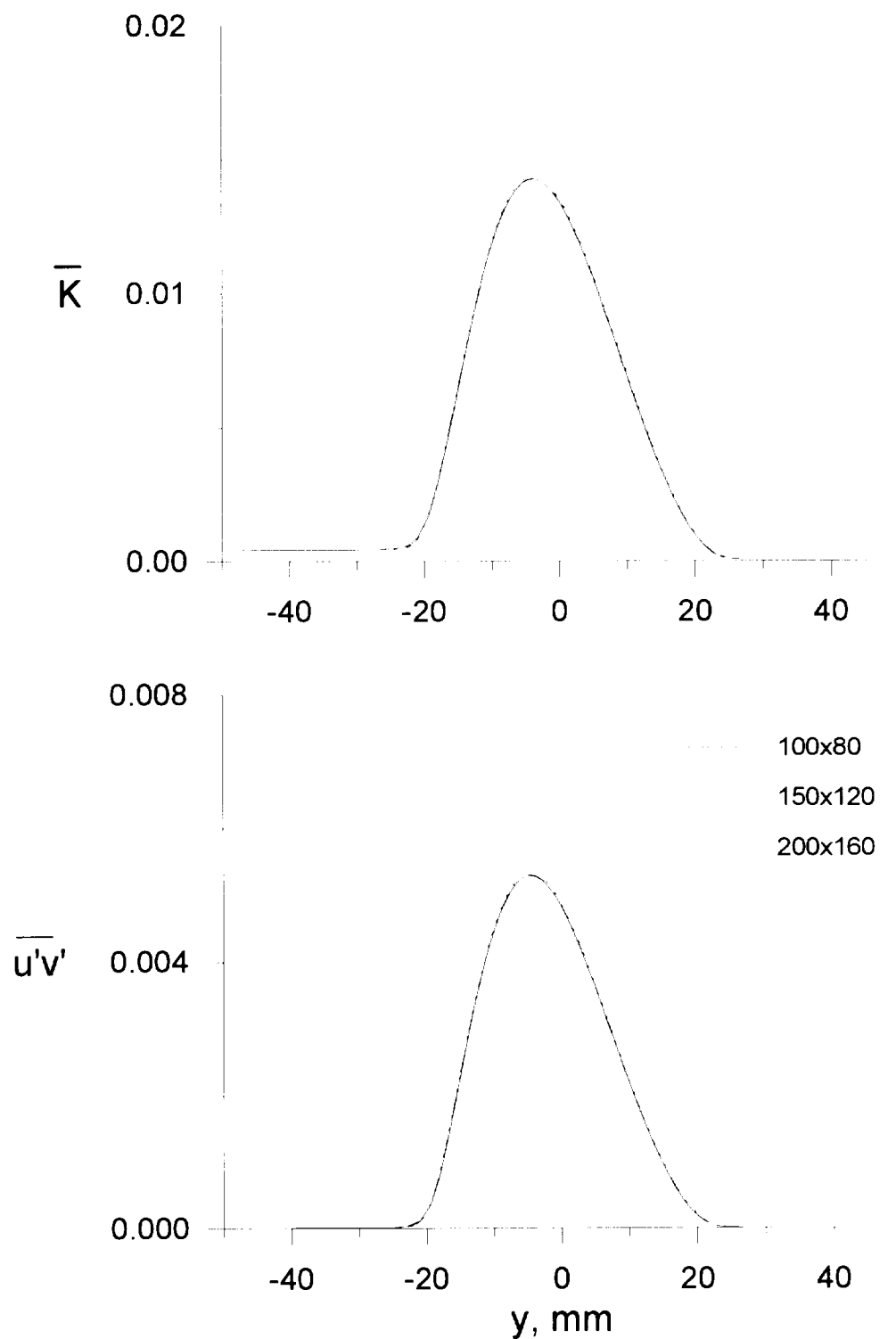
Fig.47b. Influence of discretization on calculated turbulence characteristics.
Non-reacting case. x=300 mm.
$\overline{K}=K/u_a^2$, $\overline{u'v'}=<u'v'>/u_a^2$.

Chang et al. test case.
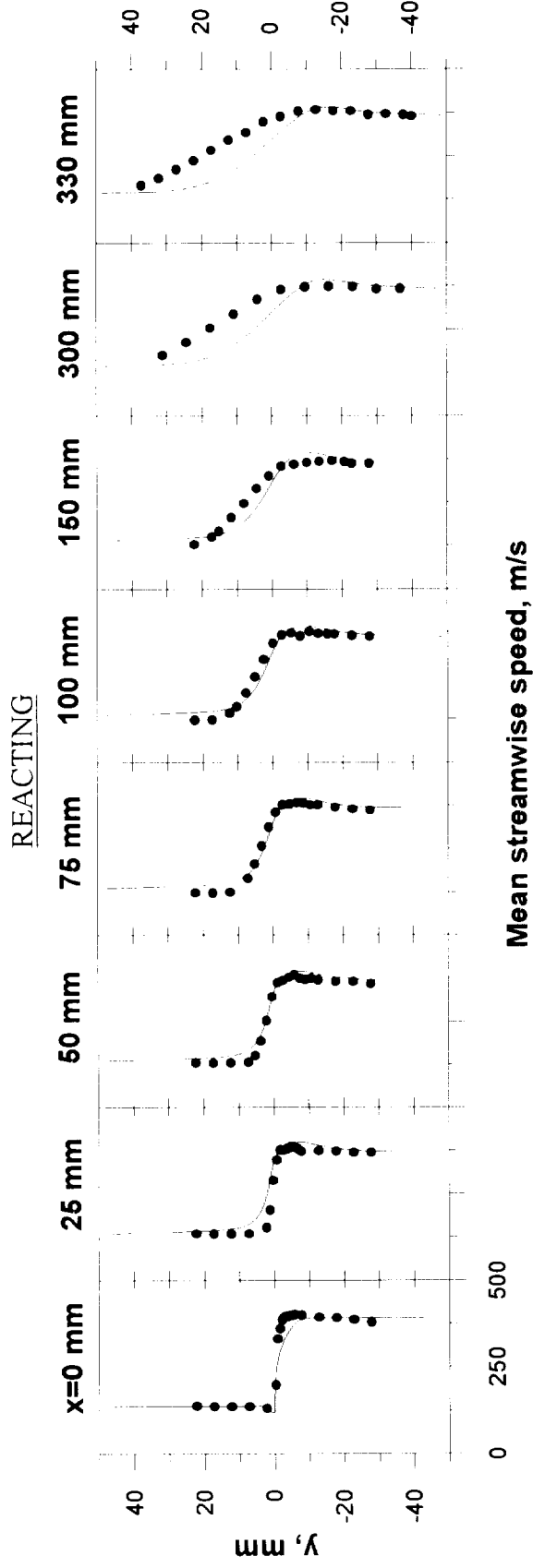
Fig. 48. Mean streamwise velocity profiles. Reacting case.

Chang et al. test case.
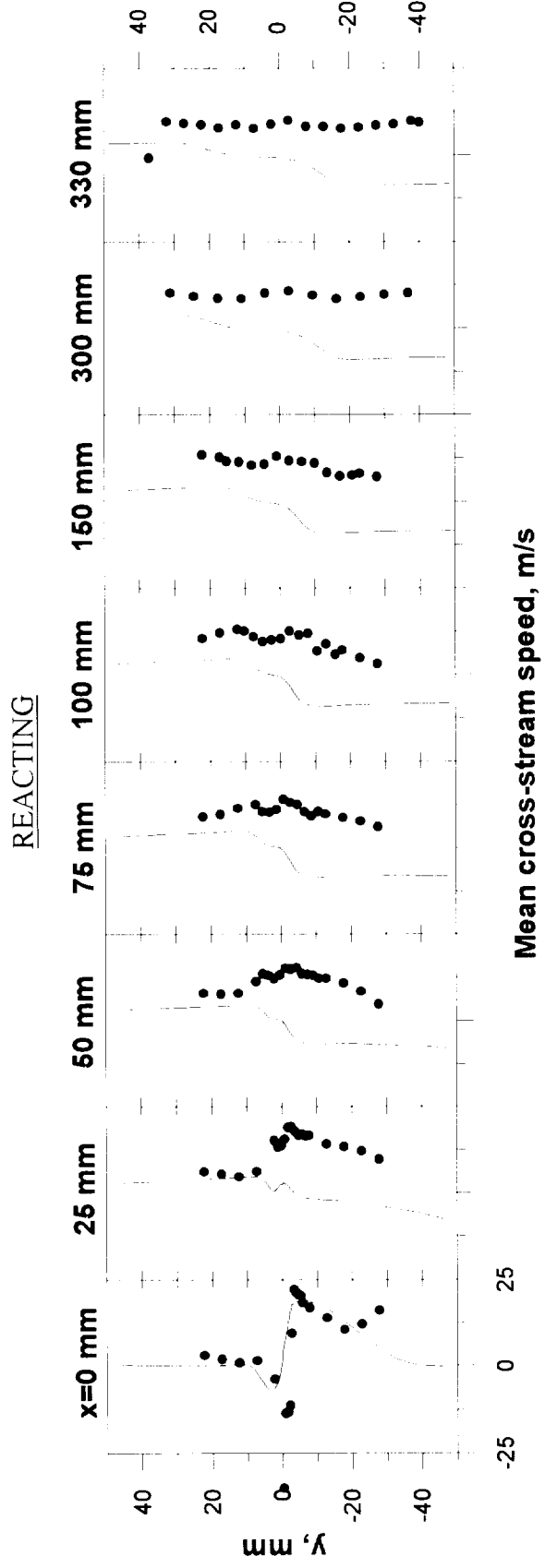
Fig.49. Mean cross-stream velocity profiles. Reacting case.

Chang et al. test case.
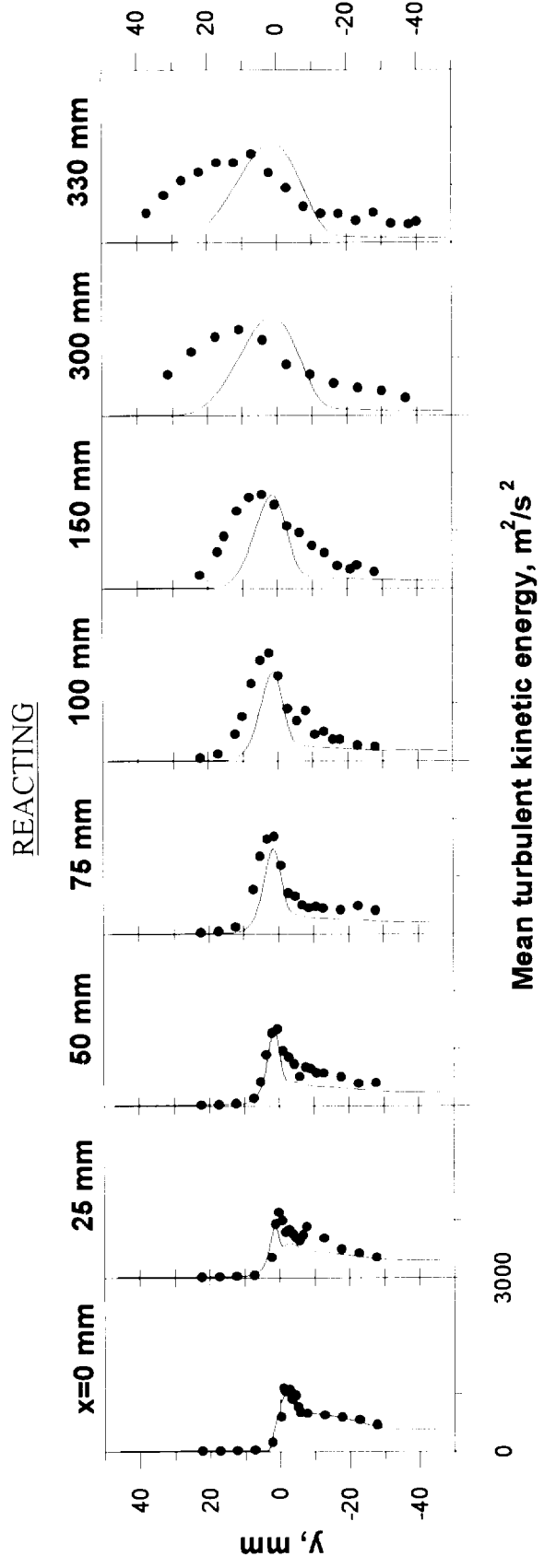
Fig.50. Profiles of turbulent kinetic energy. Reacting case.

Chang et al. test case.
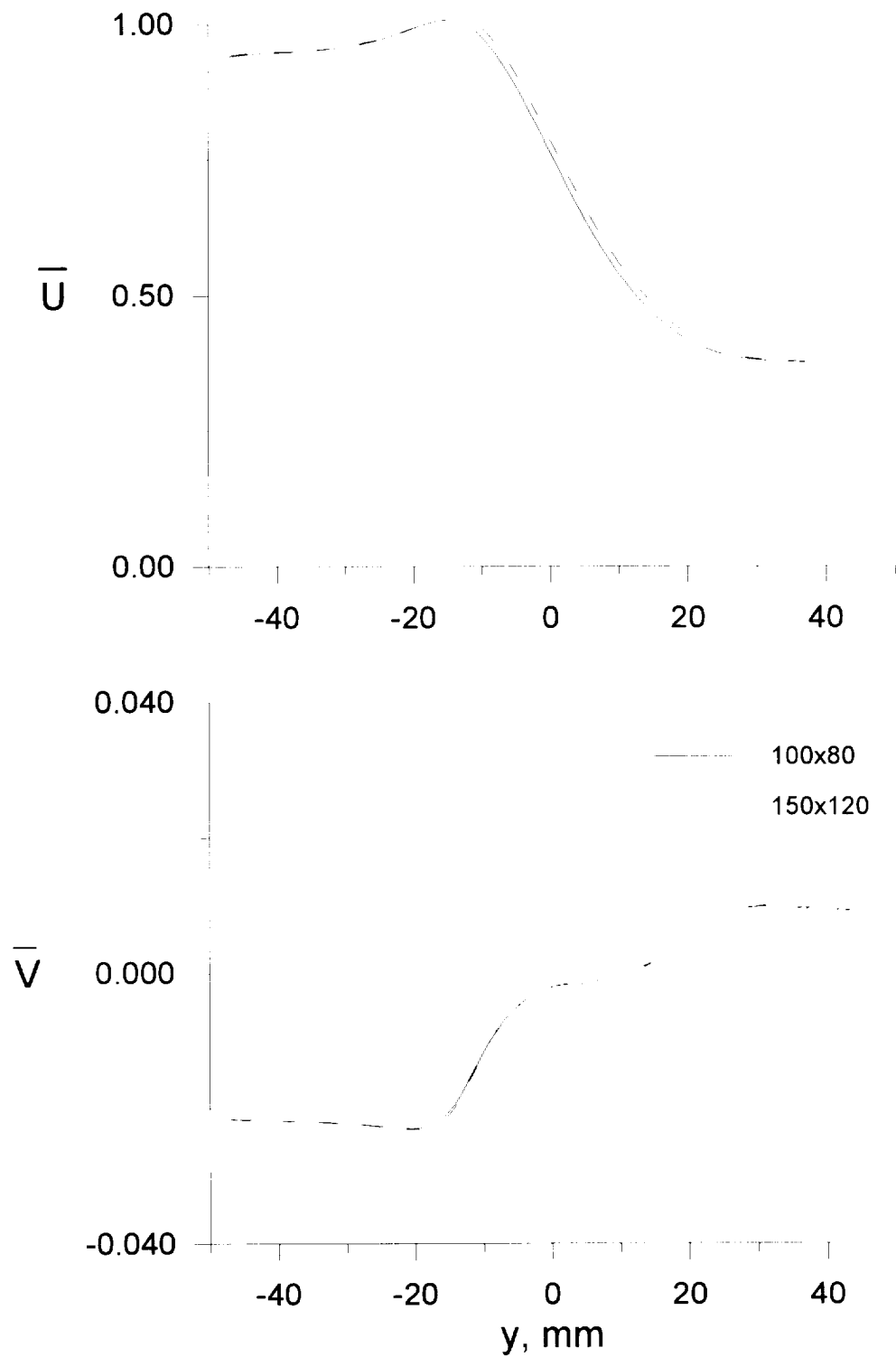
Fig.51a. Influence of discretization on calculated velocity components.
Reacting case. x=300 mm.
$\overline{U}=u/u_a$, $V=v/u_a$.

Chang et al. test case.
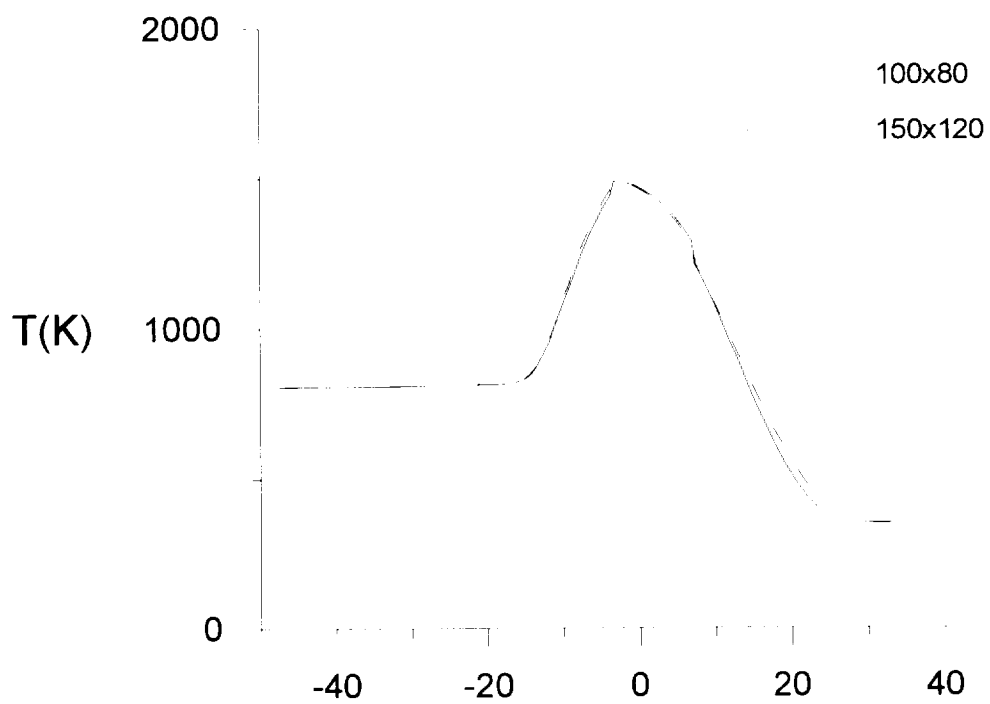
Fig.51b. Influence of discretization on calculated temperature.
Reacting case. x=300 mm.

Chang et al. test case.
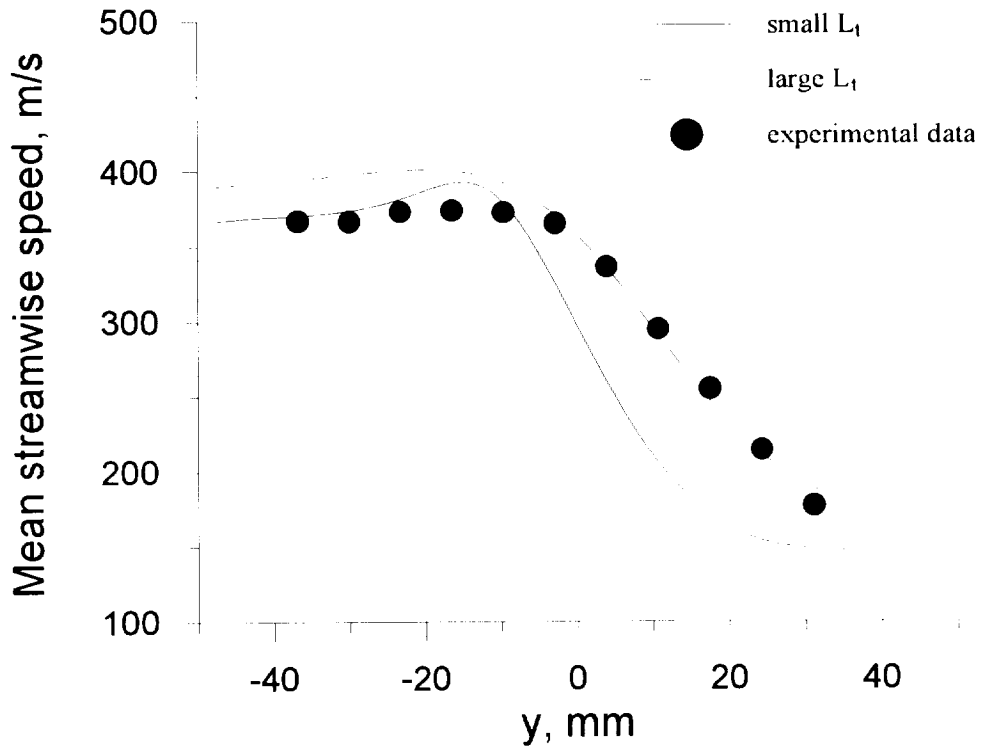
Fig.52. Influence of turbulence length scale in air stream L_t
on predicted streamwise velocity.
x=300 mm.
Chang et al. test case.
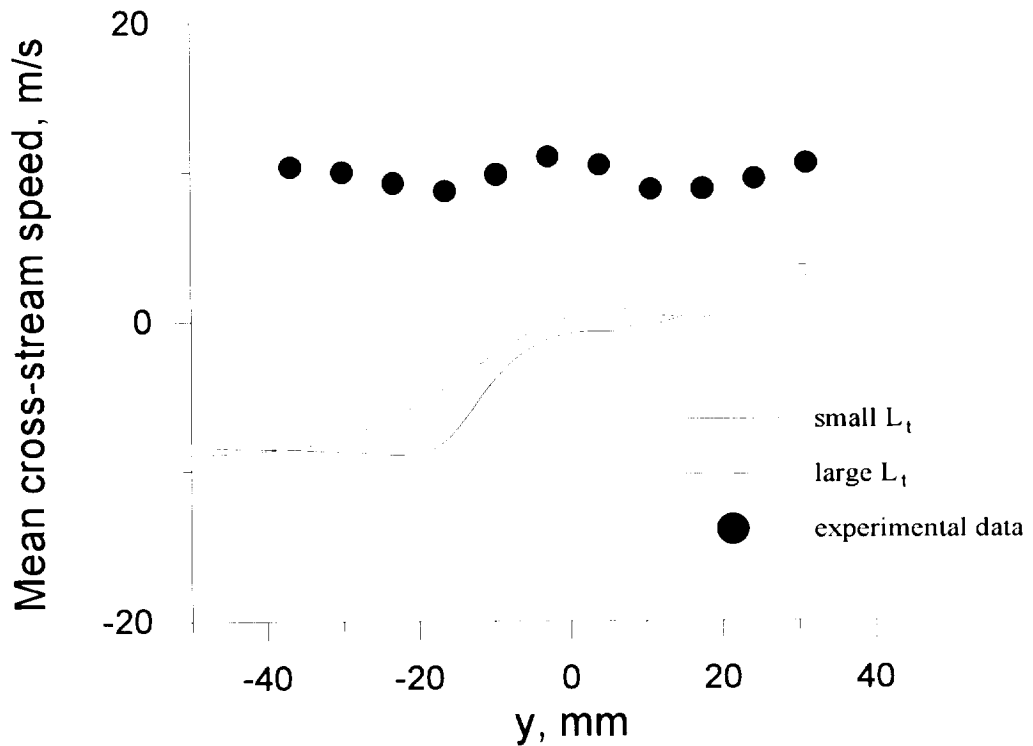
Fig.53. Influence of turbulence length scale in air stream L_t
on predicted cross-stream velocity.
x=300 mm.
Chang et al. test case.
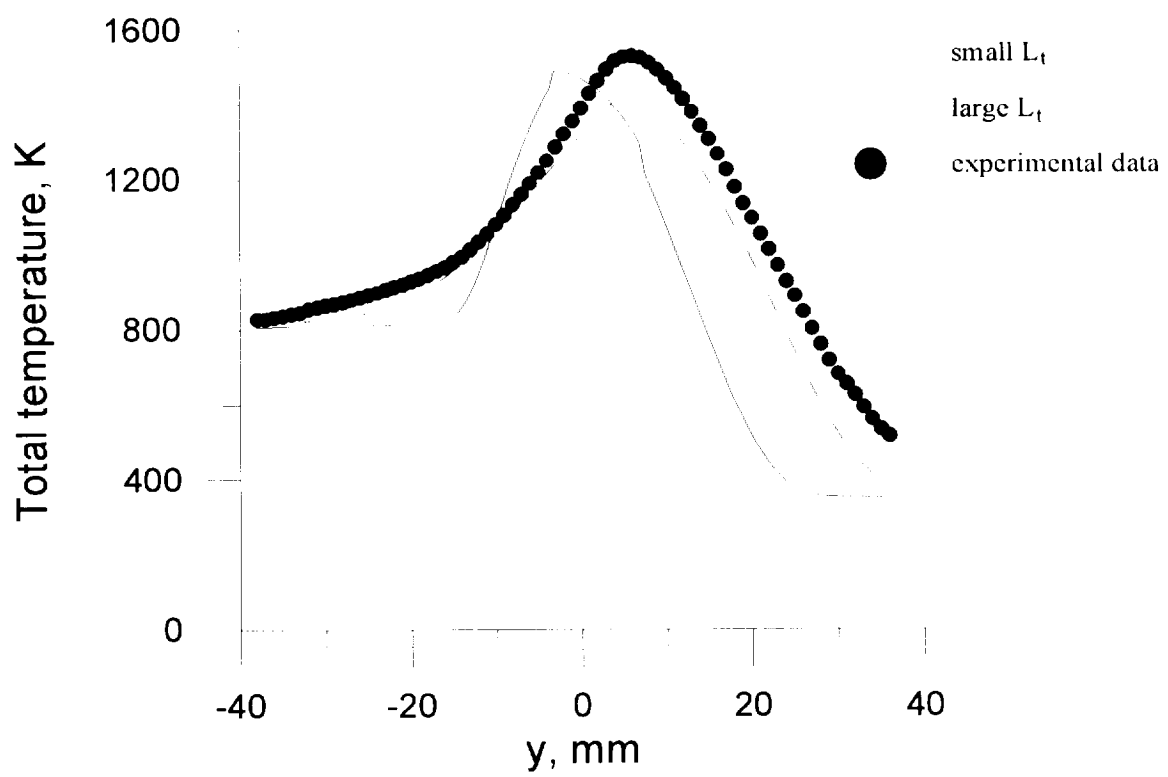
Fig.54. Influence of turbulence length scale in air stream L_t
on predicted temperature profile.
x=300 mm.
Chang et al. test case.
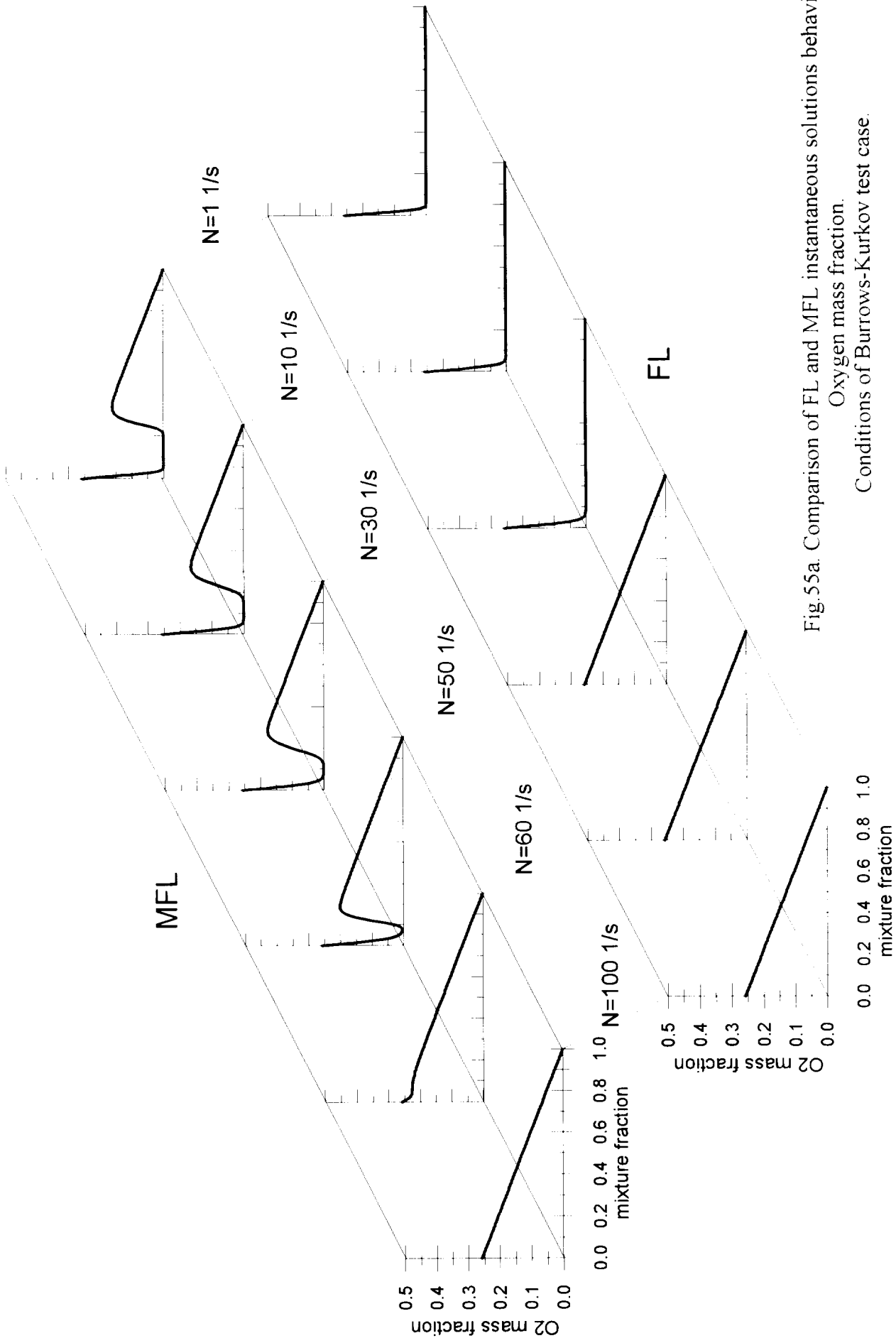
Fig.55a. Comparison of FL and MFL instantaneous solutions behavior.
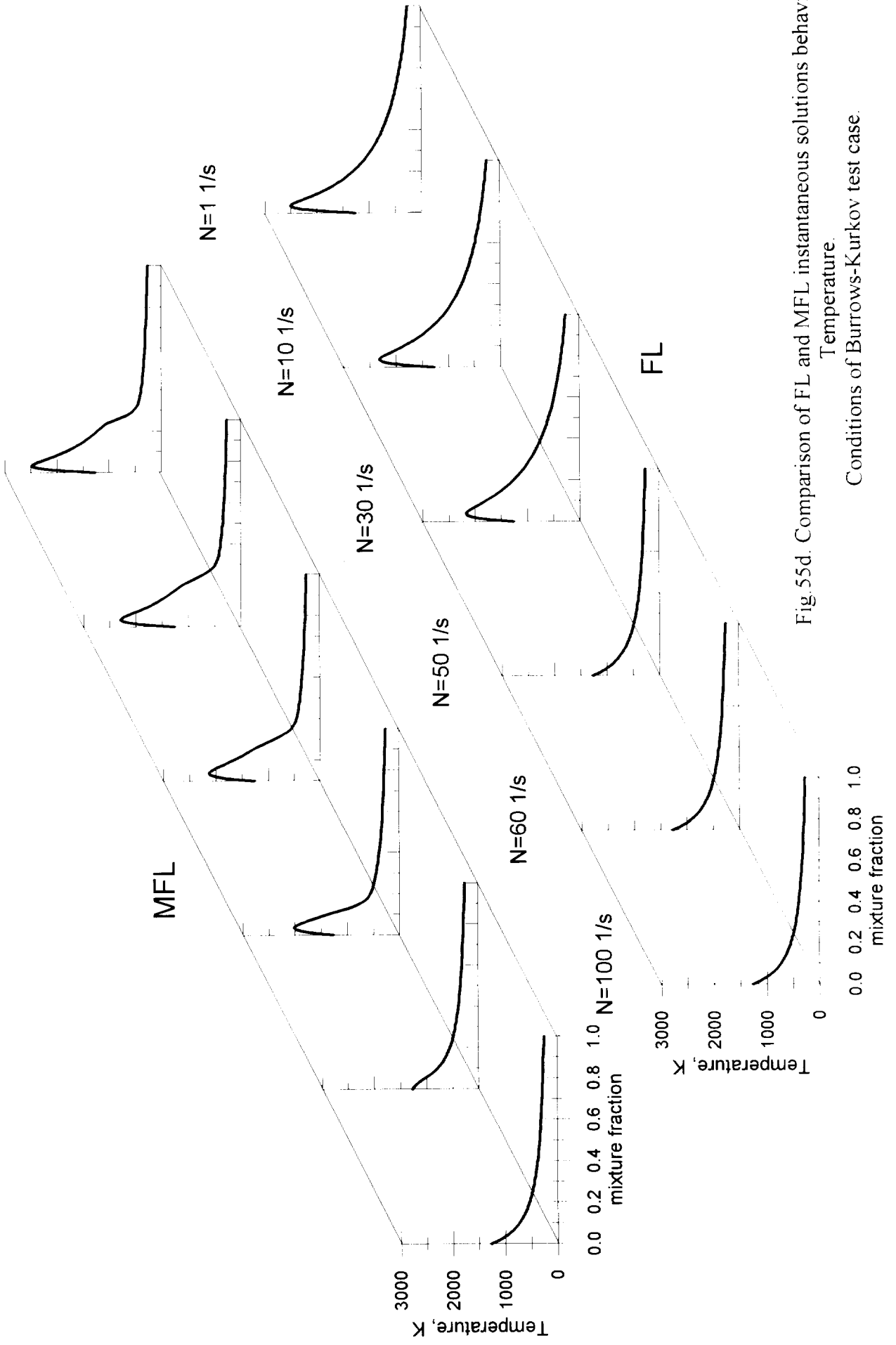Oxygen mass fraction.
Conditions of Burrows-Kurkov test case.
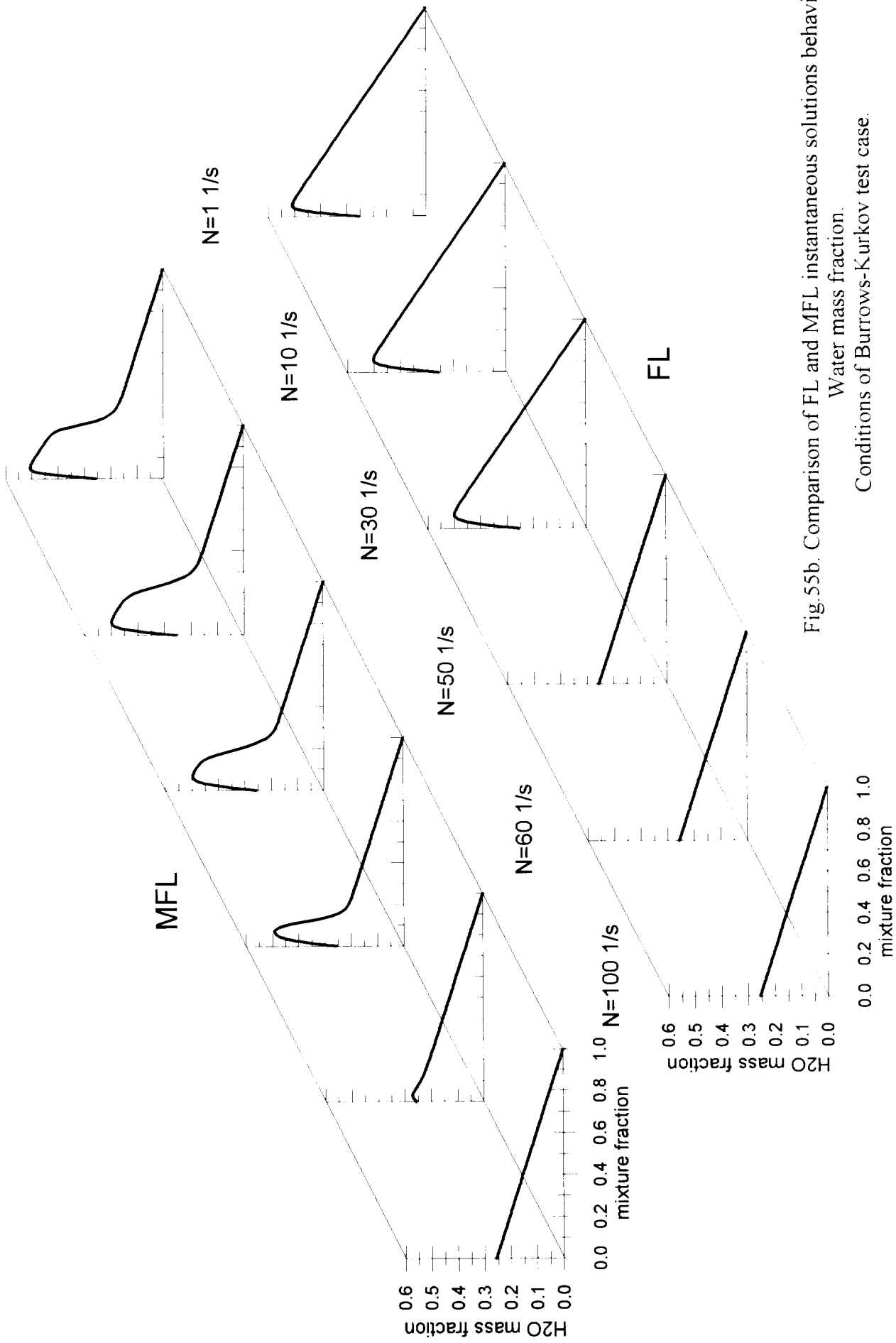
Fig.55b. Comparison of FL and MFL instantaneous solutions behavior. Water mass fraction. Conditions of Burrows-Kurkov test case.
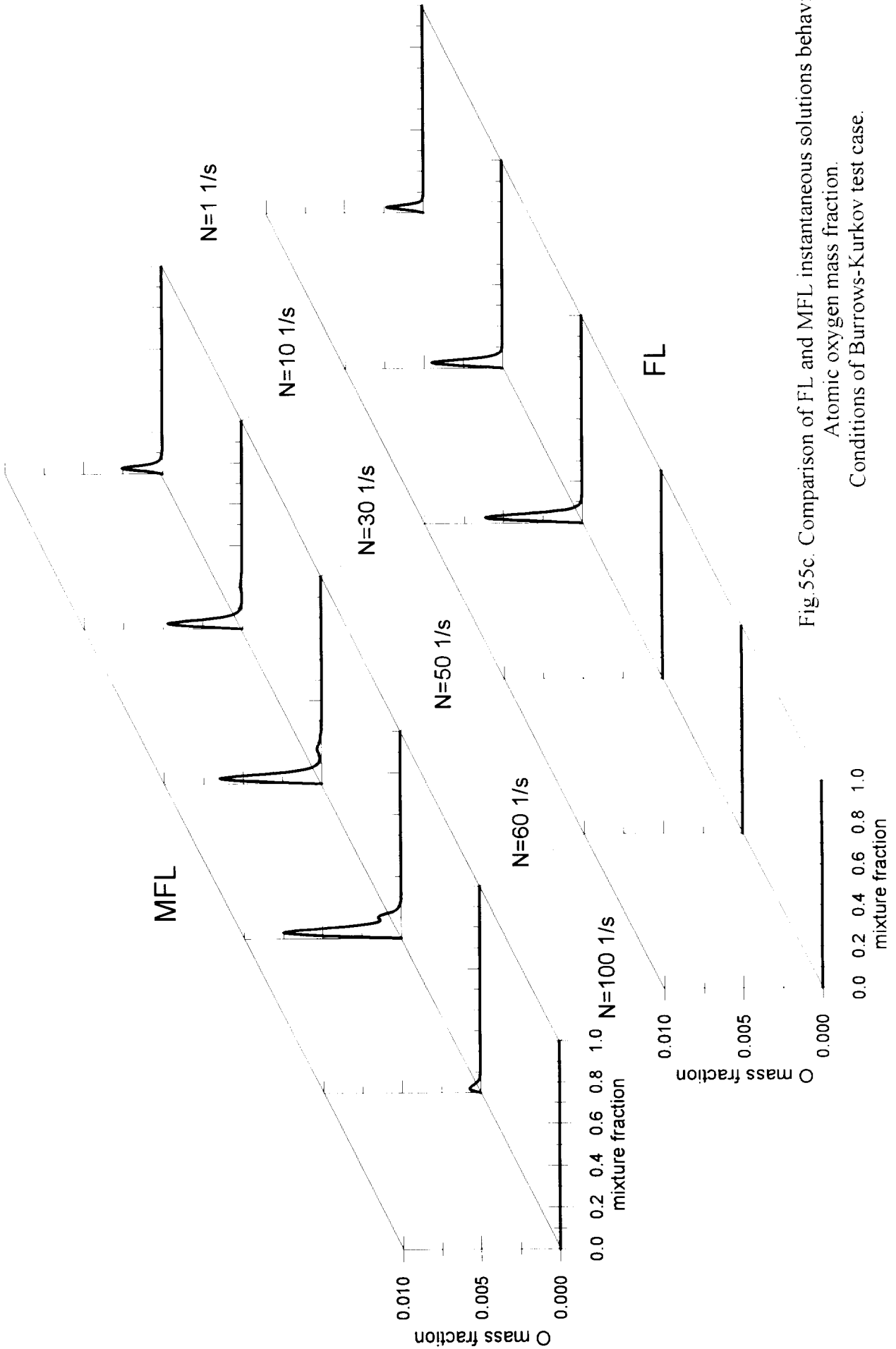
Fig.55c. Comparison of FL and MFL instantaneous solutions behavior.
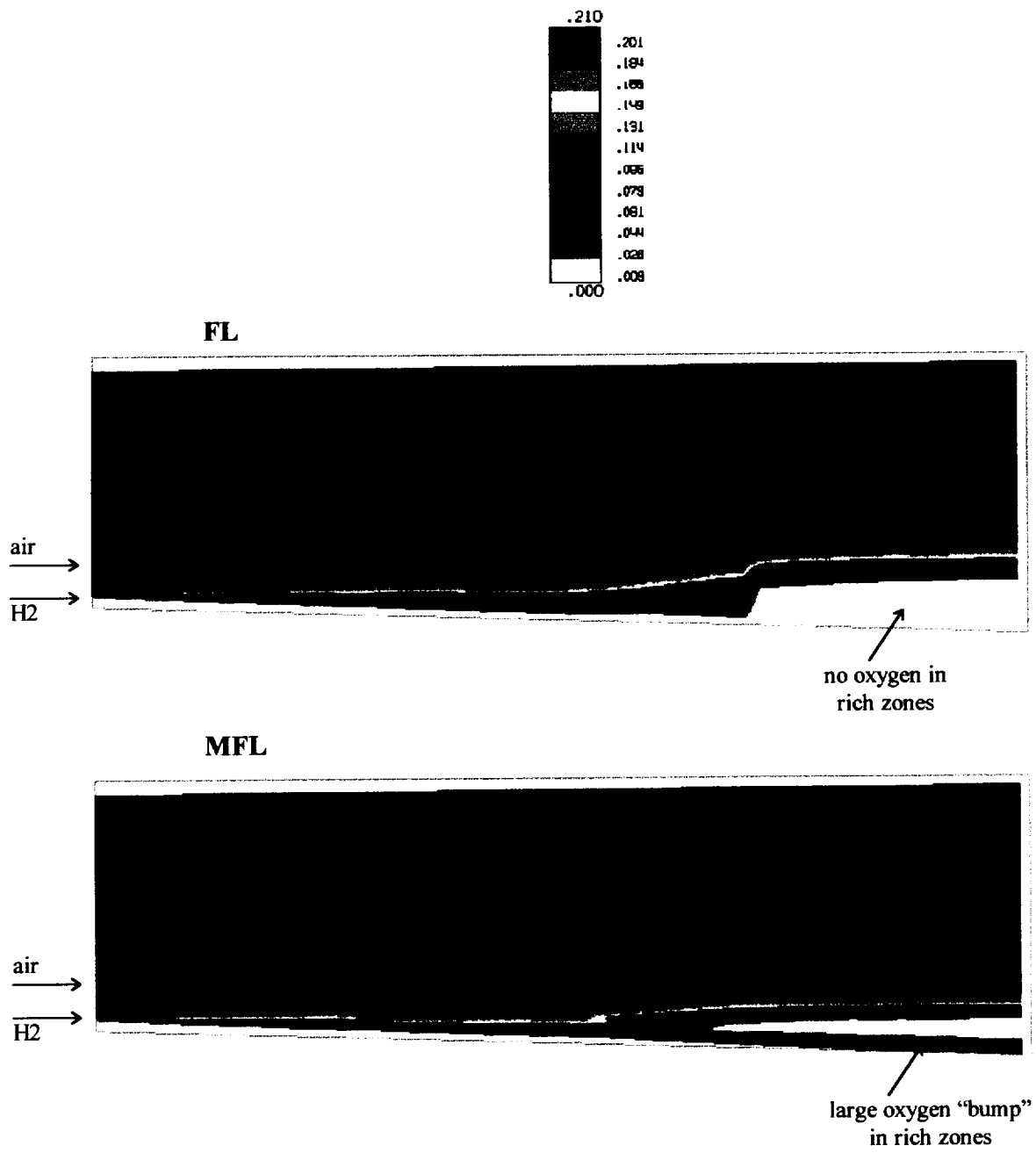Atomic oxygen mass fraction.
Conditions of Burrows-Kurkov test case.

Fig 55d. Comparison of FL and MFL instantaneous solutions behavior.
Temperature.
Conditions of Burrows-Kurkov test case.

Mean O2 mole fraction contours

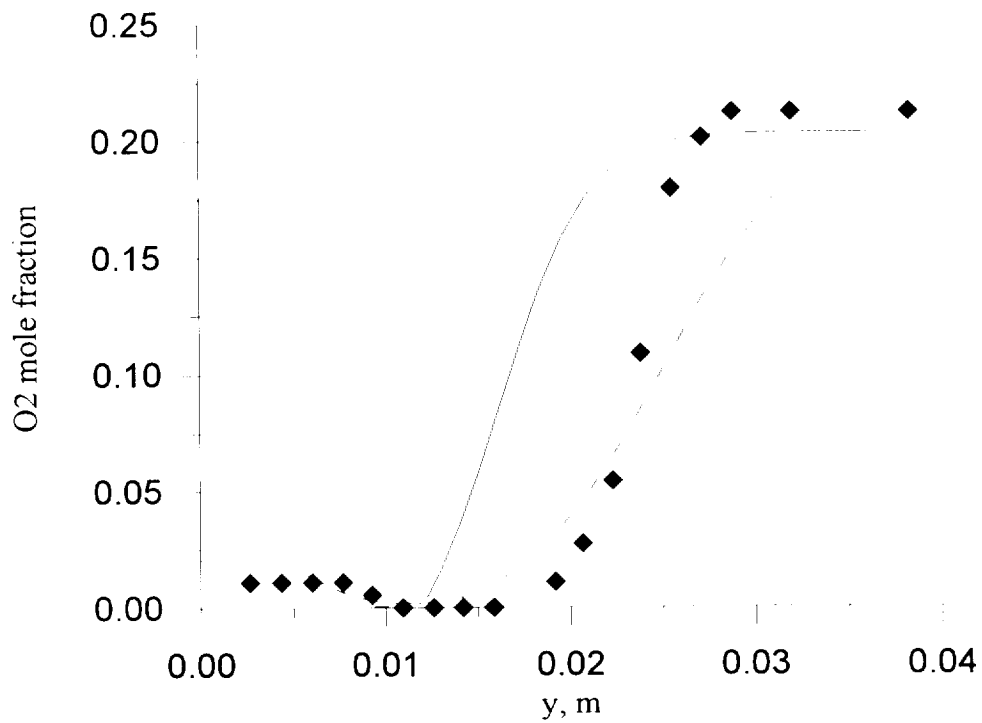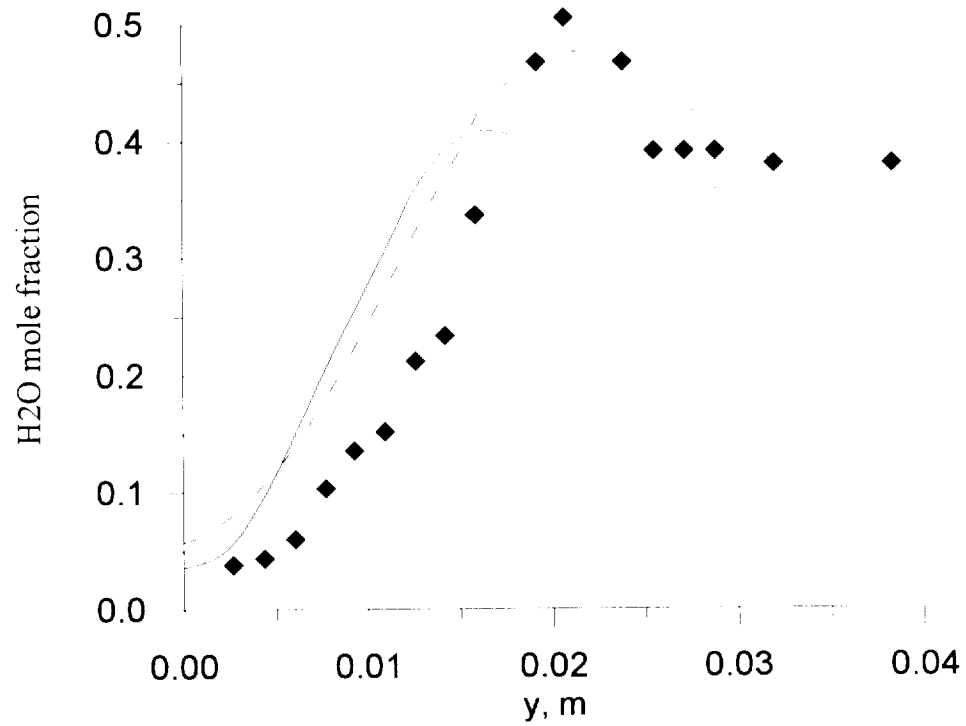Fig.56. Modeling tests of MFL approach

Burrous-Kurkov test case conditions

Fig.57. Comparison of FL and MFL predictions.

MFL

‒ ‒ FL

◆ experimental data

x=0.356 m.
Burrows-Kurkov test case conditions